Mineral Res. Expl. Bull., 140, 1-18, 2010

SEDIMENT CORE STUDIES ON THE NORTH ANATOLIAN FAULT ZONE IN THE EASTERN SEA OF MARMARA: EVIDENCE OF SEA LEVEL CHANGES AND FAULT ACTIVITY

Erol SARI * and Namýk ÇAÐATAY **

ABSTRACT.- Sediment cores BUC-10A and ÝZ-30 located on the North Anatolian Fault Zone (NAFZ), 12 km south of Büyükçekmece and Ýzmit Gulf in the eastern part of the Sea of Marmara, respectively, were studied to investigate tectonics and paleo-oceanographic processes, using sedimentological and geochemical methods. Total inorganic carbon (TIC as total calcium carbonate) and total organic carbon (TOC) contents in core BUC-10A range between 12.1-34.3 and 0.5-4.1 dry wt. %, respectively. The organic matter-rich sapropel unit was identified between 1.60 and 2.43 m below sea floor (bsf) in this core. The concentration ranges of the metals in core BUC-10A were: Cr: 55-96, Cu: 21-37, Ni: 63 39-74, Mn: 345-693, Pb: 19-34, Zn: 79-143 ppm and Fe: 2.30-3.15 dry wt. %. The concentration ranges of TOC, TIC, Cr, Cu, Fe, Ni, Mn, Pb and Zn in core ÝZ-30 were 0.40-1.70 %, 0.25-31%, 39-87 ppm, 13-32 ppm, %2.10-4.80, 18-41 ppm, 315-528 ppm, 7-21 ppm and 78-185 ppm, respectively. Chalcophile element (Fe, Mn, Cu, Pb, and Zn) concentrations in cores ÝZ-30 and BUC-10A give no evidence of hydrothermal activity. A debris flow characterized in core ÝZ-30 and dated 3276±48 a (calendar) before present (BP) was most likely triggered by tectonic activity in the Ýzmit Gulf. Sediments of 49.5 mbsf palaeo-shoreline dated 9364±64 a BP was also identified in the same core from the Ýzmit Gulf.

Key words: Sea of Marmara, Sea level change, North Anatolian Fault, hydrothermal activity, submarine mass flow.

INTRODUCTION

Sea of Marmara is connected to the Mediterranean and Black Sea via the Turkish Straits. Therefore, the Sea of Marmara has a two-layer water stratification and flow system, which separates the more saline (37.5 - 38.5 ppt) lower water layer of Mediterranean origin from the less saline upper layer of the Black Sea origin (18 - 22 ppt) (Ünlüata et al., 1990; Beþiktepe et.al., 1994). This different salinity creates a two-way system of reciprocal flow. Therefore the Sea of Marmara contains the records of climatic and tectonic changes of itself, adjacent seas and the surrounding land mass. The previous cores studies in the Sea of Marmara have indicated that the Sea of Marmara sediments deposited in the last 20 ka can be subdivided into two units according to fossil contents (Çaðatay et al., 1999, 2000). The upper Unit 1 has was deposited under marine conditions after the arrival of the Mediterranean water at about 12 kyr BP, and the lower Unit-2 was deposited under lacustrine conditions (Çaðatay et al., 2000, 2003; Abrajano et al., 2002; Mc Hugh et al., 2008).

Geometry, kinematics and seismic activity of the North Anatolian Fault (NAF) beneath the Sea of Marmara have been studied by many workers (Alpar 1999; Halbach et al., 2000, 2002; Gürbüz et al., 2000; McClusky et al., 2000; Okay et al., 2000; Ýmren et al., 2001; Gökaþan et al., 2001, 2002, 2003; Le Pichon et al., 2001, 2003; Rangin et al., 2001, 2004; Armijo et al., 2002, 2005; Alpar and Yaltýrak 2002; Meade et al., 2002; Polonia et al. 2002, 2004; Yaltýrak, 2002; Demirbað et al., 2003). Although past mass flow and cold seep activities (Patzold et al., 2000; Sarý 2004; Kuþçu et al., 2005; Sarý and Çaðatay 2006; Mc Hugh et al., 2006, Beck et al., 2007, Zitter et al., 2008)

* Ýstanbul University, Institute of Marine Sciences and Management, Vefa, Ýstanbul
** Ýstanbul Technical University Faculty of Mines, Geology Department Ayazaða, Ýstanbul, Turkey

and tsunami events (Alpar et al., 2003, 2004; Hebert et al., 2005; Altýnok and Alpar 2006; Tinti et al., 2006) have been reported from the Sea of Marmara, there is insufficient information on the effects of the NAF activity on the geochemistry of the Sea of Marmara sediments (Halbach et al., 2000, 2002; Armijo et al., 2005; Kuþçu et al., 2005; Zitter et al., 2008; Kuþçu et al., 2009). These geochemical studies mostly concentrated on the surface expression of cold seeps along the main Marmara fault. It would be expected that during a seismic event, the transpressional segments would release fluids, whereas the transtensional would be mainly areas recharge and deep circulation. It would also be assumed that the exiting fluids would react with the sediments causing significant changes in the composition.

In this paper sedimentological and geochemical properties of sediments related to the NAF activity and paleo-oceanographic changes, such as tectonic uplift, mass flows, hydrothermal activity, diagenetic changes and sea level changes were studied in two cores located on the northern strand of the NAF Zone (Figure 1). The cores ÝZ-30 and BUC-10A were recovered off the Hersek delta in the Ýzmit Gulf and from 12 km south of Büyükçekmece during the RV Urania cruise in 2001. The cores were studied using geochemical (TOC, TIC and heavy metals analysis) and sedimentological methods.

METHODS

Gravity cores ÝZ-30 and BUC-10A are 3.50 and 3.6 m long, and recovered from -46.2 and-380 m respectively. The cores were split into two halfs in laboratory and lithologically described. They were then subsampled at about 5 cm intervals, also taking into account the lithological variation. TIC, TOC and the total heavy metal content of the core samples were carried out at the Istanbul University Institute of Marine Science and Management Laboratories.

TIC content was determined using a gasometric method. This method is based on the volumetric determination of CO_2 released by acidification of the dry ground subsample with 10% HCl. The results are expressed as weight percentage of $CaCO_3$ (Loring and Rantala, 1992).

TOC analysis was performed using the Walkley - Black method, which involves the titration with ferrous aluminium sulphate of the dichromate left after a wet combustion of the sample with potassium dichromate (Gaudette et. al., 1974; Loring and Rantala, 1992).

For metal analysis, the sediment sample was treated with 10 ml HNO_3 at 120°C in an open teflon beaker for 30 min. and then heated with 5ml $HClO_4$ and 5 ml HF in closed teflon beaker for 30 min. After the formation of dense white fumes, the cover was removed to allow the $HClO_4$ to evaporate. To further digest the resistant particles, 5 ml of HF was added and the mixture allowed refluxing for a further 30 min. The remaining solution was evaporated on a hot plate at 180°C to obtain dry residues, which were redissolved in 10 ml of 1M HCl, and then diluted to 50 ml with 1M HCl and stored in a pre-cleaned plastic bottle in a deep freezer (Loring and Rantala 1992; Tessier et. al. 1979). All metals were determined by flame Atomic Absorption Spectrophotometer (AAS) after the total digestion.

Accelerated Mass Spectroscopic (AMS) ^{14}C age determination was carried out at the Woods Hole Oceanographic Institution's NOSAMS facility. Hand-picked and ultrasonicated benthic foraminifers collected from immediately below individual sediment layers were used for the analysis (Table 1). Ages were calculated as ^{14}C a BP, corrected for ^{13}C, and the error expressed as $\pm 1\sigma$. Calibrated calendar ages with a reservoir correction of 385 a (Siani et al. 2000) were calculated according to Stuiver and Braziunus (1993) reported as calendar a BP.

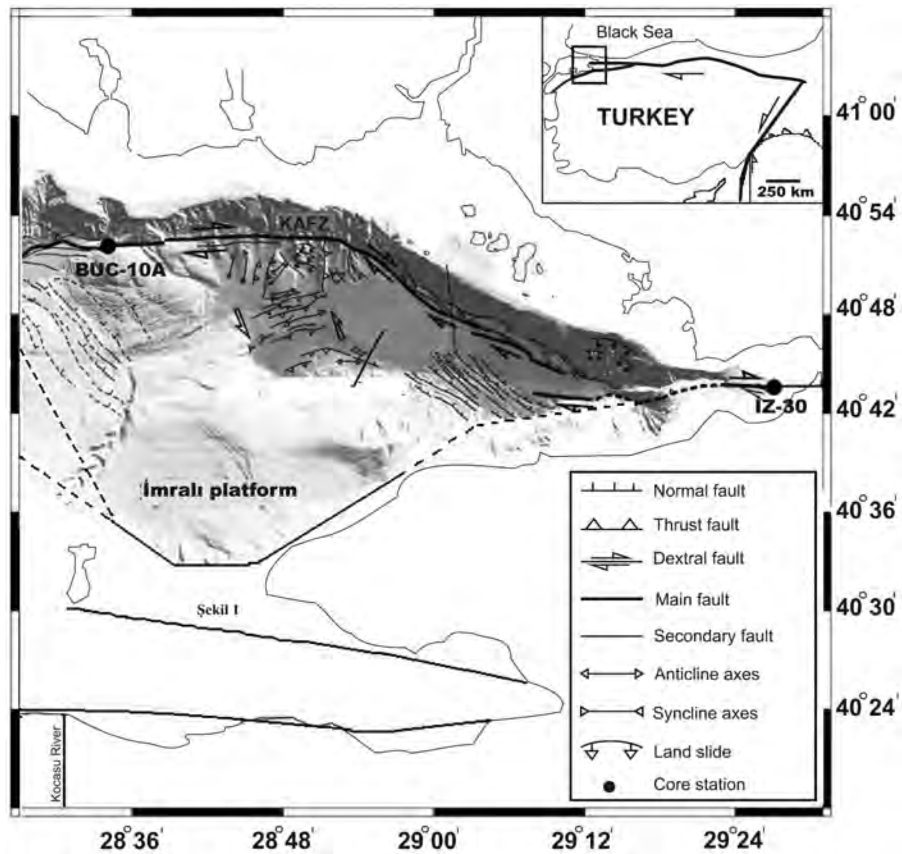

Figure 1- Bathymetric and fault map of Sea of Marmara, showing the core locations.

Table 1- Radiocarbon and calibrated ages for selected samples in the core İZ-30.

Core number	Level (cm)	Material	^{14}C date	Calibrated year (Calendar year)
İZ-30	223-224	Foraminifer	3455 $\pm$ 35	3276 $\pm$ 48
İZ-30	330	Mollusc	8740 $\pm$ 64	9364 $\pm$ 64

RESULTS

Lithological identification of cores

The sedimentary section in Core ÝZ-30 is composed of brown mud (0 - 0.70 mbsf), yellowish green mud (0.70-1.35 mbsf), greyish-green mud (1.35 - 1.72 mbsf) and dark grey green mud (1.72-2.09 mbsf). Bioturbation with whole and broken bivalve shell fragments are present at 0.39 - 0.47 mbsf and 1.72 - 1.90 mbsf intervals in the core (Figure 2). Alternations of dark green, fine sandy silt and mud lamina occur between 2.09 and 2.24 mbsf in core ÝZ-30. A poorly sorted fossil-rich sandy silt layer with sharp lower and upper contacts is present between 2.24 and 2.50 mbsf below the laminated unit. This unit presents the characteristics of mass flow. The AMS ^{14}C determination from foraminiferal tests just above its upper contact produced an age of 3276±48 a (calendar) BP. The 2.50 and 3.30 mbsf interval of Core ÝZ-30 consists of dark grey green mud that has a sharp lower contact with a 0.13 m thick dark green fine gravely silty sand unit. The gray gravelly sand unit contains Turritella turbana, and other marine bivalve shells and shell fragments. AMS ^{14}C age of an articulated marine bivalve at 3.30 mbsf above the sand layer gave an age of 9364±64 a (calendar) BP. The basal part of the core consists of 7 cm-thick dark green mud.

Core BUC-10A located 12 km offshore Büyükçekmece consists of two units (Figure 3). The upper Unit 1 is 2.70 m-thick and has been deposited under marine conditions. The uppermost 0.03 mbsf part of the unit consists of light brown mud, which is followed downward to 0.6 mbsf by light green homogeneous mud with gas voids. The middle part of Unit 1 between 0.60-0.72 mbsf and 2.43-2.64 mbsf in Core BUC-10A is composed of dark green homogenous mud, which contains black reduced spots and bands between 0.72 and 1.60 mbsf. The interval between 1.60-2.43 mbsf of the dark green mud is a sapropelic unit having a sharp upper and lower contact. The basal part of Unit 1 between 2.64 and 2.70 mbsf in core BUC-10A is laminated brown mud. Unit 2 constitutes the interval between 2.70 -3.60 mbsf, and was deposited under lacustrine conditions prior to 12 ka BP according to previous researchers (e.g., Çaðatay et al., 2000). Unit 2 consists of greyish green mud that includes black coloured and lenticular iron monosulfide bands. No macro fossils have been found in the lacustrine unit of Core BUC-10A.

The distribution of organic carbon and total carbonate in core sediment

TOC concentration of ÝZ-30 varies between 0.40 and 1.70 dry wt. %. High organic carbon values (>1.0 dry wt. %) are observed at intervals; 0-0.18, 0.55-0.63, 1.35-1.43 and 1.76-2.24 mbsf. The average organic carbon value of the total 71 samples from Core ÝZ-30 is 1.05 dry wt.%. TIC contents vary from 0.25 to 31.10 dry wt. % (as $CaCO_3$) (Figure 4). The main part of the carbonate in the core is of biogenic origin consisting of benthic carbonate shells and shell fragments. The down core distribution pattern of total carbonate content commonly displays a narrow range (0.25 -14.20 %) in core ÝZ-30 with the exception of intervals 2.36-2.37 (22.90%) and 3.30-3.33 mbsf (31.10%) (Figure 4).

The concentration of TOC in the Core BUC-10A ranges from 0.5 to 4.1 dry wt.% (Figure 5). The highest TOC values are found at 1.60-1.63 mbsf and 1.70-1.73 mbsf. All the TOC values in the dark green sapropelic mud between 1.60 and 2.43 mbsf is higher than 2 dry wt.%. The concentration of TIC in Core BUC-10A ranges from 12.10 to 34.30 dry wt.% as $CaCO_3$ with a downward increase from the core top to a maximum value at 2.83 mbsf (Figure 5). The TIC values decrease downward from its maximum at 2.83 mbsf and reach 19.30 dry wt. % at 3.53 m.

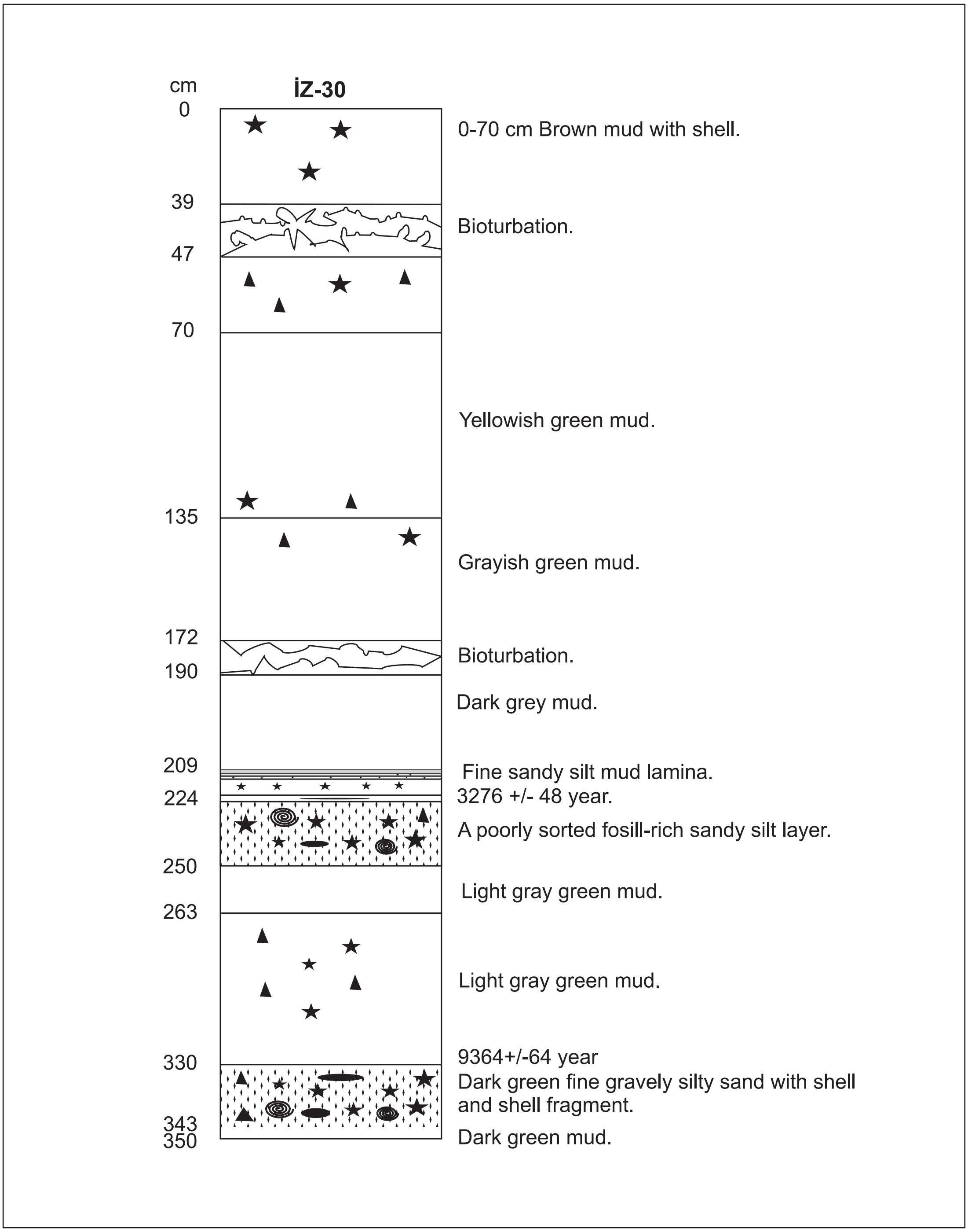

Figure 2- Lithologic log of gravity core ÝZ-30.

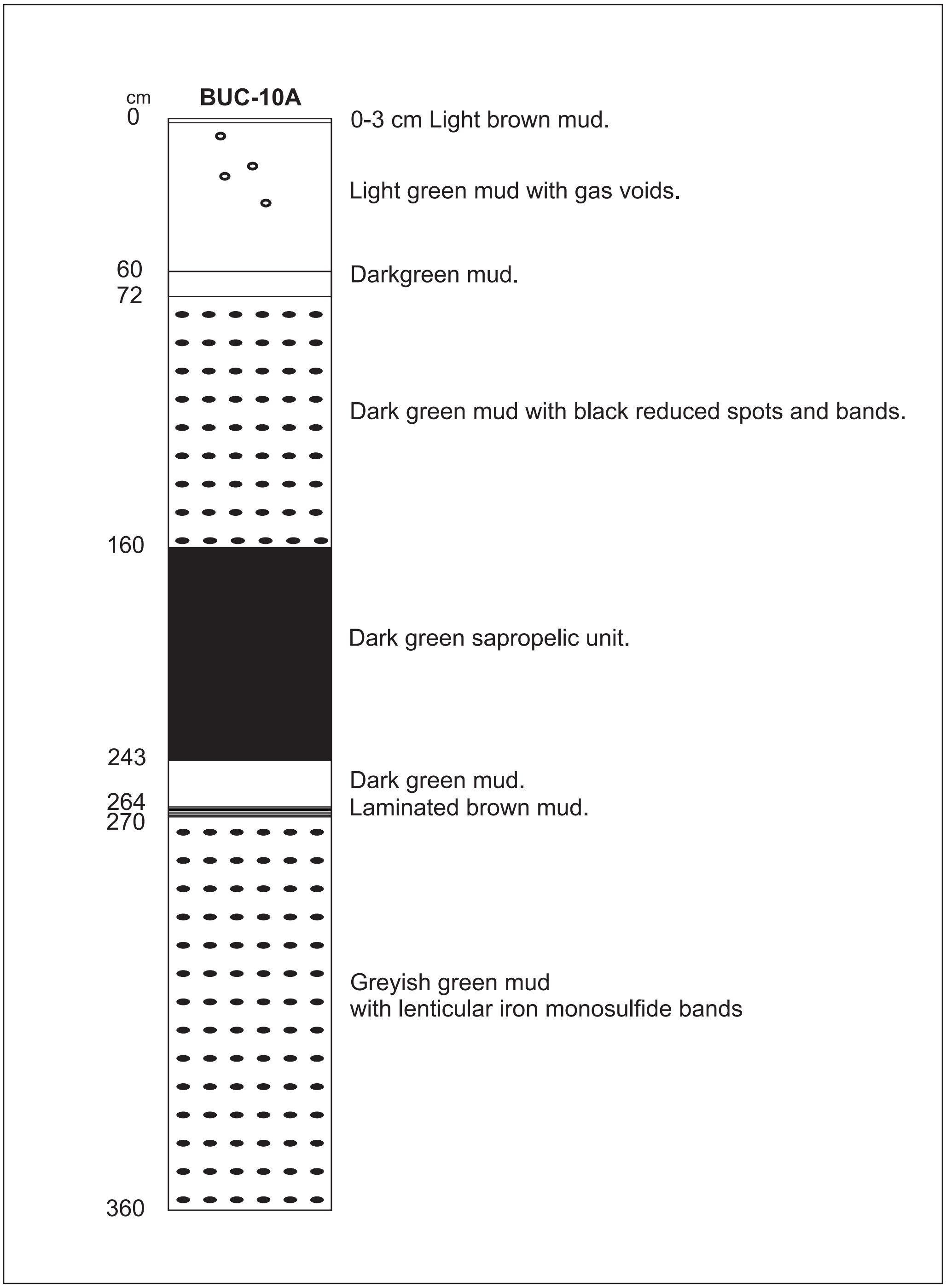

Figure 3- Lithologic log of gravity core BUC-10A.

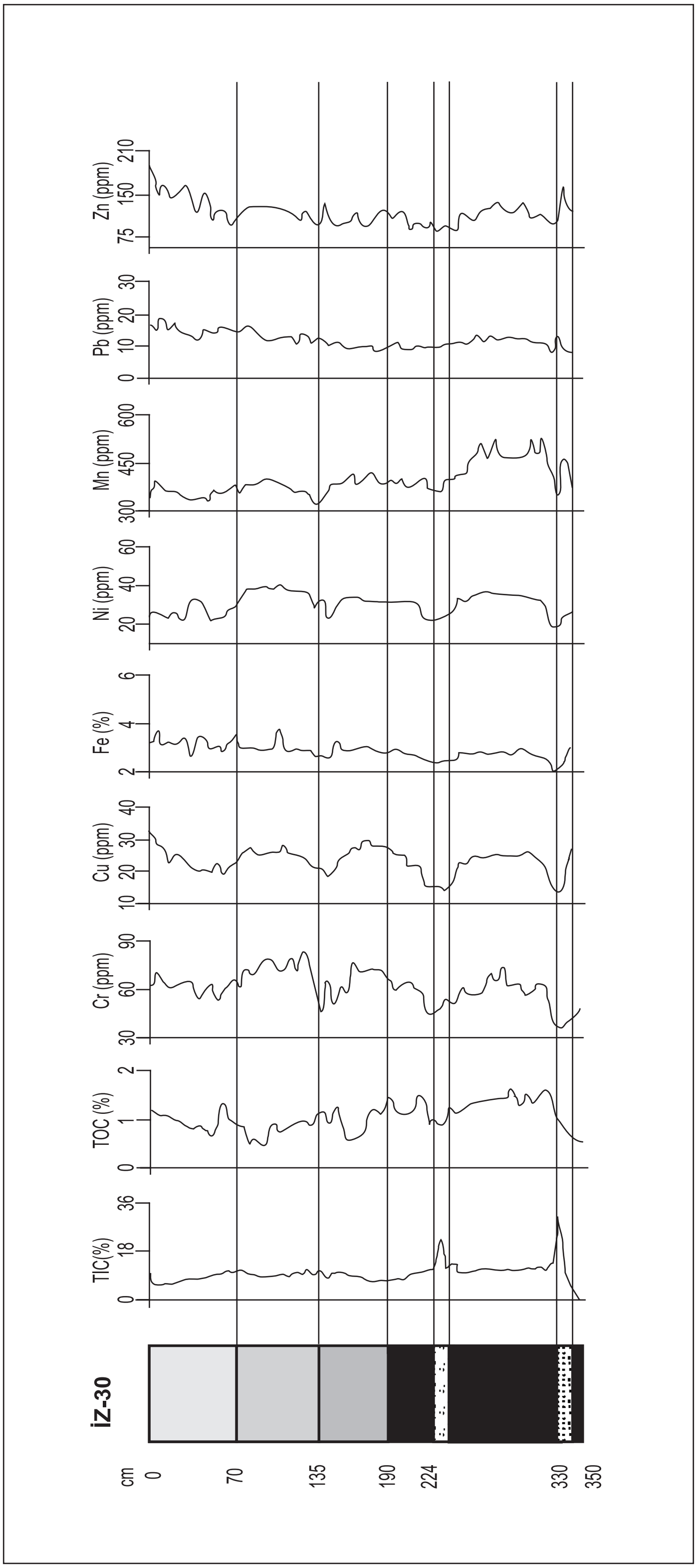

Figure 4- Distribution of TOC, TİC and metal contents in core İZ-30.

Distribution of Cr, Cu, Fe, Ni, Mn, Pb and Zn in cores

Cr, Cu, Fe, Mn, Ni, Pb and Zn contents were determined in a total of 71 sediment samples which were collected from core ÝZ-30. The heavy metal contents in this core range between 39-87 ppm Cr, 13-32 ppm Cu, 2.10-4.80 % Fe, 315-528 ppm Mn, 18-41 ppm Ni, 7-21 ppm Pb and 78-185 ppm Zn. The average concentration of the metals are 65 ppm for Cr, 23.50 ppm for Cu, 3% for Fe, 393 ppm for Mn, 31 ppm for Ni, 12 ppm for Pb and 112 ppm for Zn (Figure 4). The distribution of the Cr, Cu and Ni along Core ÝZ-30 shows similar trends (Figure 4). This similar behaviour is supported by significant positive correlation coefficients (r>0.5) between the metal values. The Fe, Mn, Pb and Zn contents display negative or weak positive correlation coefficients with TIC and TOC (Table 2). The heavy metal contents of sediments in Core ÝZ-30 are commonly lower than the shale averages (Krauskopf 1985), except for Zn, which is slightly higher.

Cr, Cu, Fe, Ni, Mn, Pb and Zn were determined in 37 sediment samples in Core BUC-10A (Figure 5). Mean values and variation ranges (in parentheses) of these elements are 80 ppm (55-96 ppm) Cr, 27 ppm (21-37 ppm) Cu, 2.75 % (2.30-3.15 %) Fe, 468 ppm (345-693 ppm) Mn, 63 ppm (39-74 ppm) Ni, 15 ppm (9-34 ppm) Pb and 118 ppm (79-143 ppm) Zn. All analyzed metal concentrations in core BUC-10A are lower than their worldwide shale averages (Krauskopf, 1985) except for Zn which is 1.43 times the shale average. Cu, Cr and Pb concentrations are the highest at the top 0.03 m part of the core, whereas the lowest metal values are observed at 2.80 - 3.00 mbsf interval which is characterized by the high amount (>30% $CaCO_3$) of total carbonate (Figure 5). The correlation coefficient matrix of metals, TIC and TOC were given in the table 3. Significant positive linear correlation coefficients are observed between the following pairs: Zn-Cu (r=0.74), Cr-Ni (r=0, 68), Ni-Fe (r=0.55) and Pb-Zn (r=0.52). Other elements display negative or weak positive linear correlations with each other.

DISCUSSION AND CONCLUSIONS

Possible effects of fluid activity on sediment composition along the fault

Being located on the NAF, the sediments in the cores ÝZ-30 and BUC-10A would be expected to have been affected by deformation and fluid activity, leaving some geochemical and sedimentological signatures. Ore group elements of Ba, Co, Cu, Ni, Pb, V and Zn are commonly enriched in hydrothermal sediments deposited close to active submarine fault zones (Hodkinson and Cronan, 1995; Gamberi et al, 1997; Kuhn et al, 2000). In the Lau Basin of the southwest Pacific, Cronan and Hodkinson (1997) have determined accumulation rates of 32.000 µg Mn cm^{-2} ka^{-1}, 52.100 µg Fe cm^{-2} ka^{-1}, 604 µg Ba cm^{-2} ka^{-1}, 234 µg V cm^{-2} ka^{-1}, 29 µg Co cm^{-2} ka^{-1}, 109 µg Ni cm^{-2} ka^{-1}, 266 µg Cu cm^{-2} ka^{-1}, 125 µg Zn cm^{-2} ka^{-1} ve 44 Pb µg cm^{-2} ka^{-1}. These studies indicate that hydrothermal sediments are highly enriched in Fe, Mn, Cu, Zn, and Pb. Such metal enrichments are not observed in sediments cores ÝZ-30 and BUC-10A located on the northern strand of the NAF (Figure 4, 5). Instead the metal values are represent concentration levels of semi-pelagic sediments. Zinc enrichment in the upper part of the cores (0-0.5 mbsf) is explained by anthropogenic inputs. Thus, it can be concluded that no hydrothermal fluid activity is present at the sites of cores ÝZ-30 and BUC-10A. Meriç and Suner (1995) and Meriç et al., (1995), based on the analysis of benthic foraminifers in the borehole samples between the Hersek Burnu and Kaba Burun promontories in the Ýzmit Gulf suggests some chemical changes in the tests that are possibly the result of fluid activity. This conclusion is supported by the fact that an increase in gas bubbles released into the water column was observed in the Ýzmit Gulf after the 1999 Kocaeli

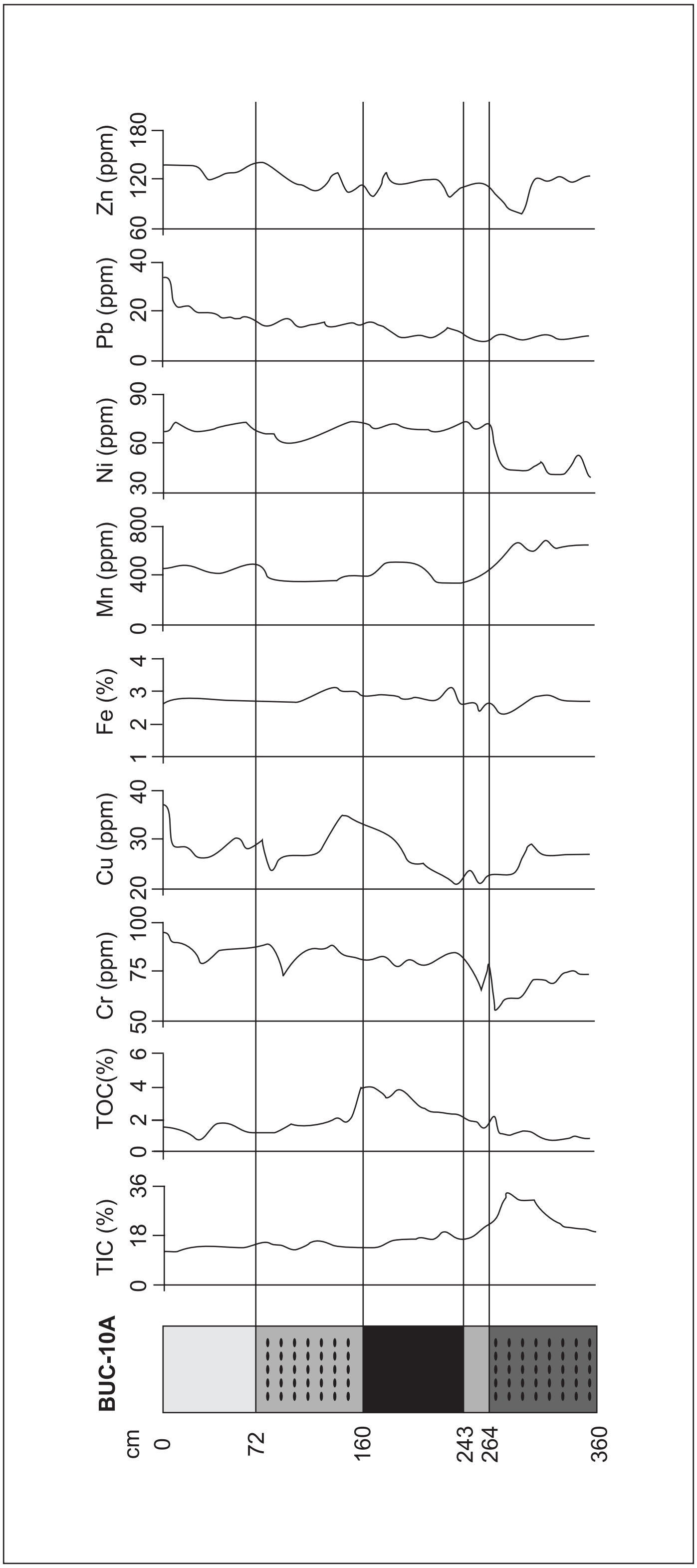

Figure 5- Distribution of TOC, TÝC and metal contents in core BUC-10A.

Table 2- Correlation coefficients between parameters in sediments samples from core ÝZ-30.

	Mn	Fe	Cu	Ni	Pb	Cr	Zn	TOC	TIC
Mn	1								
Fe	-0.24	1							
Cu	0.16	0.51	1						
Ni	0.31	0.20	0.56	1					
Pb	-0.26	0.53	0.32	0.02	1				
Cr	-0.01	0.51	0.73	0,71	0.31	1			
Zn	0.29	0.41	0.33	-0.04	0.65	0.20	1		
TOC	0.47	-0.15	0.08	0.08	-0.11	-0,02	-0.06	1	
TIC	0.26	-0.54	-0.44	-0.14	-0.30	-0.32	-0.34	0.17	1

Table 3- Correlation coefficients between parameters in sediments samples from core BUC-10A.

	Mn	Fe	Cu	Ni	Pb	Zn	Cr	TOC	TIC
Mn	1								
Fe	-0.22	1							
Cu	-0.03	0.36	1						
Ni	-0.73	0.37	0.31	1					
Pb	-0.23	0.12	0.59	0.41	1				
Zn	-0.13	0.26	0.36	0.33	0.54	1			
Cr	-0.53	0.37	0.45	0.70	0.62	0.61	1		
TOC	-0.40	0.42	0.35	0.59	0.004	-0.18	0.16	1	
TİC	0.54	-0.49	-0.56	-0.72	-0.65	-0.60	-0.84	-0.32	1

earthquake (Alpar, 1999 and Kuþçu et al., 2002, 2005). The presence of gas voids with 0.4 mm in diameter at 0-0.40 mbsf interval in Core BUC-10A suggest gas escape at the core site. Recent surveys in the Sea of Marmara have demonstrated the widespread cold fluid activity along the NAF, indicating the tectonic control on the fluid escape (Armijo et al., 2005; Zitter et al., 2008; Geli et al., 2008 and Bourry et al., 2009). However, the surveys did not discover any hydrothermal fluid activity in the Sea of Marmara.

Evidence of tectonic activity

The mud lithology of Core ÝZ-30 from Ýzmit Gulf on the NAFZ was disrupted by coarse sediment intervals with shells and shell fragments at 2.24 - 2.50 mbsf and 3.30 - 3.43 mbsf (Figure 2). These changes are supported by total inorganic carbonate distribution curve in ÝZ-30 (Figure 4). Sandy silt unit between 2.24 and 2.50 mbsf is poorly sorted, contains abundant shell and shell fragments, and displays sharp upper and lower contacts. These properties are typical characteristics of mass flow deposits (Johnson, 1970; Hampton, 1972; Middleton and Hampton, 1973; Shanmugan et al., 1995). AMS ^{14}C radiocarbon dating just above the upper contact of the unit produced an age of 3276±48 a (calendar) BP for this deposit. The possible triggering mechanisms for this mass flow during the normal marine period of deposition are; volcanic eruption, (Kastens and Cita 1981; Cita and Rimoldi 1997), high tide (Bjerrum 1971; Wisenam et al., 1986), low sea level (Hampton et al., 1996; Lee et al., 1996), rapid sedimentation on shelf edge and slope, gas activity related to gas hydrate decomposition (Hampton et al. 1996; Lee et al. 1996), as well as the earthquake (seismic) activity. No volcanic activity has been observed in the Sea of Marmara during at least a couple of millenniums. Santorini is the nearest active volcanic centre, and its last eruption took place at 3 500 a B.P. (Druitt et al. 1989). This volcanic eruption occurred 200 years before the mass flow event. Therefore, the volcanic eruption cannot be a possible triggering mechanism for the mass flow in the Ýzmit Gulf. The study area is a small inland sea and has only low-scale tidal oscillations (between 8 and 10 cm, Damoc 1971; Alpar and Yüce 1998), hence tide can be ignored as a triggering cause of mass flows. The sea level in the Sea of Marmara started rising after the reconnection at about 12 ka BP (Aksu et al., 1999, 2002; Çaðatay et al., 2000; Hiscott and Aksu 2002; Kaminski et al., 2002; Elmas et al., 2008) and stable environmental conditions reached its present shoreline in the Sea of Marmara at about 4.0 ka BP (Çaðatay et al., 2000; Mc Hugh et al. 2008). With the storm wave base level at about 10-15 m the storms can not be the cause of the mass flow. The riverine input into Gulf of Ýzmit is via some small creeks having small drainage areas. Moreover, the location of Core ÝZ-30 is far away from the mouths of streams. Thus, rapid sediment loading is not possible at the core site to provide the necessary triggering for the mass flow. Water depth in the Ýzmit Gulf is not suitable for the gas hydrate formation that usually occurs in sediments deeper than 1000 m at temperatures of 14°C, characteristic of bottom waters in the Sea of Marmara (Kvenvolden, 1993). However, direct fluid expulsion from active faults during earthquakes (Alpar, 1999; Kuþçu et al., 2004, 2009; Geli et al., 2008; Zitter et al., 2008) could cause sediment disturbance close to the fault rupture. Such a gas escape mechanism and/or seismic shaking during earthquakes are the most likely triggering mechanism of the submarine mass flow dated 3.3 ka BP in the Ýzmit Gulf. Study area is tectonically very active. 20 historical and 73 instrumental earthquakes with intensity equal to or greater than 9 and 5 having occurred in the eastern Sea of Marmara over the last 2000 years (Ambraseys and Finkel 1991; Ambraseys 2002). The association of mass flows and seismic activity in the Sea of Marmara basins is supported by the occurrence of frequent sismo-turbidite units identified in cores, which can be correlated with the historical earthquake (Baþaran 2002; Sarý and Çaðatay 2006; Mc Hugh et al., 2006).

Evidence of sea level changes

With rising global sea level after the late glacial maximum (Fairbanks, 1989), Mediterranean waters spilled through the Dardanelles Strait into the Sea of Marmara at 12 ka B.P. (Çaðatay et al. 2000, 2003; Aksu et al. 2002; Kaminski et al. 2002; Mc Hugh et al., 2008). Following this reconnection, the sea level in the Sea of Marmara has risen in tandem with global sea level. But the global transition from glacial to interglacial was interrupted by the Younger Dryas cold interstadial in the Sea of Marmara as evidenced by the presence of the -65 m paleo-shoreline and a terrace in the Sea of Marmara shelf areas (Çaðatay et al., 2003; Newman 2003; Eriþ et al., 2007), The coarse gravely sand unit with shell and shell fragments at 3.30-3.43 mbsf interval near the base of Core ÝZ-30 interrupts the homogeneous marine mud and is interpreted as the sediments of a high-energy paleo-shoreline. This paleoshoreline is dated to be about 9.4 ka BP by the AMS ^{14}C dating. This 49.5 mbsf paleo-shoreline with an age of 9.4 ka BP is in agreement with the global sea level curve (Fairbank, 1989) and the lowermost parasequences of the Kurbaðalý Dere Delta package located on the eastern side of the Istanbul Strait canyon on the northern shelf of the Sea of Marmara (Gökaþan et al., 2005; Eriþ et al., 2007).

Core BUC-10A located 12 km offshore Büyükçekmece consists of two units which have been deposited under marine (0-2.70 mbsf) and lacustrine (2.70-3.60 mbsf) conditions (Figure 3). The TOC profile of the core provides important chronostratigraphic and paleoceanographic information for the Sea of Marmara (Figure 3-5). In the sediment core BUC 10, a sapropelic sediment layer between 1.60-2.43 mbsf is identified. This layer was previously dated at 10.6-6.4 kyr (uncalib) BP (Çaðatay et al., 1999, 2000). Foraminiferal analysis indicates that the sapropel was deposited under mainly suboxic bottom water conditions (Çaðatay et al., 1999, 2000). Organic material of the sapropelic unit in the Sea of Marmara is mainly of terrestrial origin with the marine fraction becoming predominant towards the top of the unit, as global sea level rose with time and the core location became further away from the shoreline (Tolun 2002).

ACKNOWLEDGEMENTS

This study was supported by The Research Foundation of the University of Ýstanbul (project T-1189/01112001). We thank captain and crew of RV Urania for recovery of the cores. We also would like to thank referee Ismail KUÞÇU and the other two referees for their useful comments and suggestions.

Manuscript received May 5, 2009

REFERENCES

Abrajano, T., Aksu, A.E., Hiscott, R.N. and Mudie, P.J. 2002. Aspects of carbon isotope biogeochemistry of late Quaternary sediments from the Marmara Sea and Black Sea. Marine Geology, 190,151-164.

Aksu, A.E., Hiscott, R.N. and Yafiar, D. 1999. Oscillating Quaternary water levels of the Marmara Sea and vigorous outflow into the Aegean Sea from the Marmara Sea-Black Sea drainage corridor. Marine Geology, 153, 275-302.

______,______, Kaminski, M.A., Mudie, P.J., Gillespie, H., Abrajano, T. and Yafiar, D. 2002. Last glacial-Holocene palaeoceanography of the Black Sea and Marmara Sea: stable isotopic, foraminiferal and coccolith evidence. Marine Geology, 190, 119-149.

Alpar, B. 1999. Underwater signatures of the Kocaeli earthquake of 17 August 1999 in Turkey. Turkish Journal of Marine Sciences, 5, 111-130.

Alpar, B. and Yüce, H. 1998. Sea-level variations and their interactions between the Black Sea and the Aegean Sea. Estuar Coast Shelf Sciences, 46, 609-619.

______ and Yaltýrak, C. 2002. Characteristic features of the North Anatolian Fault in the eastern Marmara region and its tectonic evolution. Marine Geology, 190(1-2), 329-350.

______, Altýnok, Y., Gazioðlu, C. and Yücel, Z.Y. 2003. Tsunami hazard assesment in Ýstanbul (Ýstan bul'da tsunami tehlikesinin deðerlendirilmesi). Turkish Journal of Marine Sciences, 9(1), 3-29.

______, Gazioðlu, C., Altýnok, Y., Yücel, Z.Y. and Cengiz, Þ. 2004. Tsunami hazard assessment in Ýstanbul using by high resolution satellite data (IKONOS) and DTM, XXth Congress International Society for Photogrammetry and Remote Sensing, 12- 23 July 2004, Ýstanbul. Commission TS, WG VII/5 (printed in CD).

Altýnok, Y. and Alpar, B. 2006. Marmara Island Earthquakes of 1265 and 1935; Turkey. Natural Hazards and Earth System Sciences, 6, 999-1006.

Ambraseys, N. N. 2002. The seismic activity of the Marmara Region over the last 2000 years. Bulletin of the Seismological Society of America, 92, 1-18.

______ and Finkel, C.F. 1991. Long-term seismicity of Ýstanbul and of the Marmara Sea region. Terra, Oxford, 3, 527-539.

Armijo, R., Meyer, B., Navarro, S. and King, G. 2002. Asymetric slip partitioning in the Sea of Marmara pull-apart: a clue to propagation processes of the North Anatolian Fault? Terra Nova, 13, 80-86.

______, Pondard, N., Meyer, B., Uçarkuþ, G., Mercier de Lepinay, B., Malavieille, J., Dominguez, S., Gustcher, M.A., Schmidt, S., Beck, C., Çaðatay, N., Çakýr, Z., Ýmren, C., Eris, K., Natalin, B., Özalaybey, S., Tolun, L., Lefevre, I., Seeber, L., Gasperini, L., Rangin, C., Emre, O. and Sarýkavak, K. 2005. Submarine Fault scarps in the Sea of Marmara pull-apart (North Anatolian Fault): implications for seismic hazard in Ýstanbul. Geochemistry, Geophysics and Geosystems, 6, 1-29.

Baþaran, S. 2002. Marmara Denizi'nde kütle hareketi kökenli depolarýn sedimentolojik özellikleri. Ýstanbul Üniversitesi Deniz Bilimleri ve Ýþletmeciliði Enstitüsü Yüksek Lisans Tezi 72 sayfa (unpublished).

Beck, C., Mercier de Lepinay, B., Schneider, J.-L., Cremer, M., Çaðatay, N., Wendenbaum, E., Boutareaud, S., Menot- Combes, G., Schmidt, S., Weber, O., Eriþ, K., Armijo, R., Meyer, B., Pondard, N., Gutcher, M.-A., Turon, J.L., Labeyrie, L., Cortijo, E., Gallet, Y., Bouquerel, H., Görür, N., Gervais, A., Castera, M.H., Londeix, L., de Resseguier, A. and Jaouen, A. 2007. Late Quaternary co-seismic sedimentation in the Sea of Marmara's deep basins. Sedimentary Geology, 199 (1-2), 65-89.

Beþiktepe, T., Sur, H. I., Özsoy, E., Latif, M. A., Oðuz, T. and Ünlüata, U. 1994. The circulation and hydrography of the Marmara Sea. Progress in Oceanography, 34, 285-334.

Bjerrum, L. 1971. Subaqueous slope failures in Norwegian fjords. Norwegian Geotechnical Institute Bulletin, 88, 1-8.

Bourry, C., Chazallon, B., Charlou, J. L., Donval, J. P., Ruffine, L., Henry, P., Geli, L., Çaðatay, M.N., Ýnan, S. and Moreau, M. 2009. Free gas and gas hydrates from the Sea of Marmara, Turkey Chemical and structural characterization. Chemical Geology, 264 (1-4),197-206.

Cita, M. B. and Rimoldi, B. 1997. Geological and geophysical evidence for the Holocene tsunami deposit in the eastern Mediterranean deep-sea record. Journal of Geodynamics, 24 (1-4), 293-304.

Cronan, D. S. and Hodkinson, R. A. 1997. Geochemistry of hydrothermal sediments from ODP Sites 834 and 835 in Lau Basin, Southwest Pasific. Marine Geology, 141, 237-268.

Çaðatay, N., Algan, A., Sakýnç, M., Eastoe, C., Ongan, D. and Caner, H. 1999. A Late Holocene sapropelic sediment unit from the southern Marmara shelf and its palaeoceanographic significance. Quaternary Geology Reviews,18, 531-540.

_____, Görür, N., Algan, A., Eastoe, C.J., Tchapalyga, A., Ongan, D., Kuhn, T. and Kuþçu, Ý 2000. Late Glacial-Holocene palaeoceanography of the Sea of Marmara: timing of connections with the Mediterranean and the Black Sea. Marine Geology, 167,191-206.

______,______, Polonia, A., Demirbað, E., Sakýnç, M., Cormier, M.-H, Capotondi, L., Mc Hugh, C, Emre, Ö. and Eriþ, K. 2003. Sea level changes and depositional environments in the Ýzmit Gulf, eastern Marmara Sea, during the Late glacial-Holocene period. Marine Geology, 202, 159-173.

DAMOC 1971. Master plan and feasibility report for water supply and sewerage for Istanbul region. Prepared by the DAMOC Consortium for WHO, Los Angeles, CA, vol. III, part II and III.

Demirbað, E., Rangin, C., Le Pichon, X. and Þengör, A. M. C 2003. Investigation of the tectonics of the main Marmara Fault by means of deep-towed seismic data. Tectonophysics, 361,1-19.

Druitt, T. H., Mellors, R. A., Pyle, D. M. and Sparks, R. S. J. 1989. Explosive volcanism on Santorini, Greece. Geological Magazýne,126 (2), 95-126.

Elmas, K. E., Algan, O., Öngen, Ö. Ý, Struck, U., Altenbach A. V., Saðular, E. K. and Nazik ., A 2008. Palaeoenvironmental investigation of sapropelic sediments from the Marmara Sea: A biostratigraphic approach to palaeoceanographic history during the Last Glacial-Holocene. Turkish Journal of Earth Sciences,17, 129-168.

Eriþ, K. K., Ryan, W. B. F., Çaðatay, M. N., Sancar, U., Lericolais, G., Ménot, G. and Bard, E., 2007. The timing and evolution of the post-glacial transgression across the Sea of Marmara shelf south of Ýstanbul. Marine Geology 243, 57-76.

Fairbanks, R. G. 1989. A 17,000 - year glacio-eustatic sea level record: influence of glacial melting rates on the Younger Dryas event and deep-ocean circulation. Nature, 342, 637-642.

Gamberi, F., Marani, M. and Savelli, C. 1997. Tectonic, volcanic and hydrothermal features of a submarine portion of the Aeolian arc (Tyrrhenian Sea). Marine Geology, 140, 167-181.

Gaudette, H.,Flight, W., Tanner, L. and Folger, D.W. 1974. An inexpensive titration method for the determination of organic carbon in recent sediments. Journal of Sedimentary Petrology, 44, 249-253.

Geli, L.,Henry, P. , Zitter, T., Dupre, S., Tryon, M., Çaðatay, M.N., Mercier de Lepinay B., Le Pichon, X. , Þengör , A. M. C., Görür, N., Natalin, B., Uçarkuþ, G., Özeren, S., Volker, D., Gasperini, L., Burnard, P. and Bourlange, S. 2008. The Marnaut Scientific Party, 2008. Gas emissions and active tectonics within the submerged section of the North Anatolian Fault zone in the Sea of Marmara. Earth and Planetary Science Letters, 274, 34-39.

Gökaþan, E., Alpar, B., Gazioðlu, C., Yücel, Z.Y., Tok, B., Doðan, E., and Güneysu, C. 2001. Active tectonics of the Ýzmit Gulf (NE Marmara Sea): from high resolution seismic and multi-beam bathymetry data. Marine Geology, 175 (1-4), 271-294.

______,Gazioðlu, C., Alpar, B., Yücel, Z. Y., Ersoy, Þ., Gündoðdu, O., Yaltýrak, C. and Tok, B. 2002. Evidences of NW extension of the North Anatolian Fault Zone in the Marmara Sea; a new approach to the 17 August 1999 Marmara Sea earthquake. Geo-Marine Letters, 21, 183 - 199.

Gökaþan, E., Ustaömer, T., Gazioðlu, C., Yücel, Z.Y., Öztürk, K., Tur, H., Ecevitoðlu, B. and Tok, B. 2003. Active tectonics of the Marmara Sea. Morphotectonic evolution of the Marmara Sea inferred from multi-beam bathymetric and seismic data. Geo-Marine Letters, 23(1),19-33.

_____, Algan, O., Tur, H., Meriç, E., Türker, A. and Þimþek, M. 2005. Delta formation at the southern entrance of Ýstanbul Strait (Marmara Sea, Turkey): a new interpretation based on high-resolution seismic stratigraphy. Geo-Marine Letters, 25, 370-377.

Gürbüz, C., Aktar, M., Eyidoðan, H., Cisternas, A., Haessler, H., Barka, A., Ergin, M., Türkelli, N., Polat, O., Üçer, S. B., Kuleli, S., Barýþ, S., Kaypak, B., Bekler, T., Zor, E., Biçmen, F. and Yöruk, A. 2000. The seismotectonics of the Marmara Region (Turkey): results from a microseismic experiment. Tectonophysics, 316, 1-17.

Halbach, P., Kuþçu, Ý., Kuhn, T., Pekdeðer, A. and Seifert, R. 2000. Methane in sediments of the deep Marmara Sea and its relation to local tectonic structures: NATO Advanced Research Seminar: integration of earth sciences research on the 1999 Turkish and Greek earthquakes and needs for future cooperative research seminar abstract book 74-75, 14-17 May 2000, Ýstanbul.

_____,_____, Inthorn, M., Kuhn, T., Pekdeðer A. and Seifert, R. 2002. Methane in sediments of the deep Marmara Sea and its relation to local tectonic structures. In: Görür, N., Papadopoulos, G. A., Okay, N. (eds) Integration of Earth Science Research on the Turkish and Greek 1999 Earthquakes. Kluwer Academic Publishers, The Netherlands, NATO Science Series, IV. Earth and Environmental Sciences, 9, 71-85.

Hampton, M. A. 1972. The role of subaqueous debris flow in generating turbidity currents: Journal of sedimentary Petrology, 42, 775-793.

_____, Lee, H. J. and Locat, J. 1996. Submarine landslides. Reviews of Geophysics, 34, 33-59.

Hebert, H.,Schindele, F., Altýnok, Y., Alpar, B. and Gazioðlu, C. 2005. Tsunami hazard in the Marmara Sea (Turkey): a numerical approach to discuss active faulting and impact on the Ýstanbul coastal areas. Marine Geology, 215, 23-43.

Hiscott, R. N. and Aksu, A. E. 2002. Late Quaternary history of the Marmara Sea and Black Sea from high-resolution seismic and gravity-core studies. Marine Geology, 190, 261-282.

Hodkinson, R. A. and Cronan, D. S. 1995. Hydrothermal sedimentation at ODP sites 834 and 835 in relation to crustal evolution of the Lau Backarc Basin. Ýn: Parson, L. M., Walker, C. L., Dixon, D. R., (Eds.), Hydrothermal vents and processes. The Geological Society of London, 87, 231-248

Ýmren, C., Le Pichon, X., Rangin, C., Demirbað, E., Ecevitoðlu, B. and Görür, N. 2001. The North Anatolian Fault within the Sea of Marmara: a new interpretation based on multi-channel seismic and multi-beam bathymetry data. Earth and Planetary Science Letters, 186, 143-158.

Johnson, A. M. 1970. Physical Processes in Geology: San Francisco (Freeman, Cooper and Co) Calif., 577 p.

Kaminski, M. A., Aksu, A., Box, M., Hiscott, R.N., Filipescu, S. and Alsalameen, M. 2002. Late glacial to Holocene benthic foraminifera in the Marmara Sea: implications for Black Sea-Mediterranean Sea connections following the last deglaciation. Marine Geology, 190, 165-202.

Kastens, K. A. and Cita, M. B.1981. Tsunami induced sediment transport in the Abyssal Mediterranean Sea, Bulletin of Geological Society of America, 92, 845-857.

Krauskopf, K. B. 1985. Introduction to geochemistry, 2nd edition Mc Grawhill. Singapare, 617 p.

Kuhn, T., Burger, H., Castrodori, D. and Halbach, P. 2000. Volcanic and hydrothermal history of ridge segments near the Rodrigues Triple Junction (Central Indian Ocean) deduced from sediment geochemistry. Marine Geology, 169, 391-409.

Kuþçu, I., Okamura, M, Matsuoka, H. and Awata, Y. 2002. Active faults in the Gulf of Izmit on the North Anatolian Fault, NW Turkey: a high-resolution shallow seismic study. Marine Geology, 190, 421-443.

______, ______,______, Gökaþan, E., Awata, Y., Tur, H. and Þimþek, M. 2005. Seafloor gas seeps and sediment failures triggered by the August 17, 1999 earthquake in the eastern part of the Gulf of Izmit, Sea of Marmara, NW, Turkey. Marine Geology, 215, 193-214.

______, Halbach P, Inthorn M., Kuhn T. and Seifert R. 2008. 5The R/V Meteor Cruise Leg M44/1 in February 1999 in the Sea of Marmara: The First Multibeam Bathymetric Study and Analysis of Methane in Sediment and Water Columns. Turkish Journal of Earth Sciences, 17, 461-480.

______, Okamura, M., Matsuoka, H., Yamamori, K., Awata, Y. and Özalp, S. 2009. Recognition of active faults and stepover geometry in Gemlik Bay, Sea of Marmara, NW Turkey. Marine Geology, 260, 90-101.

Kvenvolden, K. A. 1993. Gas Hydrates-Geological Perspective and Global Change. Reviews of Geophysics, 31, 173-187.

Le Pichon, X., Þengör, A. M. C., Demirbað, E., Rangin, C., Imren, C., Armijo, R., Görür, N., Çaðatay, N., Mercier de Le´pinay, B., Meyer, B., Saatçýlar, R. and Tok, B. 2001. The active main Marmara Fault. Earth and Planetary Science Letters, 192, 595-616.

Le Pichon, X., Chamot-Rooke, N., Rangin, C. ve Þengör, A. M. C. 2003. The North Anatolian Fault in the Sea of Marmara. Journal of Geophysical Research, 108 (B4), 2179.

Lee, H. J., Chough, S. K. and Yoon, S. H. 1996. Slope-stability change from Late Pleistocene to Holocene in the Ulleung Basin, East Sea (Japan Sea). Sedimentary Geology, 104, 39-51.

Loring, D. H. and Rantala, R.T.T. 1992. Manual for the geochemical analyses of marine sediments and suspended particulate matter. Earth-Science Reviews, 32, 235-283.

McClusky, S., Balassanian, S., Barka, A., Demir, C., Ergintav, S., Georgiev, I., Gurkan, O., Hamburger, M., Hurst, K., Kahle, H., Kastens, K., Kekelidze, G., King, R., Kotzev, V., Lenk, O., Mahmoud, S., Mishin, A., Nadariya, M., Ouzounis, A., Paradissis, D., Peter, Y., Prilepin, M., Reilinger, R., Sanli, I., Seeger, H., Tealeb, A., Toksöz, M. N. and Veis, G. 2000. Global positioning system constraints on plate kinematics and dynamics in the Eastern Mediterranean and Caucasus. Journal of Geophysical Research, 105, 5695-5719.

Mc Hugh, C.M.G., Seeber, L., Cormier, M.-H., Dutton, J., Çaðatay, M. N., Polonia, A., Ryan, W. B. F., and Görür, N. 2006. Submarine earthquake geology along the North Anatolia Fault in the Marmara Sea, Turkey: A model for transform basin sedimentation. Earth and Planetary Science Letters, 248 (3-4), 661-684.

______, Gurung D., Giosan L., Ryan W. B. F., Mart Y., Sancar U., Burckle L. and Çaðatay, M. N. 2008. The last reconnection of the Marmara Sea (Turkey) to the World Ocean: A paleoceanographic and paleoclimatic perspective. Marine Geology, 255, 64-82.

Meade, B. J., Hager, B. H., McClusky, S. C., Reilinger, R. E., Ergintav, S., Lenk, O., Barka, A. and Özener, H. 2002. Estimates of seismic potential in the Marmara Sea region from block models of secular deformation constrained by global positioning system measurements. Bulletin of the Seismological Society of America, 92 (1), 208-215.

Meriç, E, Yanko, V. and Avþar, N., 1995. Ýzmit Körfezi (Hersek Burnu-Kaba Burun) Kuvaterner istifinin foraminifer faunasý. Ýzmit Körfezi Kuvaterner Ýstifi, (Ed. Meriç, E.), 105-151, Ýstanbul.

_____ and Suner, F., 1995. Ýzmit Körfezi (Hersek Burnu-Kaba Burun) Kuvaterner istifinde gözlenen termal veriler. Ýzmit Körfezi Kuvaterner istifi (Ed. E. Meriç), 81-90, Ýstanbul.

Middleton, G. V. and Hampton, M. A., 1973. Sediment gravity flows: mechanics of flow and deposition. In: Middleton, G. V., Bouma. A. H. (Eds.), Turbidites and Deep - Water Sedimentation. Pacific section Society of Economic Paleontologists and Mineralogists, Los Angeles CA, 1-38.

Newman, K. R., 2003. Using Submerged Shorelines to Constrain Recent Tectonics in the Marmara Sea, Northwestern Turkey, Department of Geology, Senior Thesis, Smith College 49 p (unpuldished).

Okay, A. I., Kaþlýlar-Özcan, A., Ýmren, C., Boztepe-Güney, A., Demirbað, E., and Kuþçu, Ý, 2000. Active faults and evolving stike-slip basins in the Marmara Sea, northwest Turkey: a multi-channel seismic reflection study. Tectonophsics, 321, 189-218.

Patzold, J., Halbach, P. E., Hempel, G. and Weikert, H., 2000. Ostliches Mittelmeer-Nordliches Rotes Meer 1999. Cruise No. 44, 22 January-16 May 1999. Meteor Berichte 00-3, Universitat Hamburg, 240 p.

Polonia, A., Cormier, M. H., Çaðatay, N., Bortoluzzi, G., Bonatti, E., Gasperini, L., Seeber, L., Görür, N., Capotondi, L., Mc Hugh, C., Ryan, W. B.F., Emre, Ö., Okay, N., Ligi, M., Tok, B., Blasi, A., Busetti, M., Eriþ, K., Fabretti, P., Fielding, E. J., Ýmren, C., Kurt, H., Magagnoli, A., Morazzi, G., Özer, N., Penitenti, D., Serpi, G. and Sarýkavak, K. 2002. Exploring submarine Earthquake Geology in the Marmara Sea. Eos, Transactýons. American Geophysical Union, 83 (21), 235-236.

Polonia, A., Gasperini, L., Amorosi, A., Bonatti, E., Bortoluzzi, G., Çaðatay, M. N., Capotondi, L., Cormier, M. H., Görür, N., Mc Hugh, C. M. G. and Seeber, L. 2004. Holoceneslip rate of the North Anatolian Fault beneath the Sea of Marmara. Earth and Planetary Science Letters, 227, 411-426.

Rangin, C., Demirbað, E., Ýmren, C., Crusson, A., Normand, A., Le Drezen, E. and Le Bot, A. 2001. Marine Atlas of the Sea of Marmara (Turkey). 11 plates and 1 booklet. Special publication (ISBN 2-84433-068-1) by IFREMER Technology Center, Brest, France.

_____, Le Pichon, X., Demirbað, E. and Ýmren, C. 2004. Strain localization in the Sea of Marmara: propagation of the North Anatolian Fault in a now inactive pull-apart. Tectonics, 23, 1-18.

Sarý E., 2004. The seaching of the fault activity by sediment geochemistry and sedimentology methods in the east of Marmara Sea. Ýstanbul Üniversitesi Deniz Bilimleri ve Ýþletmeciliði Enstitüsü Doktora Tezi, 166 sayfa (unpublished).

_____ and Çaðatay N. 2006. Turbidites and their association with past earthquakes in the deep Çýnarcýk Basin of the Marmara Sea. Geo-Marine Letters, 26, 69-76.

Shanmugam, G., Bloch, R. B., Mitchell, S. M., Beamish, G. W. J., Hodgkinson, R. J., Damuth, J. E., Straume, T., Syvertsen, S. E. and Shields, K. E. 1995. Basin - floor fans in the North Sea: sequence - stratigraphic models vs. sedimentary facies. American Association of Petroleum Geologists Bulletin, 79, 477-512.

Siani, G., Paterne, M., Arnold, M., Bard, E., Metivier, B., Tisnerat, N. and Bassinot, F. 2000. Radiocarbon reservoir ages in the Mediterranean Sea and Black Sea. Radiocarbon, 42, 271-280.

Stuiver, M. and Braziunus, T., 2003. Modelling atmospheric 14C influences and 14C ages of Marine Samples to 10,000 B.C. Radiocarbon, 35, 215-230.

Tessier, A., Cambell, P.G.C. and Bisson, M. 1979. Sequential extraction procedure for the speciation of particulate trace metals. Analytical Chemistry, 51, 844-850.

Tinti, S., Armigliato, A., Manucci, A., Pagnoni, G., Zaniboni, F., Yalçýner, A.C and Altýnok, Y. 2006. The generating mechanisms of the August 17, 1999 Ýzmit Bay (Turkey) tsunami: Regional (tectonic) and local (mass instabilities) causes. Marine Geology, 225, 311-330.

Tolun, L., Çaðatay, N. and Carrigan, W. J. 2002. Organic Geochemistry and Origin of Late Glacial-Holocene Sapropelic Layers and Associated Sediments in Marmara Sea. Marine Geology, 190, 47-60.

Ünlüata, Ü., Oðuz, T., Latif, M. A. and Özsoy, E. 1990. On the physical oceanography of the Turkish Straits. In: The Physical Oceanography of Sea Straits Pratt, L.J. (Ed.) NATO/ASI Series, Kluwer, Dordrecht, 25-60.

Wisenam, W. J. Jr., Fan, Y. B., Bornhold, B.D., Keller, G.H., Su, Z. Q., Prior, D. B., Yu, Z. X., Wright, L. D., Wang, F. Q. and Quian, Q. Y. 1986. Suspended sediment advection by tidal currents off the Huanghe (Yellow River) delta. Geo-Marine Letters, 6, 107-113.

Yaltýrak, C. 2002. Tectonic evolution of the Marmara Sea and its surroundings. Marine Geology, 190(1-2), 493-529.

Zitter, T.A.C.,. Henry, P., Aloisi, G., Delaygue, G., Çaðatay, M.N., Mercier de Lepinay B., Al-Samir, M., Fornacciari, F., Tesmer, M., Pekdeðer, A., Wallmann, K. and Lericolais, G. 2008. Cold seeps along the main Marmara Fault in the Sea of Marmara Turkey. Deep-Sea Research I, 55, 552-570.

Mineral Res. Expl. Bull., 140, 19-34, 2010

INVESTIGATIONS OF ALTERATION ZONES BASED ON FLUID INCLUSION MICROTHERMOMETRY AT SUNGUN PORPHYRY COPPER DEPOSIT, NW IRAN

Omid ASGHARI* and Ardeshir HEZARKHANI**

ABSTRACT.- The Sungun porphyry copper deposit is located in East Azerbaijan, NW of Iran. The porphyries occur as stocks and dikes ranging in composition from quartz monzodiorite to quartz monzonite. Four types of hypogene alteration are developed; potassic, phyllic, propylitic and argillic. Three types of fluid inclusions are typically observed at Sungun; (1) vapor-rich, (2) liquid-rich and (3) multi-phase. Halite is the principal solid phase in the latter. The primary multiphase inclusions within the quartz crystals were chosen for micro-thermometric analyses and considered to calculate the geological pressure and hydrothermal fluid density. In potassic zone, the average of homogenization temperature is 413.6 °C while in phyllic alteration, 375.9 °C. As expected in potassic alteration, the temperature of hydrothermal solutions is higher than that in phyllic zone. The salinity of the hydrothermal fluids has a high coherency with homogenization temperature, so the average of salinity in potassic samples is 46.3 (wt% NaCl) which is higher than phyllic samples. Based on the location of potassic alteration, as expected, the lithostatic pressure is much more than the phyllic one. Finally, the average density of hydrothermal fluids in the potassically altered samples is 1.124 (gr/cm^3) which is higher than the ones in phyllic zone (1.083 gr/cm^3).

Key words: Fluid Inclusion, Porphyry copper deposit, Potassic alteration, Phyllic alteration, Microthermometry, Sungun, Íran.

INTRODUCTION

Porphyry Copper deposits are generated where magmatic - hydrothermal fluids are expelled from a crystallizing magma (Burnham, 1979; Ulrich et al. 2001). Cooling, depressurization, and reaction between the fluids and the wall rocks cause metals to precipitate in and around the fractures, forming veins with alteration envelopes. Alteration assemblages and associated mineralization in porphyry ore deposits develop from huge hydrothermal systems dominated by magmatic and meteoric fluids (Sillitoe 1997; Hedenquist and Richards 1998). These systems develop in and adjacent to subvolcanic porphyritic intrusions that are apophyses of deeper-seated magma bodies (Dilles and Einaudi 1992; Sillitoe and Hedenquist 2003; Heinrich et al. 2003). Fluid inclusion analyses indicate that, the inclusions which are trapped in porphyry Cu deposits, typically include halite-saturated brines and low-salinity vapor inclusions (Nash, 1976; Roedder, 1984; Beane and Bodnar, 1995; Tosdal and Richards 2001; Heinrich, 2005). The formation of brine and vapor are inferred to result from a miscibility gap in the $NaCl-H_2O$ system that coincides with the pressure (< 2200 bars) and temperature (300 to 600°C) where most porphyry Cu deposits form (Sourirajan and Kennedy, 1962; Urusova, 1975; Roedder and Bodnar 1980; Beane and Bodnar, 1995; Kehayov et al. 2003).

Fluid inclusion studies in porphyry copper deposits (PCDs) have proven to be an important tool to constrain the physico-chemical conditions of the hydrothermal fluids responsible for vast and pervasive alteration and mineralization processes. These fluid inclusion studies have shown many common features in such deposits throughout the world (Nash, 1976; Chivas and Wilkins, 1977; Beane and Titley, 1981; Roedder, 1984; Quan et al., 1987; Beane and Bodnar, 1995; Ulrich et al. 2001; Redmond et al. 2004).

* Department of Mining Engineering, University of Kashan, Kashan, I.R.Iran (E-mail: O.asghari@aut.ac.ir)
** Department of Mining and Metallurgy Engineering, Amirkabir University of Technology, Tehran, Iran. (E-mail: ardehez@aut.ac.ir).

At Sungun deposit, numerous cross-cutting quartz veinlets and micro-veinlets, developed in various stages of alteration and mineralization, provided suitable material for fluid inclusion investigations. Etminan (1977) was the first to recognize the presence of porphyry-type copper mineralization at Sungun through fluid inclusion studies. Based upon systematic sub-surface sampling, more detailed studies of fluid inclusions were carried out by Mehrpartou (1993) and Calagari (1997, 2004) and comprehensive micro thermometric data were accumulated. Additional fluid inclusion work on the Sungun PCD was presented by Hezarkhani and Williams-Jones (1998), Hezarkhani (2006).

In this research, it will be illustrated the differences between potassic and phyllic alterations based on fluid inclusion data. As expected, all variables such as homogenization temperature, salinity, pressure and density have higher average values in potassic than phyllic, but as will be described in this research, none of the parameters achieved from microthermometry of fluid inclusions, individually can lead to discriminate the potassic from the phyllic alteration.

GEOLOGICAL SETTING

The Sungun porphyry copper deposit is hosted by a diorite/granodiorite to monzonite/quartz-monzonite stock (Mehrpartou, 1993), located 75 km northwest of Ahar in the Azarbaijan province of northwest Iran (Figure 1). The stock is a part of the Sahand-Bazman igneous and metallogenic belt (northern Iran), a deeply eroded Tertiary volcanic field, roughly 100 by 1700 km in extent (from Turkey to Baluchistan in southern Iran), consisting mainly of rhyolite and andesite, with numerous felsic intrusions.

The Sungun porphyries intruded into Upper Cretaceous carbonate rocks, a series of Eocene arenaceous-argillaceous rocks, and a series of Oligocene dacitic breccias, tuffs and trachy-andesitic lavas (Emami and Babakhani, 1991; Mehrpartou, 1993, Hezarkhani, 2006). The Sungun porphyries, which contain >500 Mt of sulfide reserves, grading 0.76 percent Cu and ~0.01 percent Mo, occur as stocks and dikes, and are series of calc-alkaline igneous rocks with a typical porphyritic texture (Hezarkhani and Williams-Jones 1998). They are situated at the northwestern part of a NW-SE trending Cenozoic magmatic belt (Sahand-Bazman) where the Sarcheshmeh PCD is also located. The Sungun stocks are divided into two groups: Porphyry Stock I is typically quartz monzodiorite where as Porphyry Stock II (which is investigated in this research) hosts the Sungun PCD and varies in composition from quartz monzonite through granodiorite to granite. Four series of cross-cutting dikes varying in composition from quartz monzodiorite to granodiorite, cut the Sungun stocks.

HYDROTHERMAL ALTERATION AND MINERALIZATION

Alteration assemblages and related mineralization in the Sungun porphyry copper deposit have been investigated by geological mapping and detailed mineralogical, petrographical and chemical studies of a large number of drill cores and outcrop samples from various parts of the stock (Figure 2). Hydrothermal alteration and mineralization at Sungun are centered on the stock and were broadly synchronous with its emplacement. Early hydrothermal alteration was dominantly potassic and propylitic, and was followed by later phyllic and argillic alteration.

Potassic alteration

The earliest alteration is represented by potassic mineral assemblages developed pervasively and as halos around veins in the deep and central parts of the Sungun stock (Hezarkhani et al. 1999). Potassic alteration is characterized by K feldspar. This alteration displays a close spatial association with mineralization, perhaps as much as 60 percent of the copper and all the molybde-

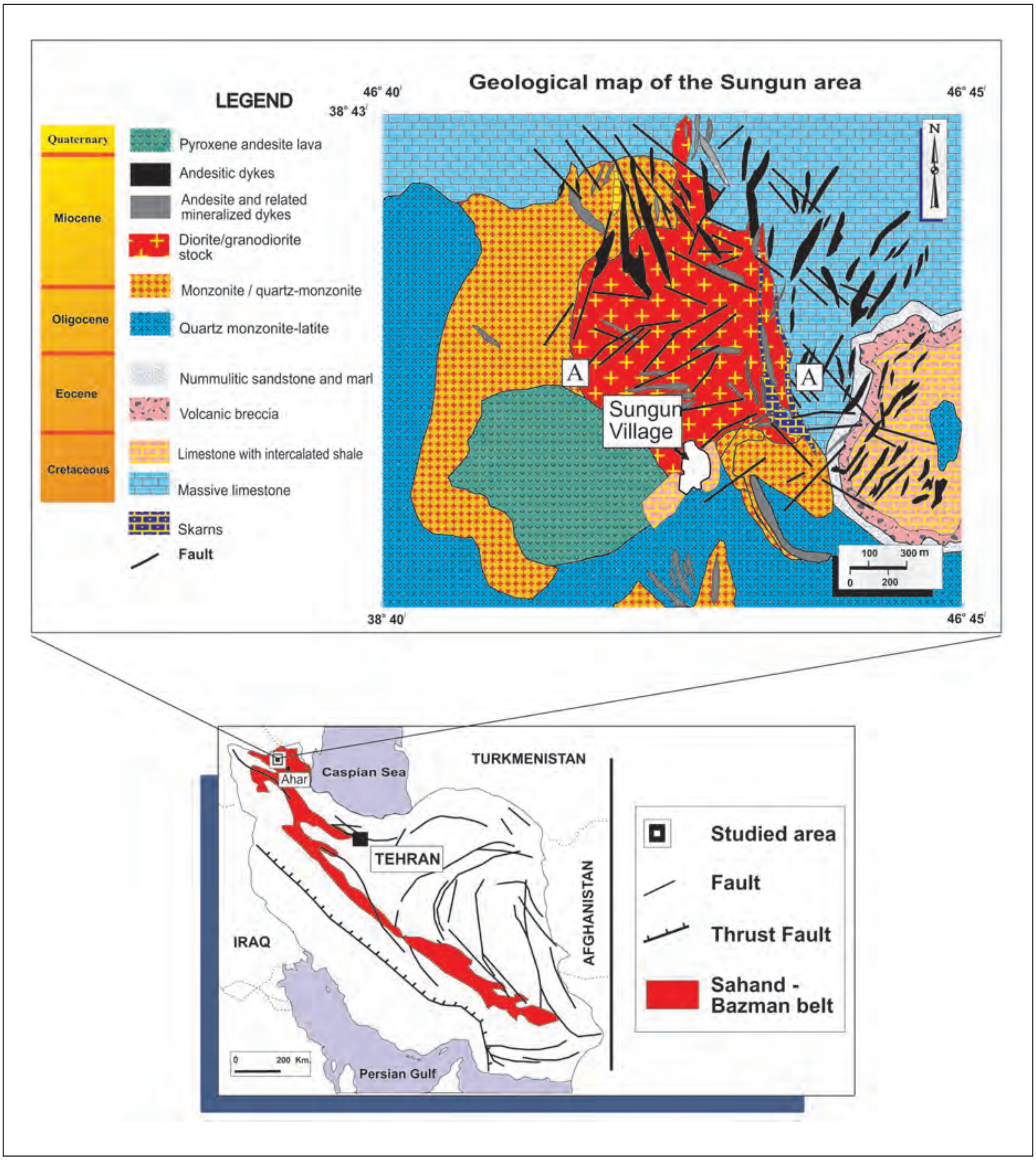

Figure 1- Below: Geological map of Iran showing Sahand-Bazman belt (modified from: Stocklin, 1976; Shahabpour, 2007); Above: Geological map of Sungun deposit area showing various types of intrusive rocks of dominantly Miosene ege and the outline of Cu-Mo porphyry type mineralizations. (Modified from Mehrparton, 1993 and Hezarkhani, 2006).

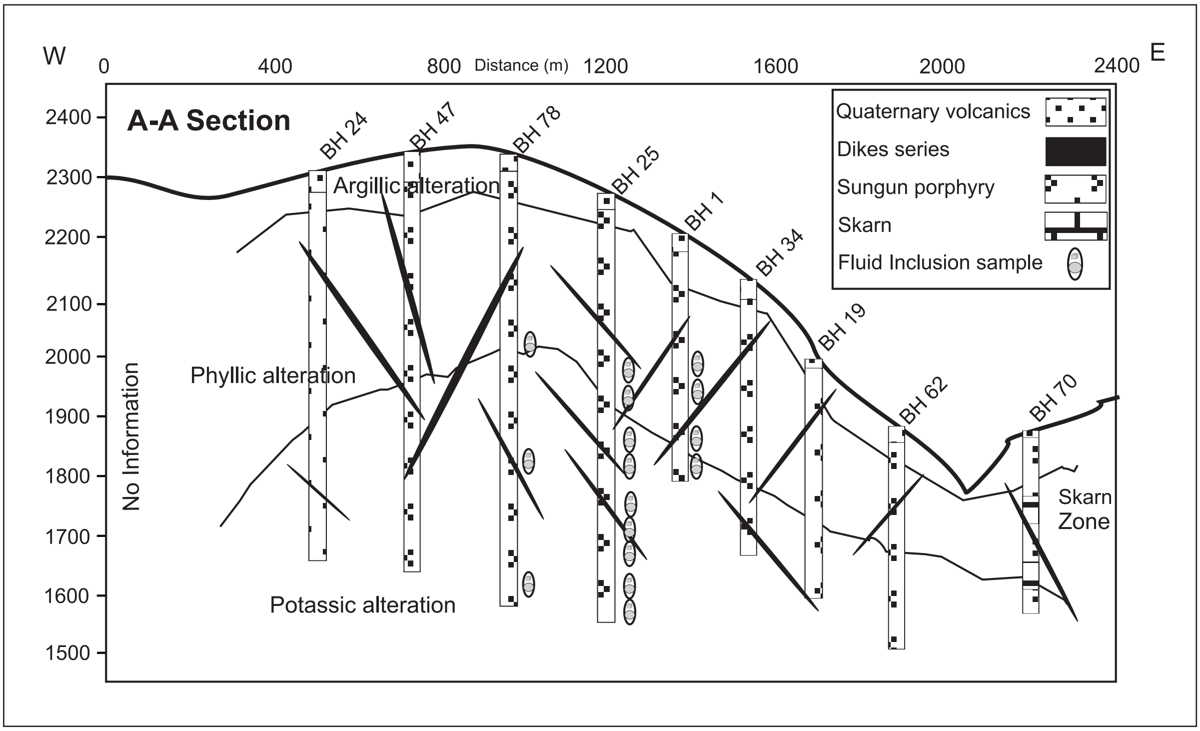

Figure 2- Profile along A-A in Figure 1 illustrating the position of diamond drill holes, dike series, and the pattern of hypogene alteration zones (potassici phyllic and argillic) in Porphyry Stock II.

num deposits were emplaced during this alteration episode (Hezarkhani and Williams-Jones 1998). On average, potassically altered rocks contain 28 percent plagioclase, 33 percent orthoclase, 20 percent quartz, 15 percent ferromagnesian minerals (mainly biotite, and sericite and chlorite after biotite) and 4 percent chalcopyrite, pyrite, zircon, scheelite, uraninite, bismuthinite, and rutile (Hezarkhani, 2006) (Figure 3a and plate 1a-1c).

Phyllic alteration

The change from transition alteration to phyllic alteration is gradual and is marked by an increase in the proportion of muscovite. Phyllic alteration is characterized by the replacement of almost all rock-forming silicates by sericite and quartz and overprints the earlier formed potassic and transition zones. Pyrite forms up to 5 vol. percent of the rock and occurs in veins and disseminations. Quartz veins are surrounded by weak sericitic halos (Plate 1d). Vein-hosted pyrite is partially replaced by chalcopyrite. Silicification was synchronous with phyllic alteration and variably affected a large part of the stock and most dikes. This observation is supported by whole-rock chemical analyses, which show that Si was added in, higher than for any other stage of the alteration (Hezarkhani and Williams-Jones 1998). In contrast to the transition zone, appreciable Cu was added to the rock during phyllic alteration. It is difficult to separate transition and phyllic alteration zones because of intense silicification during the latter alteration (Figure 3a).

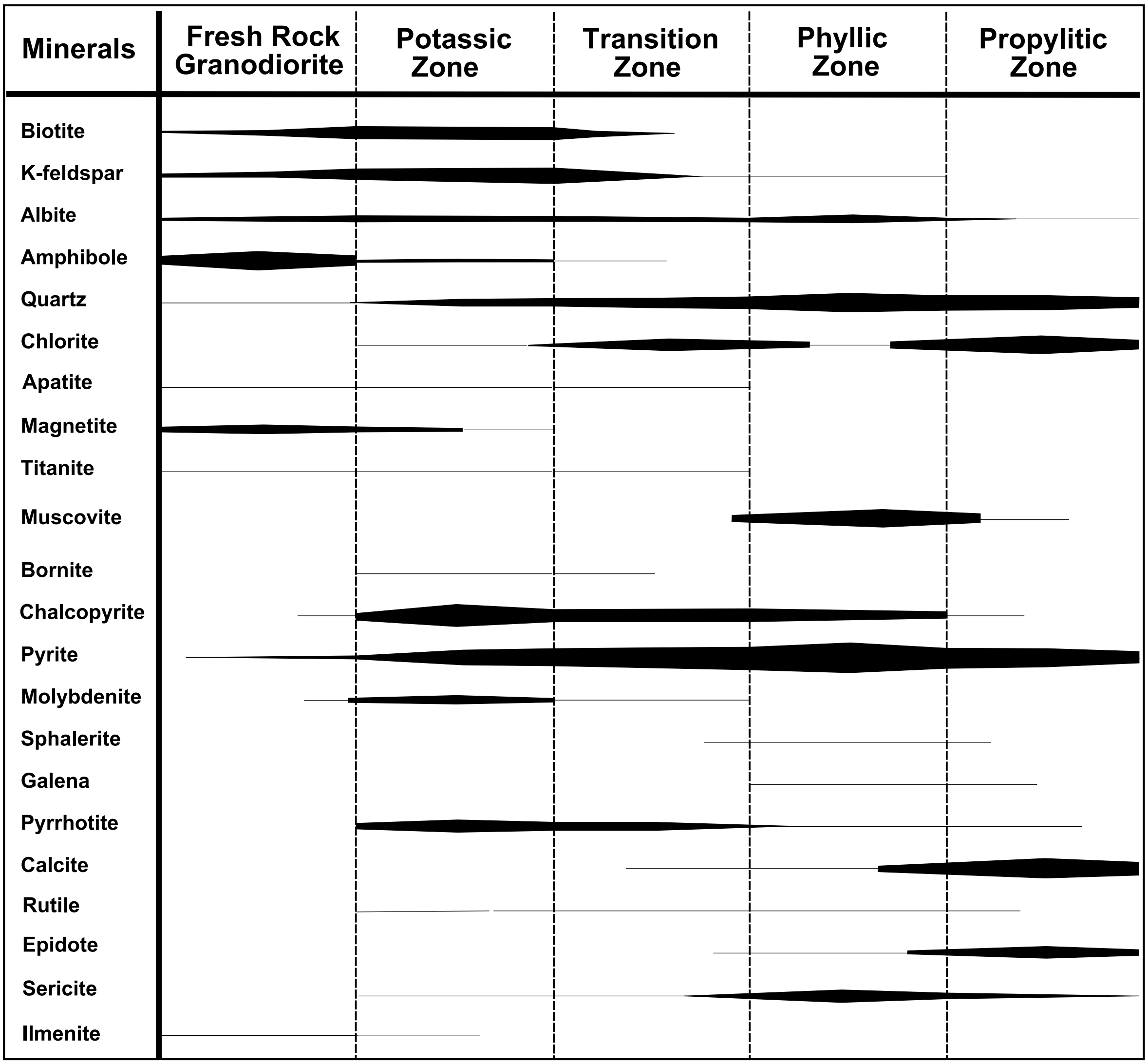

Figure 3a- Paragenetic sequence of the develpment of various alterations in porphyry stock II at Sungun. The thickness of the horizantal bars is related to the relative abundance of the mineral in the porphyry system (Hezarkhani and Williams-Jones, 1998; Calagari, 2004).

Mineralization

Hypogene copper mineralization was introduced during potassic and phyllic alteration, and exists as disseminations and veinlets form. During potassic alteration, the copper mineralization consisted of chalcopyrite and minor bornite; later hypogene copper mineralization consisted mainly of chalcopyrite (Plate 1e, 1f).

Alteration of feldspars and biotite (from potassically altered rocks) was accompanied by an increase in sulphide content outward from the central part of the stock. Copper mineralization increases toward the margins of the central potassic zone, from less than 0.20 wt % to 0.85 wt%. There is also a positive correlation between silicification and copper mineralization. The maximum Cu grade is associated with biotite, orthoclase and sericite (potassic zone) while the pyrite content is highest (3-10 vol % of the rock) in the marginal quartz-sericite (phyllic) zone. The ratio of pyrite to chalcopyrite in the zone of richest hypogene copper mineralization seen in the potassic alteration zone is as low as 4:1, but toward the margins of the stock, the ratio increases to 15:1.

FLUID INCLUSIONS PETROGRAPHY

The Sungun deposit contains well-developed stockwork mineralization that is concentrated in the potassic and transition zones (the transition zone is actually the outermost part of the potassic zone and is characterized by a low content of biotite and abundant sericitization). Based on mineralogy and cross-cutting relationships, it is possible to distinguish four main groups of veins representing four episodes of vein formation: 1) quartz + molybdenite + anhydrite ± K-feldspar with sporadic pyrite, chalcopyrite and bornite, II) quartz + chalcopyrite + pyrite ± molybdenite, III) quartz + pyrite + calcite ± chalcopyrite + anhydrite (gypsum) + molybdenite, IV) quartz, and/or calcite, and/or gypsum ± pyrite (Figure 3b).

Fluid inclusions are abundant in quartz of all vein types, and range in diameter from 1µm up to 15 µm. The majority of inclusions examined during this study had diameters of 4 12 µm. Only fluid inclusions within the quartz crystals in quartz-sulfide and quartz-molybdenite veinlets were chosen for micro-thermometric analyses for two important reasons: (1) the inclusions are intimately associated with copper and molybdenum sulfides, (2) these veinlets contain inclusions >7µm which allows for more confident thermometric analysis. The individual quartz crystals contain numerous cross-cutting microfractures along which fluid inclusions are aligned (Plate 2a).

Since hydrothermal quartz, in the very early veins (Group I), was generally too fine grained to host fluid inclusions of sufficient size for study, most of the observations were restricted to fluid inclusions in coarse-grained quartz of early mineralized veins (Group II) and later quartz-anhydrite-pyrite veins (Group III). A preliminary classification of fluid inclusions was carried out based on the number, nature and relative proportions of phases at room temperature and led to recognition of the following types of fluid inclusions:

LV inclusions consist of liquid + vapor ± solid phases with the liquid phase volumetrically dominant. These fluid inclusions are common in all mineralized quartz veins and are abundant in Group II and III veins (Plate 2b). The diameters of these fluid inclusions ranges from 3 to 12 µm. LV inclusions are found in all vein groups, but occur in variable proportions. They are most abundant in the Group II and III veins, and rare in Group I veins. Most LV inclusions are distributed along healed fractures, and are of secondary origin.

VL inclusions are found in quartz phenocrysts from fresh rocks and in Group I, II and III quartz veins. Some of these inclusions occur in growth zones in Group I and II quartz veins, where they are accompanied by LVH fluid inclusions, indicating that most of them are primary. VL inclusions are generally elongated and have rounded ends, but some have negative crystal shapes. Some of the VL inclusions have variable liquid-vapor ratios, and may have formed from the necking down of LVH inclusions or heterogeneous entrapment of liquid and vapur.

LVH inclusions are found in all veins, from the deepest, potassically altered part of the stock

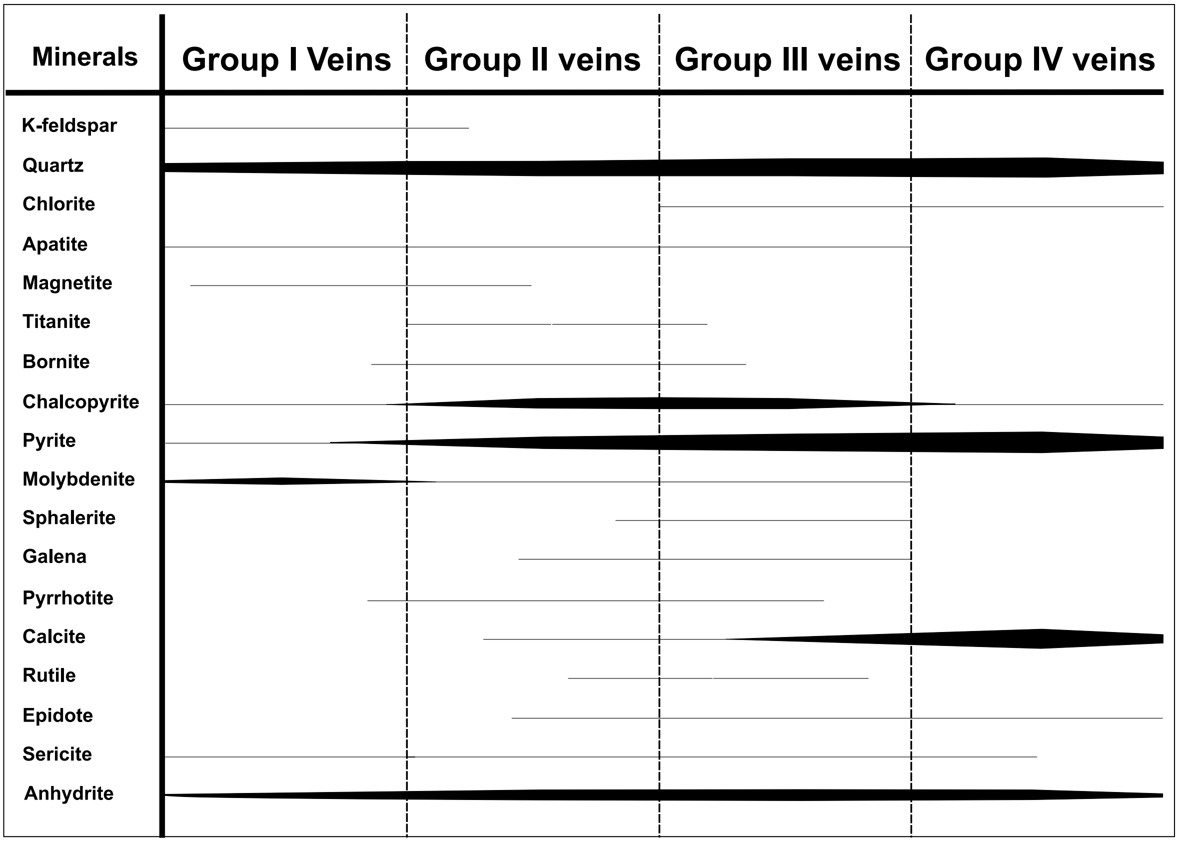

Figure 3b- Relative mineral abundances in various veins and veinlets in the Sungun deposit. Widths of bars denote qualitative abundances (Hezarkhani and Williams-Jones, 1998; Calagari, 2004).

through to the shallow level veins (Plate 2c, 2d). The fluids occupy cavities ranging from 1 µm to 15 µm in diameter. The coexistence of LVH inclusions and vapor-rich inclusions with consistent phase ratios in the growth zones of quartz grains, from potassic and phyllic alteration zones suggests a primary origin, and coexistence of two immiscible aqueous fluids.

The majority of LVH inclusions examined during this study had diameters of 4-12 µm. The 47 sub-surface samples containing quartz veinlets from diamond drill holes within the hypogene alteration zones in Porphyry Stock II, were selected for thermometric analyses.

FLUID INCLUSION INVESTIGATIONS

The samples were initially prepared for microscopic examination. Based on mineral content, the type of alteration is found and they are categorized as potassic and phyllic. The distribution pattern, shape, size, and phase content of fluid inclusions within the quartz crystals were examined applying a microscope (Table 1). Based upon their phase content, three types of inclusion are present at Sungun: (1) vapor-rich 2-phase, (2) liquid-rich 2-phase, and (3) multi-phase solid. Halite crystals are larger than the other solids and can be readily distinguished by their cubic shape. Similar characteristics are seen in fluid inclusion assemblages from other PCDs such as

Table 1- Statistical parameters of raw data based on fluid inclusion study and micro thermometry for 645 measurements in 47 samples totally and for high salinity inclusions (more than 27 wt% NaCl).

Type	Statistical	Salinity %	T_H	T_m	T_e (°C)	Size(μm^2)	L/V
High and Low Salinity	Mean	23.9	355	-7.5	-38	22.4	2.9
	Standard	18.7	93	5.5	11.7	10.4	2.7
	Variance	348	8586	30.3	138	109	7.1
	Minumum	0.2	88	-33	-67	6	0.1
	Maximum	65.5	620	-0.5	-4	70	19
High and Low Salinity	Mean	43	375	-11.6	-46.9	24.5	3.4
	Standard	7.6	82	6.4	9.1	12.4	2.1
	Variance	57	6664	40.3	82.5	154	4.3
	Minumum	29	176	-33	-67.4	8	0.3
	Maximum	65.5	600	-1.2	-26	70	9

El Salvador, Chile (Gustafson and Hunt, 1975), Santa Rita, New Mexico (Ahmad and Rose, 1980), Bingham, Utah (Roedder, 1971), Yandera and Panguna, Papua New Guinea (Watmuff, 1978; Eastoe, 1978), Copper Canyon, Nevada (Nash, 1976), Bajo de la Alumbrera and Argentina (Ulrich et al., 2001).

a- Micro-thermometric analysis

The Linkam operating unit was applied to measure the temperatures of phase changes in fluid inclusions, which operates by passing pre-heated or pre-cooled N_2 gas around the sample (Werre et al., 1979). Stage calibration was performed using synthetic and/or well-known fluid inclusions. Accuracy at the standard reference temperatures was ±0.2°C at -56.6°C (triple point of CO_2), ±0.1°C at 0°C (melting point of ice), ±2°C at 374.1°C (critical homogenization of H_2O), and ±9°C at 573°C (alpha to beta quartz transition). The heating rate was approximately 1°C/min near the temperatures of phase transitions. Thermometric analyses were performed principally on fluid inclusions which were relatively large (>7 µm). Freezing and heating experiments helped to determine the approximate salinity (wt% NaCl equivalent) and homogenization temperature (T_h); respectively (Table 1). The heating stage was used for all types of inclusion. For non-halite bearing inclusions the homogenization temperature of liquid and vapor (either L+V → L or L+V → V) was recorded. In the halite-bearing inclusions, two points: (1) $T_{s(NaCl)}$ (the temperature at which halite dissolves) and (2) $T_{h(L-V)}$ (temperature of vapor and liquid homogenization) were recorded.

b- Homogenization temperatures

The temperatures of initial (T_e) and final melting of ice ($T_{m\ ice}$) were measured on types LV, VL, and LVH fluid inclusions. The temperature of initial ice melting (T_e) of most LV fluid inclusions were between -23° and -24°C, suggesting that NaCl is the principal salts in solution. The T_e value of VL fluid inclusions ranges from - 20° to -46°C with a mode of ~-22°C, suggesting that Na and K are the dominant cations in the solution, but there may be other components for example Mg and Ca which could not be measurable by this method. The low T_e (-31°C to -46°C) for some of the VL inclusions could indicate that these inclusions are the products of necking down of LVH inclusions.

The eutectic temperatures that could be measured in LVH inclusions range from -30° to -64°C, suggesting important concentrations of Fe, Mg, Ca, and/or other components in addition to Na and K in this type of inclusion. The $T_{m\ ice}$ values for LV inclusions range from -5° to -8°C, corresponding to salinities of 5.7 wt% NaCl equivalent respectively (Sterner et al., 1988). The $T_{m\ ice}$ value for VL inclusions varies from -0.4°C to -12°C, which corresponds to a salinity of between 0.8 and 12.2 wt% NaCl equivalent.

LV fluid inclusions homogenize to liquid T_h (L+V → L) at temperatures between 523° and 298°C. Most of VL inclusions homogenize to vapor T_h (V+L → V) between 351° and 600 (°C). The frequency distribution of halite-bearing inclusions homogenizing by halite disappearance ($T_{s(NaCl)} > T_{H(L-V)}$) display a wide range of $T_{s(NaCl)}$ values, varying from 220 to 583 (°C). Salinities based on the halite dissolution tempe-rature range from 29.7 to 61.1 wt % NaCl equivalent (Table 2).

The halite-bearing inclusions homogenizing by simultaneous disappearance of halite vapor and/or by vapor disappearance ($T_{s(NaCl)} \leq T_{H(L-V)}$) show a similar range of distribution and their $T_{H(L-V)}$ values vary from 200 to 580 (°C). Some LVH inclusions homogenized by vapor disappearance and by contrast, some LVH inclusions homogenized mainly by halite dissolution. Anhydrite and chalcopyrite did not dissolve on heating to temperatures in excess of 600°C. Chalcopyrite was identified on the basis of its optical characteristics (opacity and triangular cross section) and composition in opened inclusions (SEM-EDAX analyses yielded peaks for Cu, Fe and S). Anhydrite forms transparent anisotropic prisms and was shown by SEM-EDAX analyses to consist only of Ca and S (elements lighter than F could not be analyzed) (Hezarkhani and Williams-jones, 1998).

Table 2- Descriptive statistics of primary inclusion's data for high salinity inclusions (more than 27 wt% NaCl).

Statistical parameter	Salinity	T_h	T_m	T_e	Size(μm^2)	L/V Ratio
Mean	43	375	-11.6	-46.9	24.5	3.4
Standard Deviation	7.6	82	6.4	9.1	12.4	2.1
Sample Variance	57	6664	40.3	82.5	154	4.3
Minimum	29.7	220	-33	-67.4	8	0.3
Maximum	61.1	583	-1.2	-26	70	9

c- Salinity of the inclusion fluids

Halite-bearing and non-halite-bearing liquid-rich inclusions at Sungun, exhibit a wide variation in salinity, ranging from 0.2 to 65.5 wt% (Figure 4). There are many halite-bearing fluid inclusions which have $T_{s(NaCl)} > T_{H(L-V)}$ and the discrepancy between $T_{s(NaCl)}$ and $T_{H(L-V)}$ in some inclusions may reach ~98 °C (Figure 5). These inclusions may suggest entrapment of supersaturated (with respect to NaCl) fluid or high pressure conditions of entrapment (Table 3, No. 12). However, there are still many halite-bearing inclusions whose data points lie around and below the halite saturation curve ($T_{s(NaCl)} < T_{H(L-V)}$) (Figure 5) which, in turn, denotes trapping of saturated and under saturated fluids, respectively.

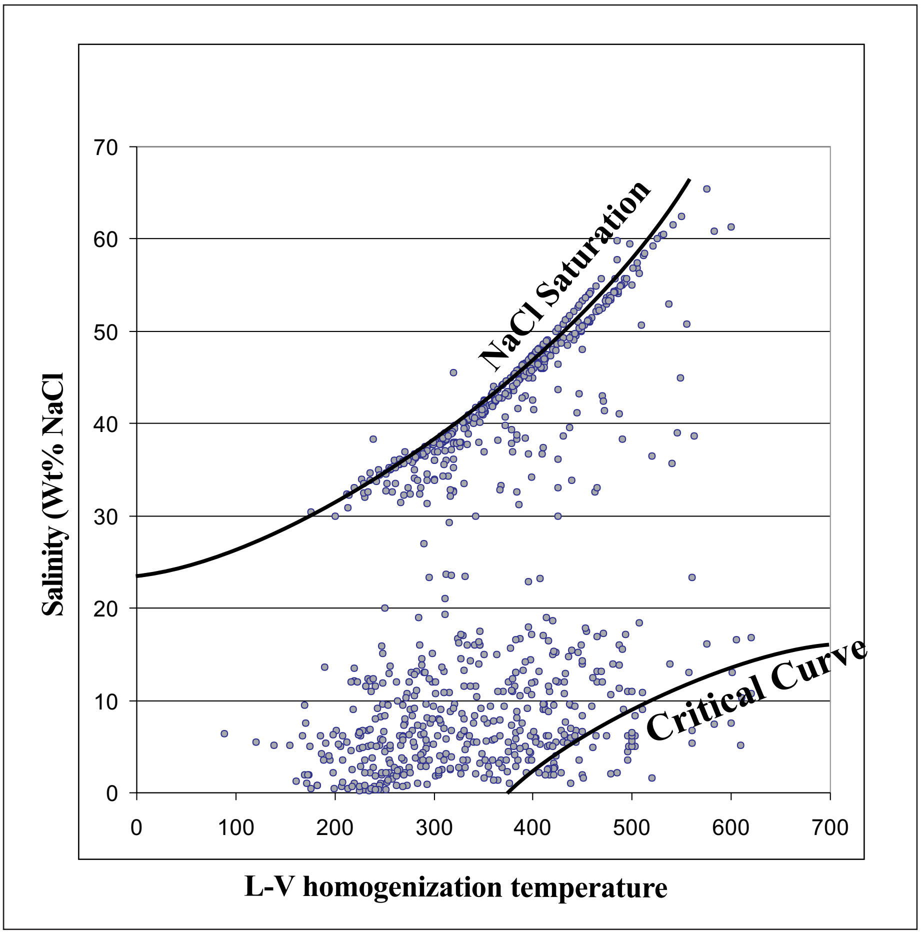

Figure 4- Salinity versus $T_{H(L-V)}$ illustrating the distribution pattern of the data points relative to the NaCl saturation and critical curves (NaCl saturation and critical curves from Cloke and Kesler, 1979). Dashed lines referring to vapor of NaCl solutions at the indicated temperatures and salinity (from Roedder, 1984).

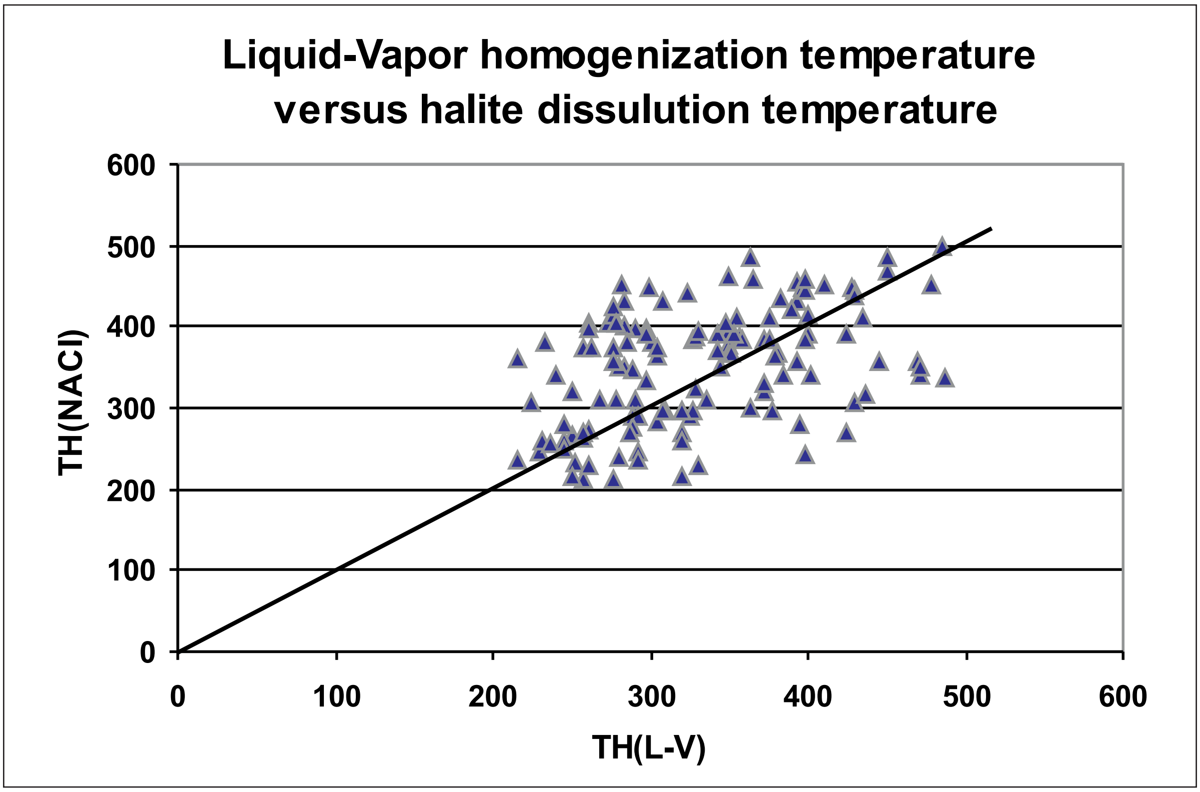

Figure 5- Liquid-vapor homogenization temperature ($T_{H(L-V)}$) versus halite dissolution temperature ($T_{H(NaCl)}$) for halite - bearing inclusions at Sungun (the diagonal line ($T_{H(L-V)} = T_{S(NACl)}$) from Shepherd et al., 1985). For calculating the pressure we used points over the diagonal line, where $T_{S(NACl)} > T_{H(L-V)}$.

Based on the Brown and Lamb (1989) is method, to measure the geological pressure the applied fluid inclusions must be halite-and gas-bearing with high salinity ones, which is why that these type of fluid inclusions are used from now on. Table 2 shows the statistical properties of the fluid inclusions with the salinities more than 27 wt% equivalent.

The point pressure and hydrothermal fluid density in the NaCl-H_2O system is calculated for 47 samples with using 3 parameters including Th → Halite (°C), Th → Vapor (°C) and salinity (wt% NaCl), based on Brown and Lamb (1989) is equation by the Flincor software (Brown, 1989). Fluid pressures varies from 261 to 2148 bars (Table 3)

COMPARING THE RESULTS IN TWO ALTERATIONS

As discussed earlier, the analyses were done on the three-phase fluid inclusions that were in the quartz veins adjacent to the mineralization (in different alterations). As we expected, this fluid inclusions shows high salinity. With the investigation of the table 4 it could be seen that the average salinity in potassic alteration is a little bit higher than the average salinity of the phyllic alteration, but they are very close to each other, as mentioned in Hezarkhani and Williams-Jones (1998).

The results show that the average of Th, salinity, pressure and density of fluids in quartz

Table 3- Achieved data from 47 locations in 13 boreholes separated into potassic and phyllic. Based on microscopic studies and XRF analysis 22 of them defined as potassic and 25 of them defined as phyllic alteration.

No.	BH No.	Alteration	Elevation (m)	Cu (%)	Th→H (°C)	Salinity (%)	Th→V (°C)	Pressure (bar)	Density (gr/cm^3)
1	BH	PHY	1848	0.73	337	39.8	297	836	1.11
2	BH	PHY	1808	0.86	351	42.5	319	770	1.15
3	BH	POT	1801	0.68	394	46.5	368	711	1.12
4	BH	POT	1774	0.64	371	44.8	350	583	1.11
5	BH	POT	1660	0.3	373	45.1	321	1165	1.14
6	BH	POT	1615	0.75	398	47.2	311	1981	1.19
7	BH	POT	1603	0.63	358	43.1	277	1688	1.16
8	BH	POT	1594	0.98	337	41.6	288	1030	1.14
9	BH	POT	1581	0.65	347	42.6	321	619	1.12
10	BH	PHY	1622	0.49	460	54.6	451	654	1.13
11	BH	POT	1592	0.7	359	43.3	298	1406	1.19
12	BH	POT	1729	0.29	398	45.5	300	2108	1.17
13	BH 1	PHY	1853	0.6	410	46	395	560	1.08
14	BH 1	PHY	1847	0.52	450	48	427	838	1.07
15	BH 1	PHY	1843	0.31	430	47.8	411	713	1.08
16	BH 1	PHY	1830	0.48	312	36	298	324	1.07
17	BH 1	PHY	1827	0.64	234	33.5	212	446	1.13
18	BH 1	PHY	1826	0.64	220	33	200	410	1.13
19	BH 1	PHY	1824	0.85	250	34	225	502	1.12
20	BH 2	PHY	1876	1.06	350	37	343	261	1.04
21	BH 2	PHY	1861	0.85	355	38	344	334	1.04
22	BH 2	PHY	1823	0.57	414	46.9	384	854	1.1
23	BH 2	PHY	1821	0.71	410	48	400	485	1.1
24	BH 2	PHY	1818	1.21	423	49	408	602	1.1
25	BH 2	PHY	1813	1.17	380	36	349	655	1.02
26	BH 2	PHY	1746	0.85	399	36	393	342	0.97
27	BH 2	PHY	1741	0.9	428	46	414	590	1.06
28	BH 3	PHY	1807	0.52	382	38.3	337	913	1.05
29	BH 3	PHY	1801	0.53	425	46.4	407	664	1.07
30	BH 4	POT	1707	0.1	356	42	331	599	1.1
31	BH 5	PHY	1711	0.12	404	46	390	528	1.08
32	BH 6	POT	1647	0.72	385	45.5	381	303	1.09
33	BH	POT	2080	0.41	461	52.7	424	1257	1.13
34	BH	POT	1813	1.31	431	47.7	398	965	1.09
35	BH	POT	1661	0.63	444	49.9	403	1210	1.12
36	BH	POT	1780	0.42	442	49.7	410	1020	1.11
37	BH	POT	1543	0.23	455	51.1	403	1483	1.13
38	BH	PHY	1671	0.76	404	45.4	388	557	1.08
39	BH	POT	1792	0.61	418	47.3	355	1503	1.13
40	BH	POT	1685	0.65	583	60.9	550	2148	1.13
41	BH	POT	1673	0.32	475	53.6	432	1452	1.13
42	BH	POT	1659	0.4	406	46.7	362	1098	1.12
43	BH	PHY	1959	0.66	394	45.2	358	875	1.11
44	BH	PHY	1918	0.47	389	44.5	335	1214	1.12
45	BH	PHY	1783	0.55	388	43.8	363	646	1.09
46	BH	POT	1676	0.42	462	32.6	408	998	1.14
47	BH	POT	1631	0.79	447	38.5	404	962	0.99

Table 4- Descriptive statistics of 25 samples from phyllic alteration and 22 samples from potassic alteration.

	Descriptive	Elevation (m)	Cu (%)	Th→H (°C)	Salinity (%NaCl)	Th→V (°C)	Pressure (bar)	Density (gr/cm^3)
Potassic	Mean	1695	0.57	414	46.3	368	1195	1.12
	S.D.	116	0.27	56	5.7	63	498	0.04
	Var.	13351	0.07	3181	32.7	3925	247652	0.002
	Min	1543	0.10	337	32.6	277	303	0.98
	Max	2080	1.31	583	60.9	583	2148	1.19
Phyllic	Mean	1811	0.68	376	42.5	354	623	1.08
	S.D.	71	0.25	64	5.8	66	222	0.04
	Var.	5092	0.06	4039	34	4374	49497	0.002
	Min	1622	0.12	220	33	200	261	0.97
	Max	1959	1.21	460	54.6	451	1214	1.15
Total	Mean	1757	0.63	394	44.2	360.	891	1.1

veinlets of potassic alteration are more than the ones in phyllically altered samples.

- In potassic alteration, the average homogenization temperature is 413.6 °C while in phyllic alteration it is 375.9 °C. As it is expected in potassic alteration, the temperature of hydrothermal is higher than the phyllic one, but there is not much difference between them.

- The salinity of the hydrothermal fluid has a high coherency with homogenization temperature, so the average amount of salinity in potassic samples is 46.3 (wt% NaCl) which is a little bit higher than that of the phyllic samples (42.5 wt% NaCl). As discussed above, the analyses were done on the three-phase fluid inclusions and as expected, this type of fluid inclusion shows high salinity in both alterations.

- Based on the location of potassic alteration, which is located beneath the phyllic alteration, we expect the lithostatic pressure is much more than the phyllic one, so it is realized that the average pressure in the potassic alteration is 1195 (bar) while the pressure average in phyllic is about 623 (bar).

- The density depends on the amount of the salinity of hydrothermal fluid, so the average density of the samples in potassic alteration is 1.124 (gr/cm^3) which is higher than the phyllic one (1.083 gr/cm^3).

CONCLUSIONS

Based on various comprehensive studies on Sungun Copper deposit, it is illustrated that the Sungun deposit is a porphyry system and the potassic and phyllic alterations contain copper sulfide minerals extensively. The primary multiphase inclusions within the quartz crystals in quartz-sulfide and quartz-molybdenite veinlets (quartz associated with sulfide minerals) were chosen for micro-thermometric analyses and considered to calculate the geological pressure and hydrothermal fluid density.

Early hydrothermal alteration produced a potassic assemblage (orthoclase-biotite) in the central part of the Sungun stock. Propylitic alteration occurred contemporaneously with potassic alteration. But in the peripheral parts of the stock, phyllic alteration occurred later, overprinting these earlier alterations. Based on fluid inclusion studies in the Sungun deposit, potassic alteration and associated Cu mineralization were caused by a high temperature and high salinity fluid of dominantly magmatic origin. The early hydrothermal fluids are represented by high temperature (337 °C to 583 °C), high salinity (up to 60 wt % NaCl equiv.) liquid-rich fluid inclusions, and high temperature (320 °C to 550 °C), low-salinity, vapor-rich inclusions. Phyllic alteration and copper leaching resulted from the inflow of oxidized and acidic meteoric waters with decreasing temperature (ranging from 220-460 °C, with a mean of 376 °C) of the system.

The average of all four measured variables (homogenization temperature, salinity, pressure and density) is higher in potassic samples than phyllic ones, but it is not possible to draw a vertical line and separate the two alteration samples. It means the thermodynamic conditions for those alterations are close together and other parameters could affect the mineral precipitation and mineral assemblages in the alteration zones.

Manuscript received March 3, 2008

REFERENCES

Ahmad, S.N., and Rose, A.W., 1980. Fluid inclusions in porphyry and skarn ore at Santa Rita, New Mexico. Economic Geology 75, 229-250.

Beane, R. E. and Titley, S.R., 1981. Porphyry copper deposits: Part II. Hydrothermal alteration and mineralization: Economic Geology 75th Anniversary Volume, 235-269.

_____ and Bodnar, R.J., 1995. Hydrothermal fluids and hydrothermal alteration in porphyry copper deposits. In: Wahl, P.W., Bolm, J.G. (Eds.), Porphyry Copper Deposits of the American Cordillera, Tucson, Arizona, Arizona Geological Society, Arizona, 83-93.

Brown, P. E., 1989. FLINCOR: a microcomputer program for the reduction and investigation of fluid inclusion data. American Mineralogist, 74, 1390-1393.

_____ and Lamb, W.M., 1989. P- V-T properties of fluids in the system H_2O-CO,-NaCI: New graphical presentations and implications for fluid inclusion studies. Geochimica et Cosmochimica Acta, 53, 1209-1221.

Burnham, C. W., 1979. Magmas and hydrothermal fluids. In: H. L. Barnes (ed), Geochemistry of Hydrothermal ore deposits, John Wiley & Sons, 71-136.

Calagari, A. A., 1997. Geochemical, stable isotope, noble gas, and fluid inclusion studies of mineralization and alteration at Sungun porphyry copper deposit, East Azarbaidjan, Iran: Implication for genesis. Unpublished PhD Thesis. Manchester University, Manchester, 537 p.

Calagari, A. A., 2004. Fluid inclusion studies in quartz veinlets in the porphyry copper deposit at Sungun, East-Azarbaidjan, Iran, Journal of Asian Earth Sciences 23, 179-189.

Chivas, A.R. and Wilkins, R.W.T., 1977. Fluid inclusion studies in relation to hydrothermal alteration and mineralization at the Koloula porphyry copper prospect, Guadalcanal. Economic Geology, 7,153-169.

Cloke, P.L. and Kesler, S.E., 1979. The halite trend in hydrothermal solutions. Economic Geology 74, 1823-1831.

Dilles, J.H. and Einaudi, M.T., 1992. Wall-rock alteration and hydrothermal flow paths about the Ann-Mason porphyry copper deposits, Nevada-a 6-km vertical reconstruction. Economic Geology, 87, 1963-2001.

Eastoe, C. G., 1978. A fluid inclusion study of the Panguna porphyry copper deposit, Bougainville, Papua New Guinea: Economic Geology, 73, 721 748.

Emami, M.H., and Babakhani, A.R., 1991. Studies of geology, petrology, and litho-geochemistry of Sungun Cu-Mo deposit, Iranian Ministry of Mines and Metals, 61.

Etminan, H., 1977. The discovery of porphyry copper-molybdenum mineralization adjacent to Sungun village in the northwest of Ahar and a proposed program for its detailed exploration. Confidential Report, Geological Report, Geological Survey of Iran, 26 p.

Gustafson, L. B., and Hunt, J. P., 1975. The porphyry copper deposit at El Salvador, Chile: Economic Geology, 70, 857 912.

Hedenquist, J.W. and Richards, J.P., 1998. the influence of geochemical techniques on the development of genetic models for porphyry copper deposits. In: Richards JP, Larson PB (eds) Techniques in hydrothermal ore deposits geology. Rev Economic Geology 10, 235-256.

Heinrich, C.A., 2005. The physical and chemical evolution of low-salinity magmatic fluids at the porphyry to epithermal transition: a thermodynamic study Mineralium Deposita, 39, 864-889.

_____, Pettke, T., Halter, W.E., Aigner-Torres, M., Audetat, A., Gunther, D., Hattendorf, B., Bleiner, D., Guillong, M. and Horn, I., 2003. Quantitative multi-element analysis of minerals, fluid and melt inclusions by laser-ablation inductively-coupled-plasma mass-spectrometry. Geochimica et Cosmochimica Acta, 67, 3473-3497

Hezarkhani, A., 2006, Petrology of Intrusive rocks within the Sungun Porphyry Copper Deposit, Azarbaijan, Iran. Journal of Asian Earth Sciences. 73, 326-340.

_____ and Williams-Jones, A.E., 1998. Controls of alteration and mineralization in the Sungun porphyry copper deposit, Iran: Evidence from fluid inclusions and stable isotopes. Economic Geology, 93, 651-670.

_____ Williams-Jones, A. E. and Gammons, C. H., 1999. Factors controlling copper solubility and chalcopyrite deposition in the Sungun porphyry copper deposit, Iran, Mineralium Deposita, 34, 770-783.

Kehayov, R., Bogdanov, K., Fanger, L., von Quadt. A., Pettke, T. and Heinrich, C.A., 2003. The fluid chemical evolution of the Elatiste porphyry Cu-Au-PGE deposit, Bulgaria. In: Eliopoulos DG (ed) Mineral exploration and sustainable development. Millpress, Rotterdam, 1173-1176.

Mehrpartou, M., 1993. Contributions to the geology, geochemistry, Ore genesis and fluid inclusion investigations on Sungun Cu-Mo porphyry deposit, northwest of Iran. Unpublished PhD Thesis. University of Hamburg, Germany, 245 p.

Nash, J. T., 1976. Fluid inclusion petrology data from porphyry copper deposits and applications to exploration: U.S. Geological Survey Proffessional Paper, 907 D, 16p.

Quan, R.A., Cloke, P.L., and Kesler, S.E., 1987. Chemical analyses of halite trend inclusions from the Granisle porphyry copper deposit, British Columbia. Economic Geology, 82, 1912-1930.

Redmond, P.B., Einaudi, M.T., Inan, E.E., Landtwing, M.R. and Heinrich, C.A., 2004. Copper deposition by fluid cooling in intrusioncentered systems: new insights from the Bingham porphyry ore deposit, Utah. Geology 32(3), 217-220.

Roedder, E., 1971. Fluid inclusion studies on the porphyry copper-type ore deposits at Bingham (Utah), Butte (Montana), and Climax (Colorado). Economic Geology, 66, 98-120.

_____, 1984. Fluid inclusions, Reviews in Mineralogy, vol. 12. Book Crafters, Inc, Michigan, 644 p.

_____ and Bodnar, R.J., 1980. Geologic pressure determination from fluid inclusion studies. Annual Review of Earth and Planetary Science 8, 263-301.

_____, 1984. Fluid inclusions: Reviews in mineralogy, Ribbe, P. H. (ed), 12, 644 p.

Shepherd, T., Rankin, A.H., and Alderton, D.H.M., 1985. A Practical Guide to Fluid Inclusion Studies, Blackie, London, 239 p.

Sillitoe, R.H. and Hedenquist, J.W., 2003. Linkages between volcanotectonic settings, ore-fluid compositions and epithermal precious metal deposits. In: Simmons SF, Graham I (eds) Volcanic, geothermal and ore-forming fluids: rulers and witnesses of processes within the earth. Economic Geology Special Publucation, 343 p.

Sillitoe, R.H., 1997. Characteristics and controls of the largest porphyry copper-gold and epithermal gold deposits in the circum- Pacific region. Australian Journal of Earth Sciences, 44(3), 373-388.

Sourirajan, S., and Kennedy, G.C., 1962. The system H_2O-NaCl at elevated temperatures and pressures. American Journal of Science, 260, 115-141.

Sterner, S. M., Hall, D. L., and Bodnar, R. J., 1988. Synthetic fluid inclusions. V. Solubility of the system NaCl-KCl-H_2O under vapor-saturated conditions. Geochimica et Cosmochimica Acta, 52, 989- 1005.

Stocklin, J.O., 1977. Structural correlation of the Alpine ranges between Iran and Central Asia. Mem. H. Aser. Geological Society of France, 333-353.

Tosdal R.M. and J.P. Richards., 2001. Magmatic and structural controls on the development of porphyry Cu±Mo±Au deposits. In: Richards, J.P. and Tosdal, R.M. (eds), Structural controls on ore genesis. Reviews in Economic Geology, 157-180

Ulrich, T., Gunther, D., and Heinrich, C.A., 2001. The evolution of a porphyry Cu-Au deposit, based on La-ICP-MS analysis of fluid inclusions, Bajo de la Alumbrera, Argentina. Economic Geology 96, 1743-1774.

Urusova, M.A., 1975. Volume properties of aqueous solutions of sodium chloride at elevated temperatures and pressures. Russian Journal of Inorganic Chemistry 20, 1717-1721.

Watmuff, G., 1978. Geology and alteration-mineralization zoning in the central portion of the Yandera porphyry copper prospect, Papua New Guinea. Economic Geology 73, 829-856.

PLATES

PLATE I

Figure a- Scanning electron photomicrographs: Molybdenite with associated anhedral bismuthinite and pyrite.

Figure b- Quartz associated with pyrite altered to chalcopyrite. All fluid inclusions have been measured from quartz veins associated with ore minerals.

Figure c- Plagioclase and calcite veins in potassically altered sample from BH104-351m (optical microscope, crossed polars).

Figure d- Quartz veins are surrounded by weak sericitic halos in phyllically altered samples from BH2-145m.

Figure e and f copper mineralization in chalcopyrite from potassic and phyllic samples.

Abbreviations: Bi= bismuthinite, Cp=chalcopyrite, Mo=molybdenite, Py=pyrite, Qtz=quartz.

PLATE - I

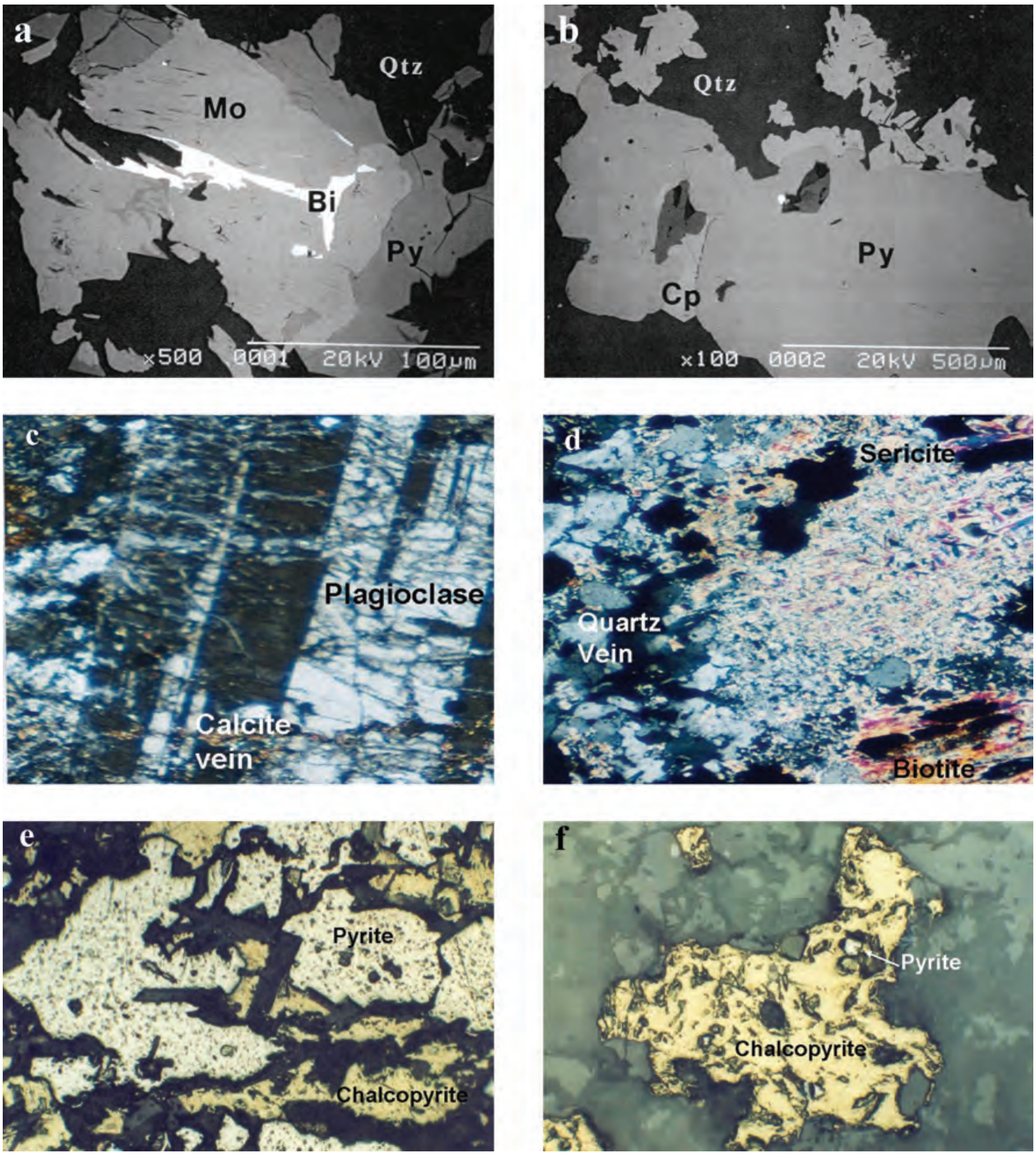
a
Qtz
Mo
Bi
Py
×500 0001 20kV 100µm
b
Qtz
Py
Cp
×100 0002 20kV 500µm
c
Plagioclase
Calcite
vein
d
Sericite
Quartz
Vein
Biotite
e
Pyrite
Chalcopyrite
f
Pyrite
Chalcopyrite

PLATE II

Photomicrographs of different inclusion types within mineralized quartz vein from Sungun.

Figure a- Secondary fluid inclusions;

Figure b- Secondary biphase (VL and LV) inclusions,

Figure c- primary polyphase inclusion from potassic alteration assemblage (sample no. 42) and

Figure d- primary inclusion from Phyllic alteration assemblage (sample no.18).

All photographs were taken at ambient laboratory temperature. See text for discussion.

PLATE - II

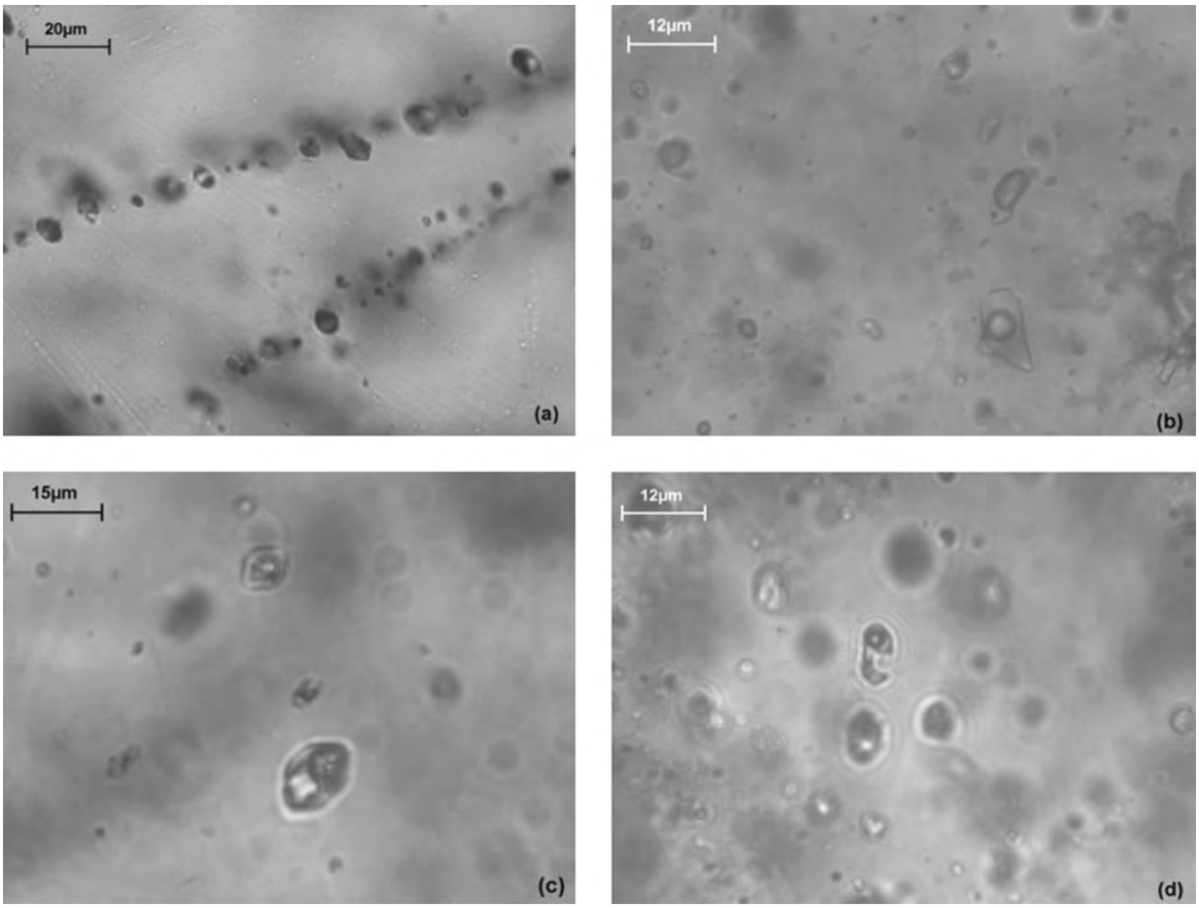

BOS SAYFA

Mineral Res. Expl. Bull., 140, 35-53, 2010

ACTUAL BLOEDITE MINERAL PRECIPITATION IN A SEASONAL LAKE IN ÇANKIRI-ÇORUM BASIN

Ýlhan SÖNMEZ *

ABSTRACT - Bloedite ($Na_2Mg(SO_4)_2.4H_2O$) which is an economically important sodium sulfate mineral currently precipitates through evaporation in Lake Ýshaklý, a small seasonal lake (playa lake) situated to the north of Ýshaklý Village (Bayat - Çorum) in Çankýrý-Çorum Basin. Lake Ýshaklý, in which actual bloedite precipitation has been determined for the first time by this work in Turkey, extends in East-West direction and covers an area of approximately 220.000 m^2. During winter and spring months it becomes a lake with a depth of more than 2 m. However, during hot periods when evaporation becomes effective, the lake dries up and is covered with a white mineral crust. Mineralogical determinations, chemical analyses and SEM examinations were carried out on the representative samples taken from conspicuous zonings in the lake. According to the results of the analysis, it has been determined that the predominant mineral in the area is bloedite; however, thenardite (Na_2SO_4), very little halite ($NaCl$) and gypsum ($CaSO_4.2H_2O$) accompany this precipitation. The sodium sulfate crustification (bloedite + thenardite), which reaches an average thicknes of 3 cm over an evaporation area of approximately 187.500 m^2 in Lake Ýshaklý, has economical potential with its proven reserve of about 12.500 tons.

Key words: Bloedite, actual evaporite precipitation, playa lake, Çankýrý-Çorum Basin

INTRODUCTION

Lake Ýshaklý, a playa lake in which actual bloedite precipitation has been determined for the first time in Turkey, is situated to the north of Ýshaklý Village, Bayat township, Çorum province (Figure 1 a,b,c). Lake water is very saline and its maximum depth exceeds 2 m in rainy seasons (Figure 2). During hot periods when evaporation is effective this pond dries up and it is covered with a mineral crust (bloedite + thenardite) that reaches a maximum thickness of 10 cm in the middle of the lake and has an average thickness of 3 cm over an evaporation area of about 187,500 m^2 (Figure 3).

Although there exists no specific source to feed the lake during evaporation periods, it is thought that there may be a source at the bottom to feed the lake.

With the thought that this actual mineralization formed at the surface might be indicative of a buried Na-sulfate deposition in the area, a core hole of 966.45 m depth was drilled at the west shore of Lake Ýshaklý. During this drilling work a total of 592 m halite (NaCl) mineral was cut in the salt dome after 225 m depth. No clear evidence of bloedite-thenardite association was observed. This current bloedite-thenardite formation, determined in a small, playa type lake in Çankýrý-Çorum Basin may be fed by a buried fossil Na-sulfate deposit precipitated earlier in the evaporitic environment. Nevertheless, when one considers that the ophiolitic rocks lying at the base of the basin are rich in magnesium, the gypsums are rich in sulfate and volcanics are rich in sodium and these might feed the groundwater, it is also possible that this mineralization takes place as a result of surface evaporation and temperature variations following this ionic equilibrium.

This work has been prepared based on the preliminary findings of the data obtained in the field and in the laboratory. It will be possible to explain the origin and formation of this precipitation by means of the new data to be obtained

*MTA Genel Müdürlüðü Maden Etüt ve Arama Dairesi, Ankara.

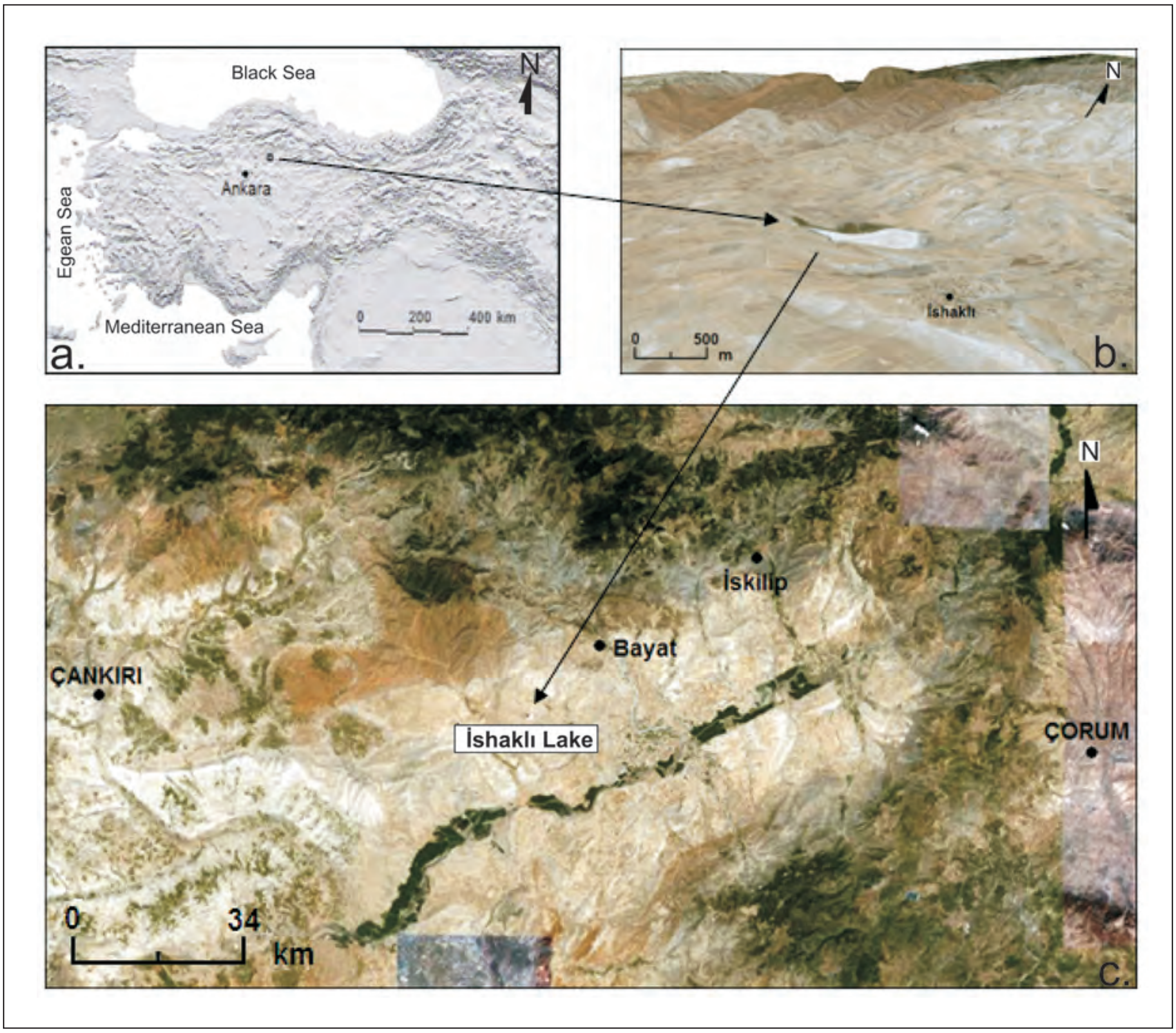

Figure 1- a,b,c: Location map of Ýshaklý Lake (image taken from "Google Earth).

from the works which are being carried out and which will be carried out in the basin.

In addition, it is another matter requiring detailed data to explain the relationship of the ionic concentration feeding this current formation with the thick halite mineral zone which was cut during the drilling beneath the playa lake.

The aim of this study is to state the existence of this actual mineralization which has been determined for the first time in Çankýrý-Çorum basin, and by opening up for discussion the origin of the occurrence and the system of precipitation, to contribute to the production of new indicators to be used in the exploration for Na-sulfate in this basin or in Turkey.

Although Na-sulfate forms numerous minerals in the nature, the most important Na-sulfate minerals, from the standpoint of economy and mineability, are mirabilite $(Na_2SO_4).10H_2O$, the-

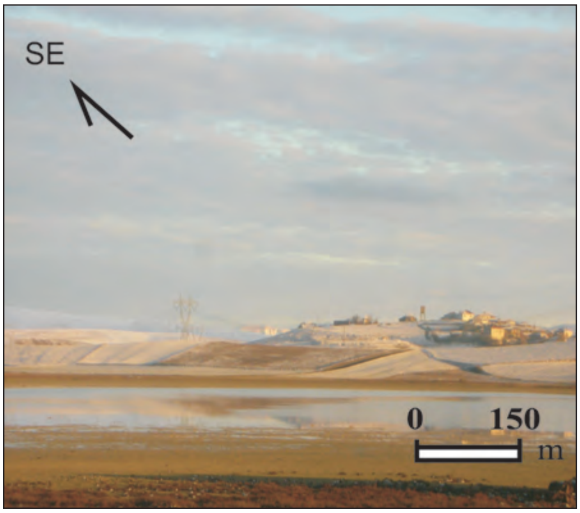

Figure 2- Ýshaklý Lake, rainy season (November-April).

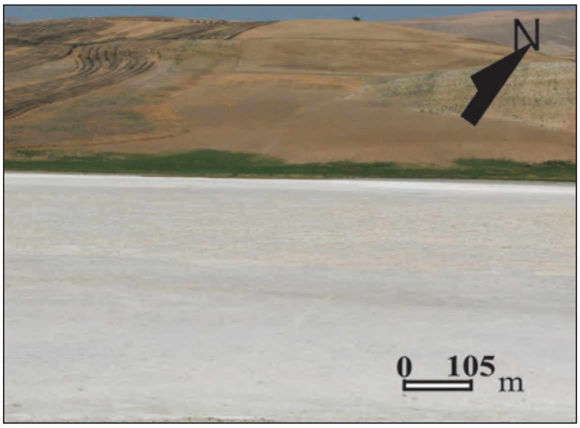

Figure 3- Ýshaklý Lake, dry season (May-October).

nardite (Na_2SO_4), glauberite ($Na_2Ca(SO_4)_2$) and bloedite ($Na_2Mg(SO_4)_2.4H_2O$). Na-sulfate minerals are minerals that have hardnesses of around 2-3, colorless in pure state transparent, readily soluble in water, having bitter and salty taste, having densities of around 1.49-2.8 gr/cm^3, formed in evaporitic terrestrial environments and that cannot be preserved under atmospheric conditions.

Na-sulfate is obtained in our country as in other countries of the world, primarily from alkaline lakes having saline and brackish waters, from buried solid sedimentary deposits and from chemical processes as a byproduct (synthetically).

In the our country 99% of the natural Na-sulfate produced is obtained from alkaline lakes having saline and brackish waters, and the remaining 1% from buried solid sedimentary deposits (Türkel and Ertok, 2001).

The most important production sites for Na-sulfate in Turkey are: Acýgöl (Denizli); Tersakan, Bolluk (Konya) alkaline lakes (Figure 4). From these lakes, sulfate minerals such as mirabilite (glauber's salt) and thenardite are produced (Gündoðan, 1994).

Figure 4 - Locations of Na-sulfate production in Turkey.

Apart from these, Çayýrhan (Ankara) deposit in Beypazarý Basin is an example of buried sedimentary Na-sulfate deposits which are scarce in the world (Çelik et al., 1987).

Çayýrhan deposit in Beypazarý Basin takes place in the Kirmir Formation by intercalating with, gypsum-bearing evaporite levels, which is of Upper Miocene age and deposited in playa lake environment. Within this deposit Na-sulfate exists as glauberite and thenardite (Helvacý et al.,1989). It has been observed that Na-sulfate occurrences in the formation are mostly composed of idiomorphic glauberite minerals and the thenardite minerals among them which bind the glauberite minerals by replacement and/or cementation (Gündoðan 2000; Gündoðan and Helvacý, 2001). In Çankýrý-Çorum and Beypazarý basins of Central Anatolia there exist evaporitic formations deposited in playa lake environment during Miocene and contain Na-sulfate. The presence of Na-sulfate in Çankýrý-Çorum basin was first determined by Gündoðan (2000). He states that the peculiar textures observed in pseudomorphic secondary gypsums, formed as a result of the alteration of glauberites observed in some levels within the Upper Miocene Bozkýr Formation which have got the properties to be used as key indicators in the exploration for Na-sulfate and points to the importance of petrographical studies.

In addition to these formations, Oligocene Upper Evaporite Formation in Valence Basin of France (Dromart and Dumas, 1997) and Folces gypsum formation in Ebro Basin of Spain (Salvany, 1997) contain glauberite.

Depositions similar to Upper Miocene Çayýrhan Na-sulfate (thenardite-glauberite) mine are observed in the world in Lower Miocene Calatayud gypsums in Calatayud Basin (Orti and Rosell, 2000) and in Lower Miocene saline unit in Madrid- Tajo Basin (Ordonez and Garcia del Cura, 1994) in Spain. In addition, in Spain's Ebro Basin, Lower Miocene Lering gypsum formation (Salvany and Orti, 1994) and Zaragoza gypsum formation (Salvany et al., 2007) contain glauberite.

REGIONAL LOCATION AND PREVIOUS WORKS

The study area is situated in Çankýrý-Çorum Basin which is one of the largest sedimentary basins of Turkey. This basin lies approximately between longitudes 33.5°- 35° east and latitudes 39.5°- 41° north in Central Anatolia (Figure 5).

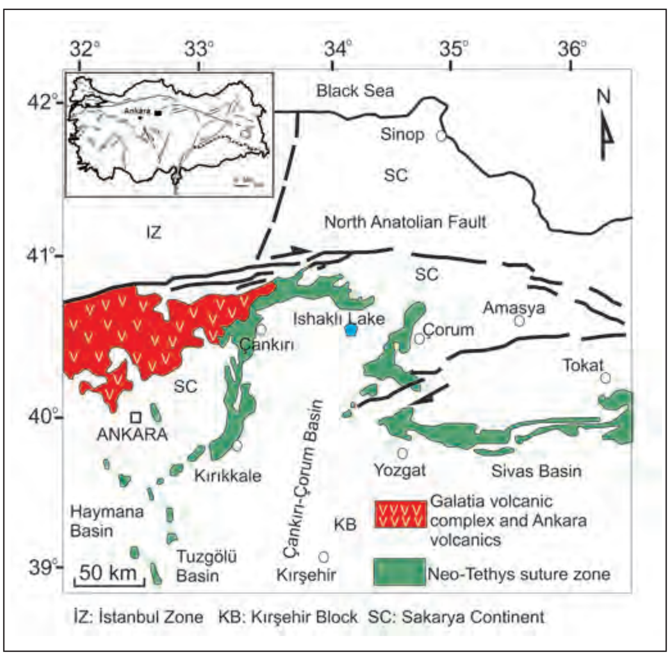

Figure 5- Simplified geological map of Çankýrý-Çorum basin (Karadenizli et al., 2004).

Çankýrý-Çorum Basin is surrounded in the west by Elmadað-Eldivan mountain, in the north by Ilgaz mountains, and in the east by Köse mountain (Tüysüz and Dellaloðlu,1992). Exist there are thick deposits of rock salt (halite) within this evaporitic basin which were deposited during various evaporitic periods and which are still being exploited.

In the fieldwork and drilling, performed in the vicinity of Ýshaklý Lake, it has been observed that this playa lake overlies the Plio-Quaternary Deðim Formation deposited in the environment of alluvial fan which constitutes the covering unit of the Çankýrý-Çorum Basin. Underlying this covering unit is the Upper Miocene-Pliocene Bozkýr Formation which is the first evaporitic unit of the basin, deposited in lacustrine environment and composed of gypsum- claystone succession (Figure 6).

Previous works about Çankýrý-Çorum Basin include some works on Tertiary geology and stratigraphy by Birgili et al. (1975), Akyürek et al. (1982), Yoldaþ (1982) and Hakyemez et al. (1986). In addition to these works, Koçyiðit (1991) and Kaymakçý (2000) established new findings regarding the tectonics and the stratigraphy of the basin.

Seyitoðlu et al. (1997, 2001) introduced the fault systems effective in the tectonics of the

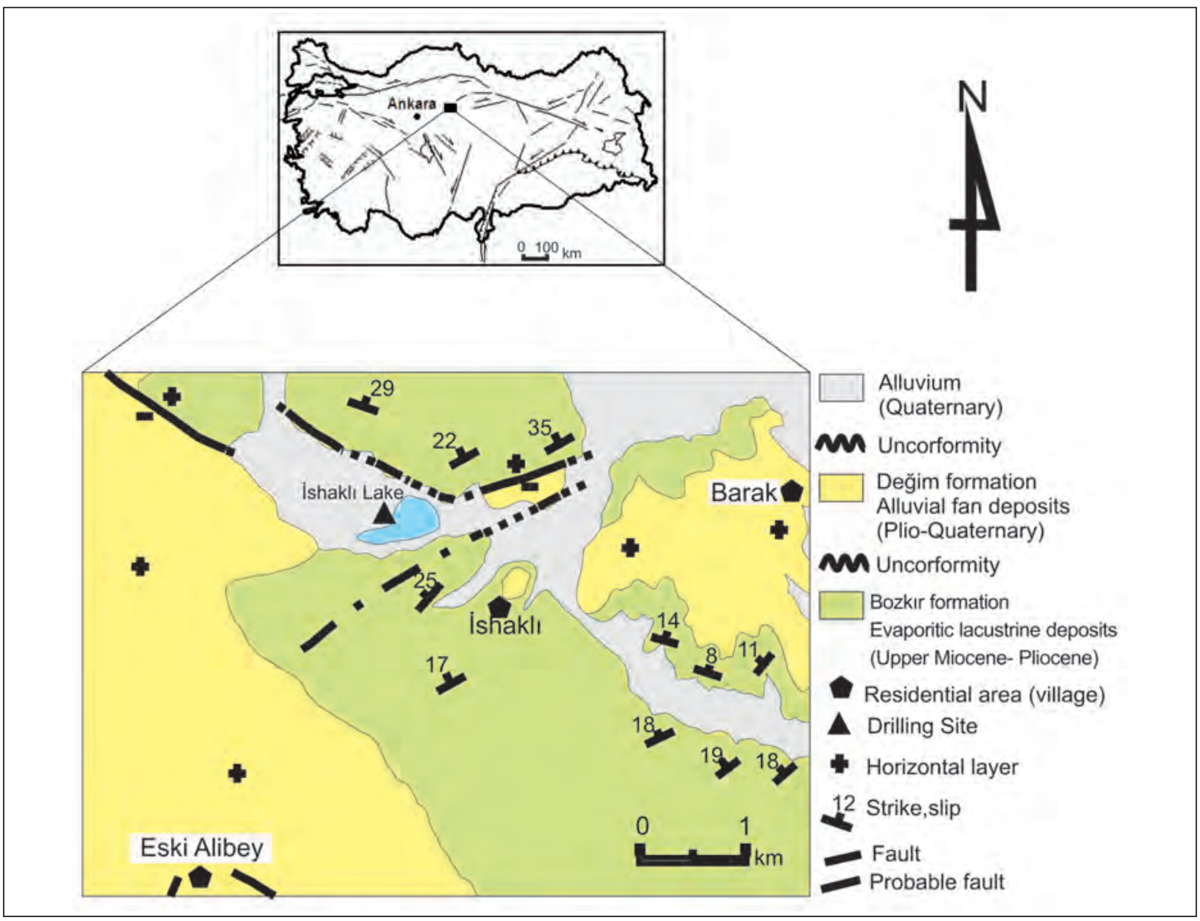

Figure 6- Geological map of the near vicinity of Ýshaklý Lake (modified after Aziz, 1972).

basin and the rockfall sediments developed under their control. There are also some studies carried out by Ergun (1977), Karadenizli and Kazancý (2000), Karadenizli (1999), Karadenizli et al. (2004), Gündoðan (2000), Gündoðan and Helvacý (2001), Varol et al. (2002) regarding the evaporite stratigraphy in the region.

In addition, General Directorate of MTA has been conducting an exploration work with drilling for industrial raw materials since 2006.

TECTONIC SETTING

Çankýrý - Çorum Basin, which is one of the most important Tertiary basins of the Central Anatolia, is located within the Anatolide Tectonic Unit, in a complex region formed by Sakarya and Kýrþehir Continents and Ankara - Erzincan Suture. The units at the bottom of the basin are made up of units belonging to Sakarya, Kýrþehir Continents and Ýzmir - Ankara - Erzincan Suture zone. While the basin is surrounded from the north and west by an ophiolithic melange, from the south by Kýrþehir Massif bounds the basin from the south. It is observed that it has a narrow connection with Haymana-Polatlý and Tuz Gölü Basins in the southwest.

The northern branch of the Neothetys (Ýzmir-Ankara - Erzincan Ocean) began to be depleted under Sakarya Continent with a northward subduction in Early Cretaceous; Sakarya and Kýrþehir Continents were closed by Tokat and Galatia Massifs in Late Cretaceous and the Neothetys, the northern flank of which was closed in Late Cretaceous-Upper Eocene, created a complex tectonic model (Þengör and Yýlmaz,1981). The regions subjected to sqeeze between irregular plates are named as Central Anatolian Basin (Görür et al., 1984). The Central Anatolian Basin is composed of Çankýrý - Çorum, Tuz gölü, Haymana-Polatlý, Beypazarý and Sivas Basins (Birgili et al., 1975; Görür et al., 1984). All these basins are defined as depression basins between rising plates.

GENERAL GEOLOGY

It is known that there exists a sediment infill which continued from Paleocene to Pliocene; Paleogene rocks are marine, and Neogene rocks are composed of terrestrial, clastic and evaporitic rocks.

The basement of the Çankýrý - Çorum Basin is composed of ophiolites of Mesozoic age. Paleocene - Eocene flysch unconformably overlies these. This flysch is composed of evenly stratified sandstone-shale succession and these are cut by Eocene volcanites of basaltic origin (Bayat formation). Oligo-Miocene sediments overlies all these units. In the basin there is a very thick sedimentary sequence continuing from Late Cretaceous to Pliocene without interruption. The part of this sequence up to Oligocene was deposited in marine environment, and the post - Oligocene rock units were deposited in terrestrial environment.

Evaporitic units of the Tertiary Çankýrý - Çorum basin were formed during four different geologic times. During Late Eocene, when the first evaporite deposition took place (Kocaçay formation), marine environment was dominant. In the evaporite depositions during Oligocene (Ýncik formation), Miocene (Bayýndýr formation) and Upper Miocene-Pliocene (Bozkýr formation) lacustrine environment was completely dominant.

All rock units in the basin are unconformably overlain by Deðim formation of Plio-Quaternary age deposited in fluvial and fan environment.

METHODOLOGY

In this field, which was discovered as a result of the works carried out wihin the scope of a project implemented by the General Directorate of MTA, revision of the geological map (scale: 1/25000) stratigraphic section preparation, intense field observations were carried out and in order to check the presence of a buried deposition, a reconnaissance core drill of 966.45 m was bored.

For mineralogical examinations, the map of the conspicuous zonings observed in the lake area were made and ten different representative samples were collected in (A-A') direction (Figure7). On these samples, XRD and chemical anayses were performed; SEM examinations were carried out to determine mineral relations.

Mineralogical analyses were realized using Philips PW XRD equipment in the laboratory of MTA's MAT Department. Diffractograms were obtained using Cu-K radiation, 2,5°-70° and 2θ. During chemical analyses samples were dried at 105°C. Analyses were performed using XRF equipment, IQ+program, again in MTA's laboratory.

During SEM examinations, from 4 selected samples (B4-B7-B9-B10), under FEI Quanta 400 MK2 model scanning electron microscobe, a total of 18 secondary electron detector (SE) images and 7 adet EDS (Energy Dispersive X Ray Spectrometer) point analysis results were obtained. EDS point analysis results are semi-quantitative elemental and oxide analysis results obtained using EDAX Genesis XM4I model EDS detector. Elemental point analyses were carried out under the detector conditions of kV: 25.00 Tilt: 0.00 Take-off: 34.94 AmpT: 102.4 Det Type: SUTW, Sapphire Res: 130.54 Lsec:10.

MINERALOGY

In the Ýshaklý playa lake, four different mineralogical zones were distinguished using the "google earth" image of the region and field observations (Figure 7). These zones are, starting from the outermost; 1. zone: gypsum+calcite zone, 2. zone: gypsum + calcite + bloedite zone, 3. zone: bloedite + gypsum zone and 4. zone: bloedite + thenardite zone. By XRD examinations of the representative samples taken from these zones approximately in the east - west direction (A-A'), mineralogical contents of these zones were determined and by XRF analysis, the

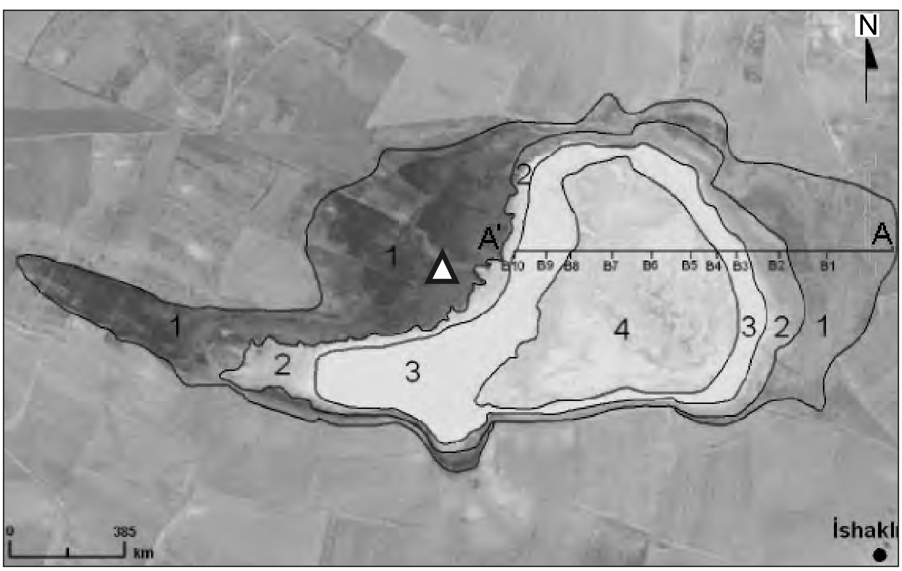

Figure 7- The map showing the zoning in Ýshaklý Pond (image taken from "Google Earth") A-A': sampling direction, 1: gypsum + calcite zone, 2: gypsum + calcite + bloedite zone, 3: bloedite + gypsum zone, 4: bloedite + thenardite zone Δ: Drilling location.

chemical analyses of the same samples were made and basic oxide percentages were determined (Table-1). In addition, SEM examinations were carried out in order to understand the micromorphologies and relations of the minerals.

According to the results of the analyses, mineralogical and chemical variations in the zones are clearly observed. In figure 7, in the samples taken in A-A' direction, towards the bloedite-thenardite zone, a net increase in the proportions of Na_2O and SO_3, and a net decrease in the proportions of Al_2O3, SiO_2, CaO_3 and Fe_2O3 is observed. MgO percentage varies between 4.9-8.7 in all the zones, and Cl persentage in all of the zones is constant and 0.02, which is very low. this shows that the think halite (NaCl) mineral, cut during the drilling, has almost no effect on the mineral formation at the surface

1. Zone: Gypsum + Calcite Zone

This zone, represented by green clays, corresponds to the lake's flood plain and has a length of approximately 215 m in (A-A') direction in figure 7 (Figure 8). In the samples taken from this zone gypsum, calcite, quartz, amorphous substance and very little anhydride have been determined. (Figure 9). In addition, it has been determined that the sample is rich in MgO, SO_3, Fe_2O_3 and CaO (Table-2).

2. Zone: Gypsum+Calcite+Bloedite Zone

It is the zone in which mineralization is weak and in the form of "efflorescence" (Figure 10). Its length is around 80 m along A-A' direction. In XRD analysis of the representative sample taken to determine the mineralogical composition of this zone gypsum, calcite, amorphous substance, bloedite, quartz and very little thenardite

Table 1- Results of analyses of the distinguished zones (oxide values are given as weight %).

Sample No	Na_2O	MgO	Al_2O_3	SiO_2	CaO	Fe_2O_3	SO_3	Cl	A.K.	XRD mineralogical composition	Zones
B1	1,2	5,7	7,0	24,9	17,1	6,0	15,7	0,02	19,50	Gypsum,Calcite,Quartz, Amorphous substance, very very little Anhydride	Gypsum-Calcite zone
B2	6,7	4,9	3,0	10,8	14,7	3,0	21,3	0,02	34,00	Gypsum,Calcite, Amorphous sustance, **Bloedite,** Quartz, very little Thenardite	Gypsum-Calcite-Bloedite Zone
B3	13,0	8,0	0,6	2,2	6,3	2,1	36,4	0,02	30,75	**Bloedite**,Gypsum,little **Thenardite**,very little Halite	Bloedite - Gypsum Zone
B4	23.3	7.4	0,1	0.4	1.3	0,1	50.1	0.02	17,10	**Bloedite, Thenardite**, Halite, very little Gypsum	Bloedite - Thenardite Zone
B5	27.5	5.7	<0.1	0.1	0.5	0,1	52.4	0.02	13,50	**Thenardite, Bloedite**,little Halite	
B6	21.0	8.7	0.3	1.1	5.4	0,2	49.1	0.02	13,85	**Bloedite**, Halite, **Thenardite**, little Gypsum	
B7	23.2	7.7	0.3	0.8	3.3	0,1	52.4	0.02	12,00	**Thenardite, Bloedite**, very very little Halite	
B8	29.9	6.2	0.1	0.3	0.2	0,1	53.2	0.02	9,95	**Thenardite,Bloedite**, little Halite	
B9	24.7	6.7	0.1	0.3	1.8	0,1	50.3	0.02	15.80	**Bloedite, Thenardite**, Halite, little Gypsum	Bloedite - Gypsum zone
B10	26.1	5.7	0.1	0.6	1.4	0,2	47.1	0.02	18.65	**Thenardite,Bloedite** little Gypsum,little Halite	

Table 2- Chemical analysis of Sample B1 (oxide values are given as weight %).

Sample No:	Na_2O	MgO	Al_2O_3	SiO_2	K_2O	CaO	Fe_2O_3	SO_3	Cl	MnO	P_2O_5	TiO_2	SrO	LOI
B1	1,2	5,7	7,0	24,9	1,0	17,1	6,0	15,7	0,02	0,2	0,1	0,5	0,49	19,50

have been determined (Figure 11). Results of the sample's chemical analysis are given in table 3.

3. Zone: Bloedite + Gypsum Zone

It is the zone in which mineralization begins to intensify in a rough and foamlike "efflorescent" appearance and a mineral crust with an average thickness of 3-5 cm is observed (Figure 12 a,b). This zone has an approximate length of 93 m at the east side of the pond, along A-A' direction. In the XRD analysis of the sample taken from this zone plenty of bloedite, gypsum, little thenardite, very little feldspar and trace amount of halite have been determined (Figure 13). The result of the chemical analysis clearly shows the increase in the proportions of Na_2O, MgO and SO_3 and the decrease in the proportion of CaO (Table-4).

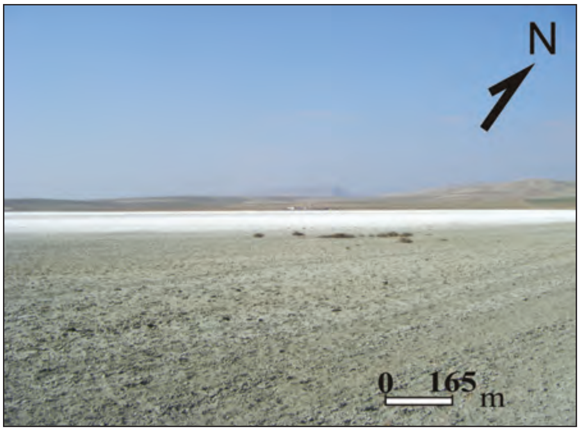

Figure 8- Gypsum+calcite zone at the lakeflat.

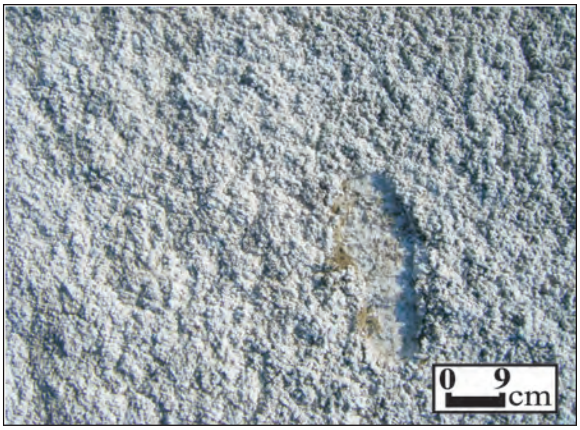

Figure10 - Weak, efflorescence mineralization surface representing gypsum + calcite+bloedite zone.

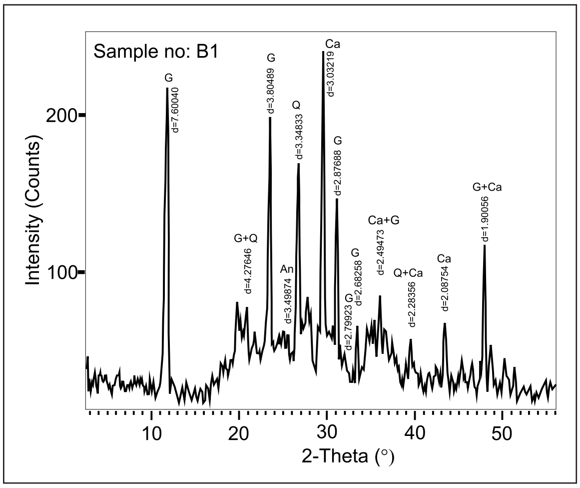

Figure 9- XRD diffractogram of Sample B1; G:Gypsum, Q: Quartz, Ca: Calcite, An: Anhydride.

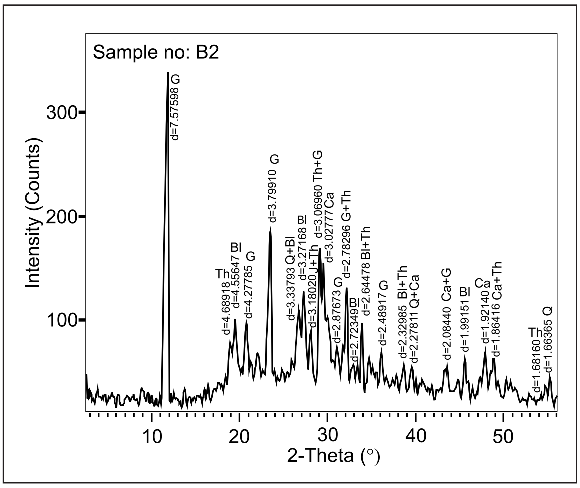

Figure11- XRD diffractogram of Sample B2 G:gypsum, Bl:bloedite, Th:thenardite, Q:quartz, Ca:calcite.

Table 3- Chemical analysis of Sample B2 (oxide values are given as weight %).

Sample No:	Na_2O	MgO	Al_2O_3	SiO_2	K_2O	CaO	Fe_2O_3	SO_3	Cl	MnO	P_2O_5	TiO_2	SrO	LOI
B2	6,7	4,9	3,0	10,8	0,5	14,7	3,0	21,3	0,02	0,1	0,1	0,5	0,33	34,00

Table 4 - Chemical analysis of Sample B3 (Oxide values are given as weight %).

Sample No	Na_2O	MgO	Al_2O_3	SiO_2	K_2O	CaO	Fe_2O_3	SO_3	Cl	MnO	P_2O_5	TiO_2	SrO	LOI
B3	13,0	8,0	0,6	2,2	0,2	6,3	2,1	36,4	0,02	<0,1	0,1	<0,1	0,20	30,75

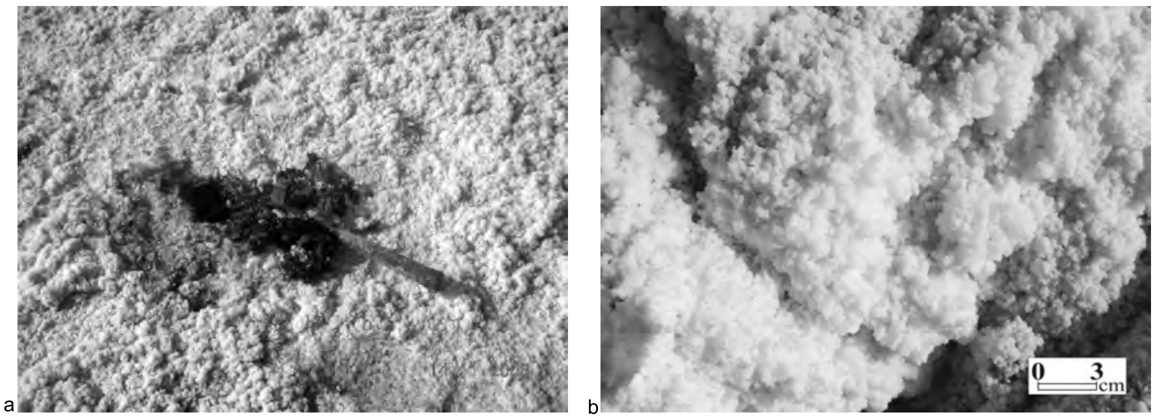

Figure 12- Foamlike "efflorescence" mineralization surface representing bloedite + gypsum zone a: general view b: detailed view.

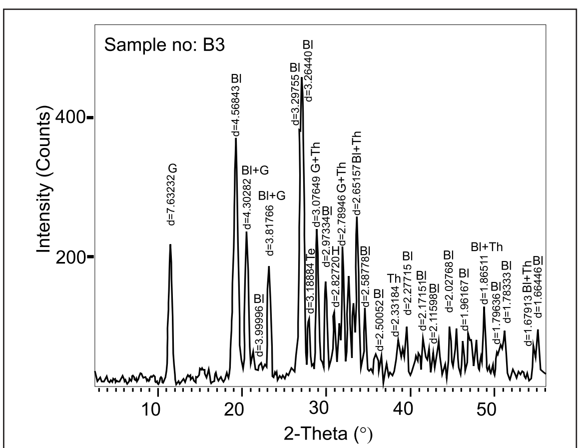

Figure 13- XRD diffractogram of Sample B3; G:gypsum, Bl: bloedite Th:thenardite, H:halite.

4. Zone: Bloedite + Thenardite Zone

This zone is represented by bloedite-thenardite assocation and has the thickest mineralization with a crust thickness of 5-10 cm (Figure 14 a,b). It has a length of about 285 m along A-A' direction. The plants growing in this salty zone intensifing in mid-lake accelerate evaporation and by absorbing salty water feed the precipitation (Figure 15 a, b). In this zone are abundantly present tepee structures (Figure 16 a,b), rodlike bloedite crystals (Figure 17), polygonal desiccation cracks (Figure 18) and bloedite crystals within the brecciated structure developed under the influence of desiccation (Figure 19). XRD analyses of the representative samples of this zone, B4, B5, B6, B7, B8 show bloedite-thenardite association and very little halite and very little gypsum (Figure 20a, b, c,d, e). And the results of the chemical analyses support this association (Table 5).

In the XRD analyses performed on the representative samples B9 and B10 corresponding to

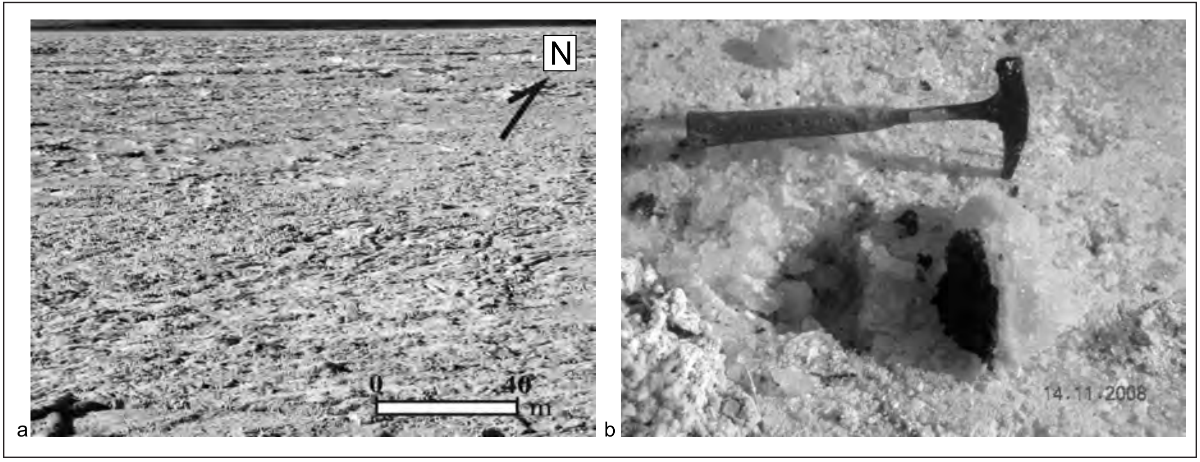

Figure 14- Large-scale desiccation cracks and crustifications observed in bloedite-thenardite zone.

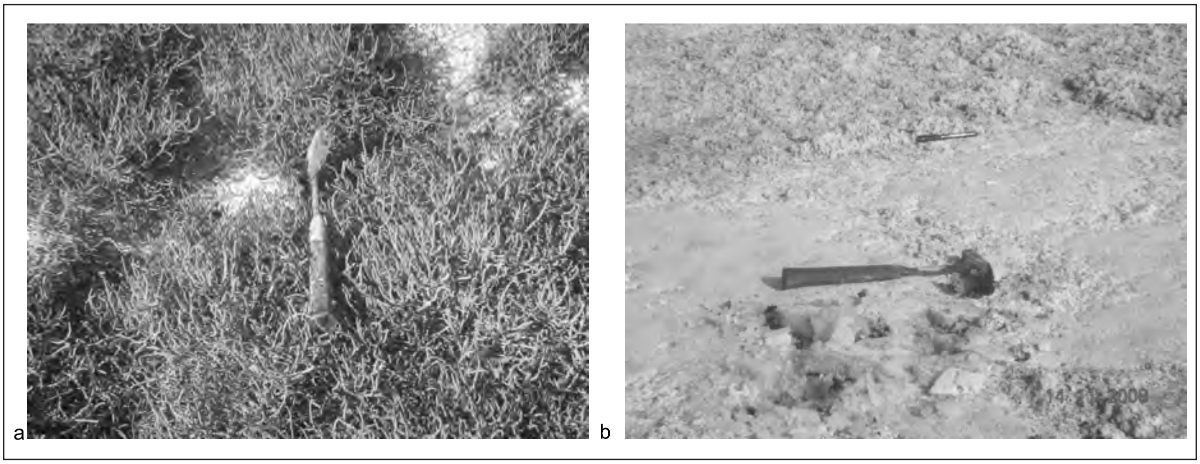

Figure 15- a: General view of the haloduric plants at lake shore, b: plant remains completelly covered by bloedite mineral in mid-lake.

Table 5- Chemical analyses of Samples B4, B5, B6, B7, B8 (Oxide values are given as weight %).

Sample No	Na_2O	MgO	Al_2O_3	SiO_2	K_2O	CaO	Fe_2O_3	SO_3	Cl	MnO	P_2O_5	TiO_2	SrO	LOI
B4	23.3	7.4	0,1	0.4	0,1	1.3	0,1	50.1	0.02	<0,1	<0,1	<0,1	0,04	17,10
B5	27.5	5.7	<0.1	0.1	<0.1	0.5	0,1	52.4	0.02	<0,1	<0,1	<0,1	0,03	13,50
B6	21.0	8.7	0.3	1.1	0.1	5.4	0,2	49.1	0.02	<0,1	<0,1	<0,1	0,16	13,85
B7	23.2	7.7	0.3	0.8	<0.1	3.3	0,1	52.4	0.02	<0,1	<0,1	<0,1	0,13	12,00
B8	29.9	6.2	0.1	0.3	<0.1	0.2	0,1	53.2	0.02	<0,1	<0,1	<0,1	0,01	9,95

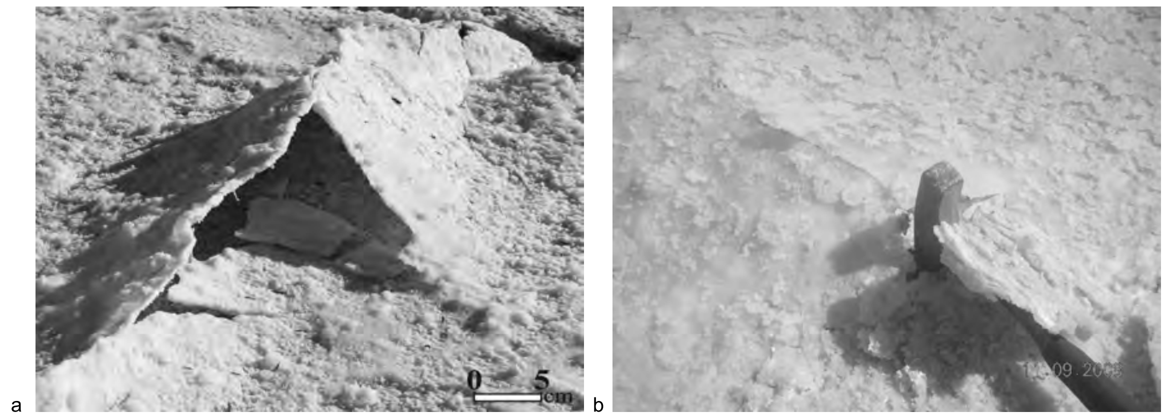

Figure 16- Tepee structures a: well-developed, b:weak.

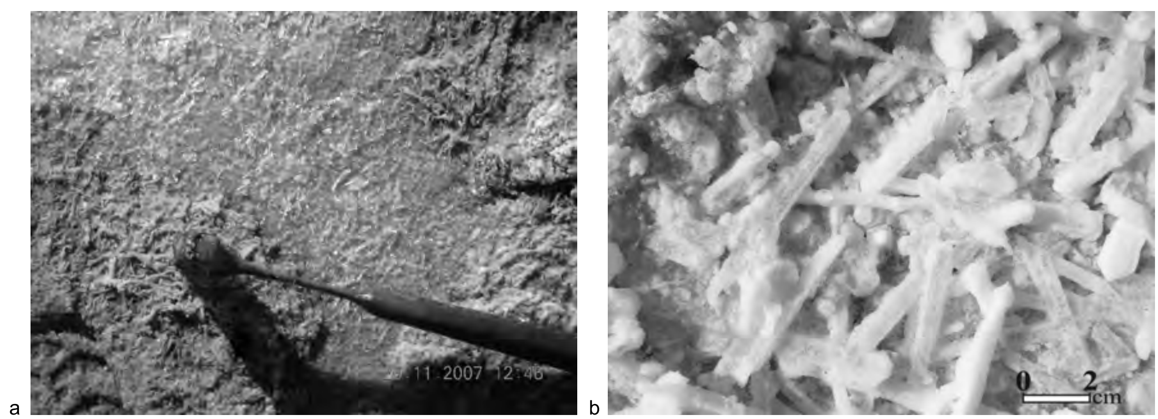

Figure 17- Rodlike bloedite crystals a: general view b: detailed view.

Figure 18- Mid-lake polygonal desiccation cracks.

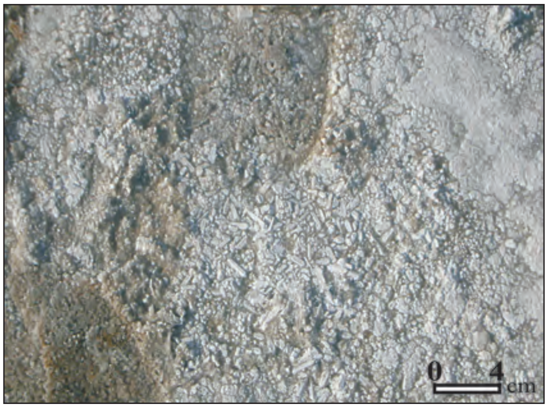

Figure19- Bloedite crystals within brecciated structure developed under the influence of desiccation.

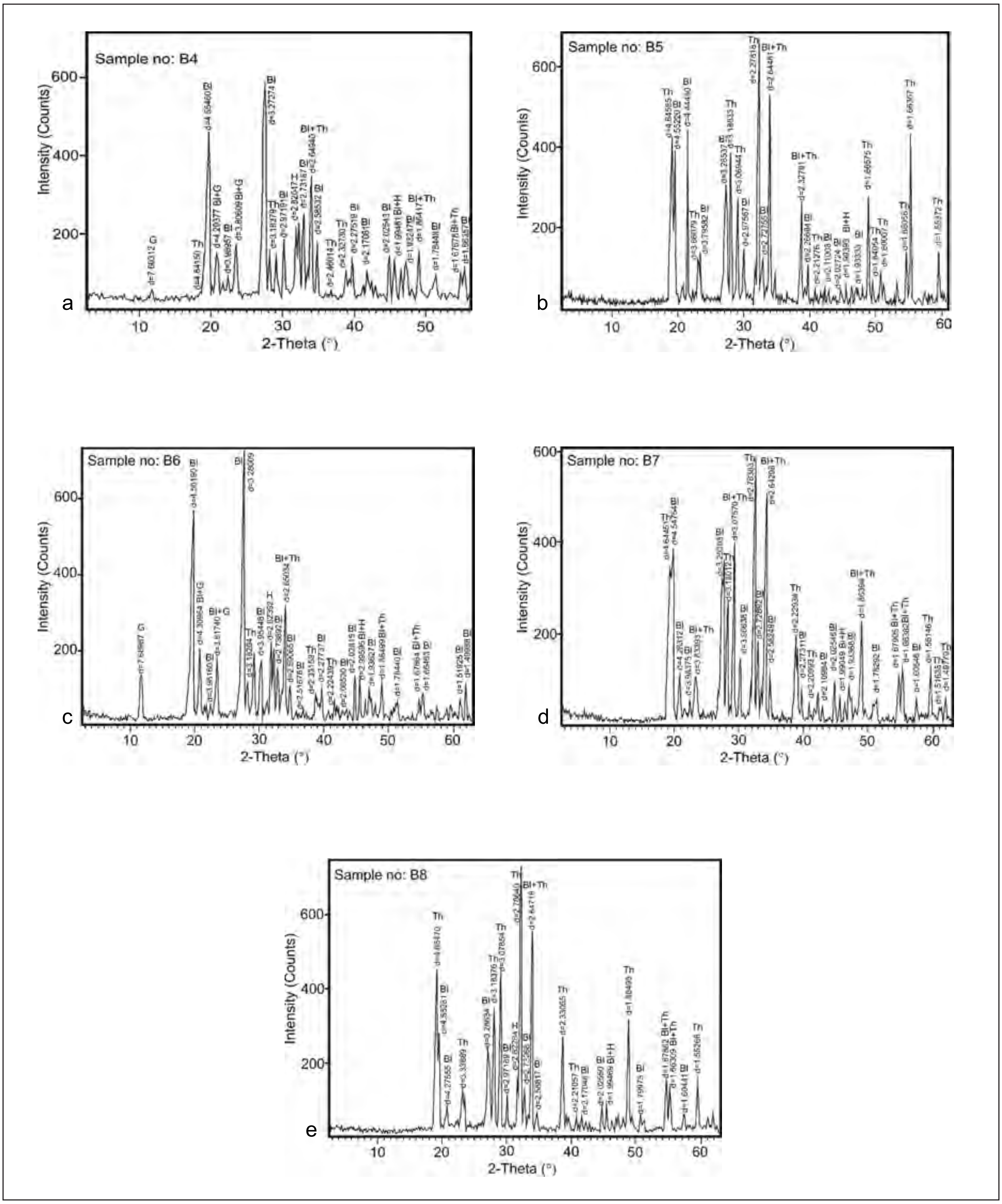

Figure 20- XRD diffractograms of the samples taken from Bloedite+Thenardite zone; G:gypsum, Bl:bloedite, H:halite, Th:thenardite, a:sample B4, b:sample B5, c:sample B6, d:sample B7, e:sample B8.

the bloedite - gypsum zone lying to the west of Ýshaklý playa lake bloedite, thenardite, halite and very little gypsum have been determined (Figure 21 a,b). And the chemical analyses of these samples show high proportions of Na_2O and SO_3 (Table 6).

The fact that the bloedite + gypsum zone lying to the west of Ýshaklý playa lake contains higher proportions of Na_2O and SO_3 compared to the zone lying to the east of the lake, according to the results of the analyses, and the mineralization seems to be thicker in the west side compared to the east side makes one think that feeding from the west might be more effective in the lake.

Through SEM examinations the mineralogical relation of the bloedite-thenardite association determined by XRD analyses was tried to be defined. Besides, by performing EDS point analyses on the crystals (Figure 22 b, d, f), (Figure 23 b), different forms of the minerals were defined. It has been observed that thenardite minerals, seen as rodlike and zoned (Figure 23 a, c) have grown on semi-idiomorphic, tabular bloedite crystals (Figure 22 a, c, e) and crystallized after bloedite (Figure 24 a, b).

CONCLUSIONS

In Turkey, the existence of actual precipitation of bloedite, which is an economically important Na-sulfate mineral, has been determined for the

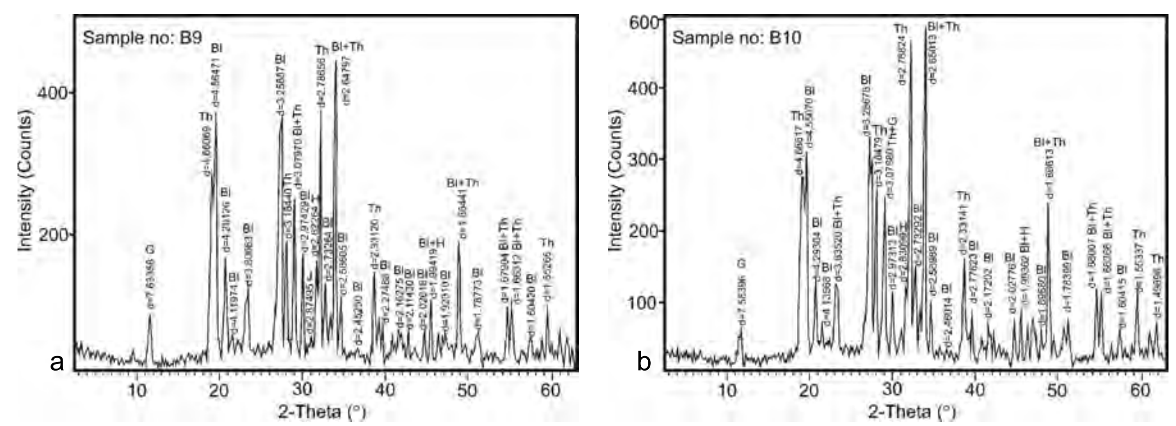

Figure 21 - XRD diffractograms of Samples B9 and B10; G: gypsum, Bl: bloedite, H: halite Th: thenardite a: Sample B9, b: Sample B10.

Table 6- Chemical analyses of Samples B9 and B10 (Oxide values are given as weight %).

Sample No	Na_2O	MgO	Al_2O_3	SiO_2	K_2O	CaO	Fe_2O_3	SO_3	Cl	MnO	P_2O_5	TiO_2	SrO	L O I
B9	24.7	6.7	0.1	0.3	0,1	1.8	0,1	50.3	0.02	<0,1	<0,1	<0,1	0,05	15.80
B10	26.1	5.7	0.1	0.6	0.1	1.4	0,2	47.1	0.02	<0,1	<0,1	<0,1	0,05	18.65

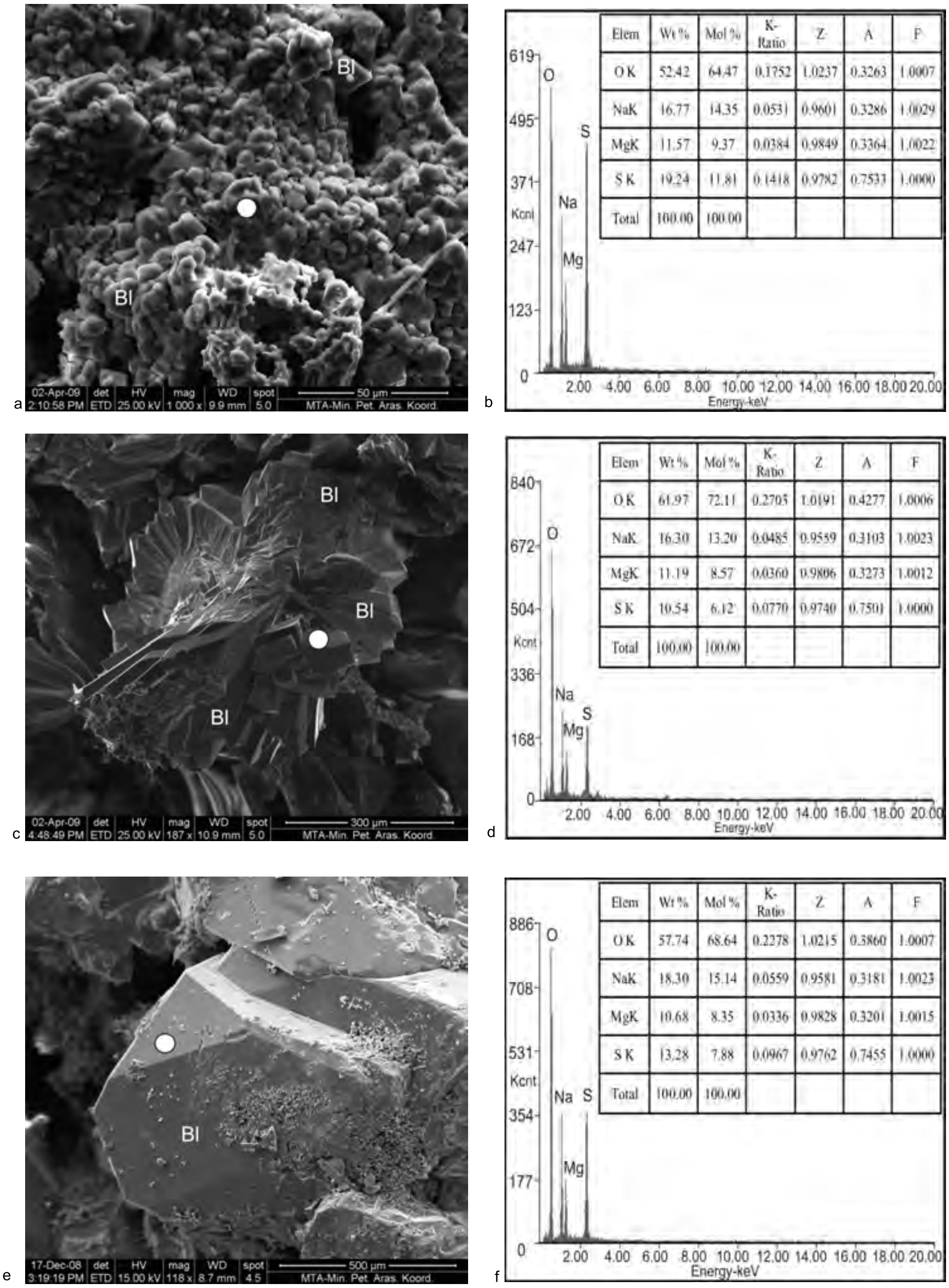

Elem	Wt %	Mol %	K-Ratio	Z	A	F
O K	52.42	64.47	0.1752	1.0237	0.3263	1.0007
NaK	16.77	14.35	0.0531	0.9601	0.3286	1.0029
MgK	11.57	9.37	0.0384	0.9849	0.3364	1.0022
S K	19.24	11.81	0.1418	0.9782	0.7533	1.0000
Total	100.00	100.00				

Elem	Wt %	Mol %	K-Ratio	Z	A	F
O K	61.97	72.11	0.2705	1.0191	0.4277	1.0006
NaK	16.30	13.20	0.0485	0.9559	0.3103	1.0023
MgK	11.19	8.57	0.0360	0.9806	0.3273	1.0012
S K	10.54	6.12	0.0770	0.9740	0.7501	1.0000
Total	100.00	100.00				

Elem	Wt %	Mol %	K-Ratio	Z	A	F
O K	57.74	68.64	0.2278	1.0215	0.3860	1.0007
NaK	18.30	15.14	0.0559	0.9581	0.3181	1.0023
MgK	10.68	8.35	0.0336	0.9828	0.3201	1.0015
S K	13.28	7.88	0.0967	0.9762	0.7455	1.0000
Total	100.00	100.00				

Figure 22- Bloedite crystals a: Blodite mineral associaton (B4), b:EDS point analysis done on bloedite crystal (B4), c: Tabular bloedite crystal (B7), d: EDS point analysis done on tabular crystal (B7), e: Semi-idiomorphic bloedite crystal (B10), f: EDS point analysis done on semi-idiomorphic bloedite crystal (B10), (O: EDS analysis measurement point on the crystal).

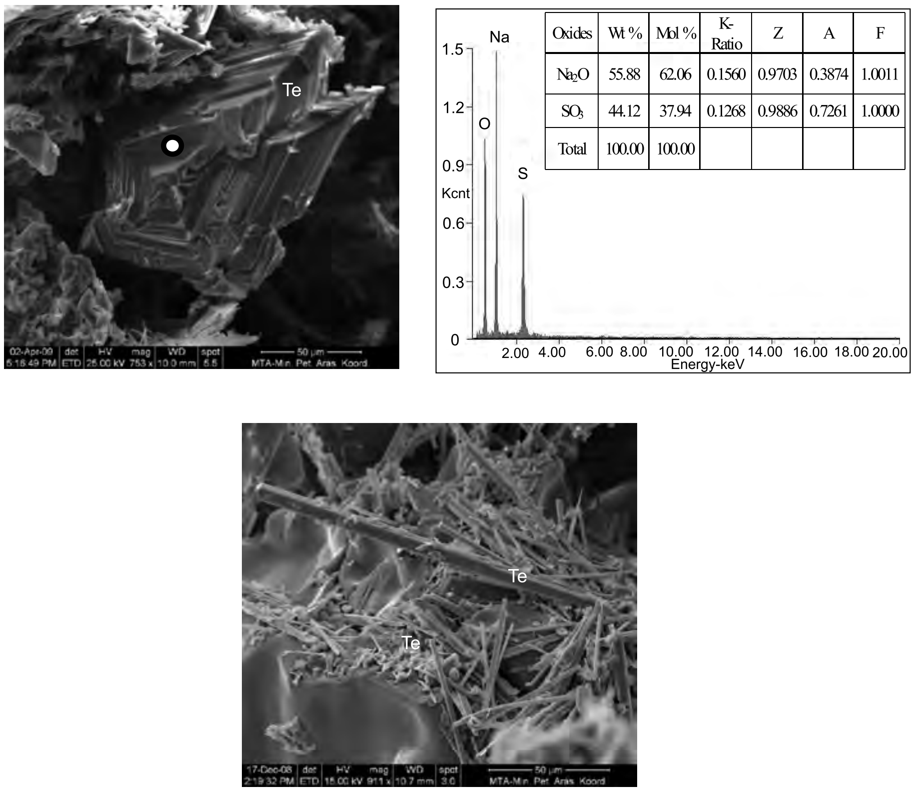

Oxides	Wt %	Mol %	K-Ratio	Z	A	F
Na_2O	55.88	62.06	0.1560	0.9703	0.3874	1.0011
SO_3	44.12	37.94	0.1268	0.9886	0.7261	1.0000
Total	100.00	100.00				

Figure 23- Thenardite crystals a: thenardite crystals in zoned structure (B9), b: EDS point analysis done on thenardite crystal in zoned structure (B9), c: rodlike thenardite crystals (B9).

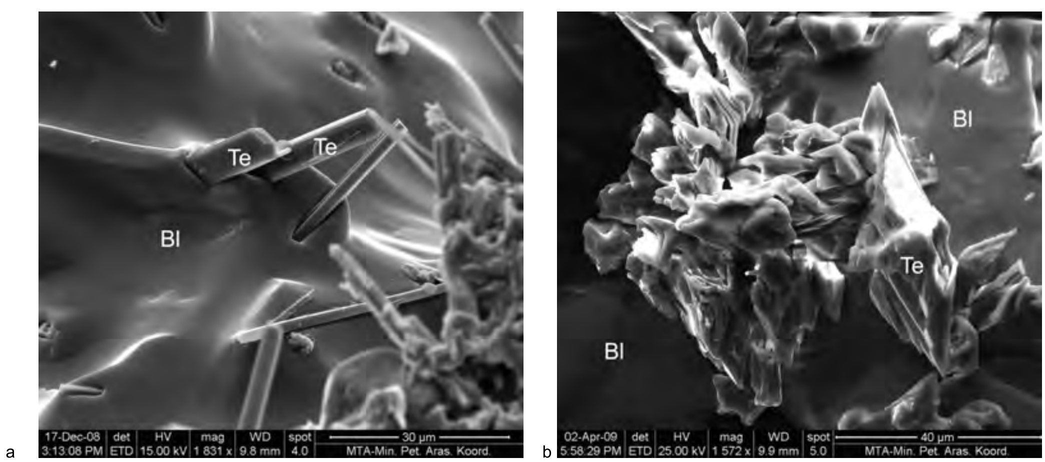

Figure 24- Thenardite crystals on bloedite crystal a: rodlike thenardite crystal (B9), b: disc-shaped thenardite crystal (B9).

first time in Ýshaklý playa lake in Çankýrý-Çorum Basin. Through analyses it has been determined that thenardite, very little halite and gypsum accompany this occurrence.

According to the mineralogical zone map of the Ýshaklý playa lake, lake area has been divided into four different zones. These are from the outermost to the innermost: 1. zone: gypsum+ calcite zone, 2. zone: gypsum + calcite + bloedite zonu, 3. zone: bloedite + gypsum zone and 4. zone: bloedite + thenardite zone. According to the results of the analyses of the samples taken from these zones, the fact that the bloedite-gypsum zone mineralization lying to the west of the lake is thicker and contains higher proportions of Na_2O and SO_3 makes one think that feeding from the west side of the lake might be more effective.

During SEM examinations it has been clearly determined that in the bloedite-thenardite association thenardite mineral grows on bloedite crystals and crystallizes after bloedite.

In the core drilling performed in the gypsum-calcite zone forming the mudflat of the lake, a halite layer of 592 m in total has been cut. Although no net evidence of bloedite - thenardite association has been observed, detailed analyses and drillings have been continuing.

This mineralization, currently formed through evaporation of lake water, corresponds to a proven economical reserve of around 125,000 tons (bloedite+thenardite) with an average mineral thickness of 3 cm over a pond area of about 187,500 m^2. However, after harvesting this precipitated reserve, the duration and thickness of the new precipitation should be observed. Only after these data have been obtained, it will be possible to decide whether the field is economic in terms of Na-sulfate or not.

More detailed works are needed in order to determine whether this surface mineralization is fed by a buried deposit or it develops through the process of evaporation at the surface which follows the ionic enrichment (Na,Mg) in the ground water.

Besides, the reason why the very thick halite (NaCl) mineralization cut in the basin does not accompany this actual precipitation should be searched. In addition, detailed data should be produced taking into consideration such factors as the origin of the chemistry of ground water feeding the system, actual tectonics and hydrogeology.

ACKNOWLEDGMENTS

This work includes some data obtained within the scope of Central Anatolian Industrial Raw Materials Exploration Project conducted by the General Directorate of the Mineral Research and Exploration (MTA). I would like to express my thanks to Prof. Dr. Baki Varol (Ankara University) for his contributions to the field and office works, to Ýnciser Girgin (MTA) and Okan Zimitoðlu (MTA) for their contributions to XRD and SEM examinations, to Haþim Aðrýlý (MTA) for his encouragement and to M. Ali Yastý (MTA) for his help in drawings.

Manuscript received April 8, 2009

BIBLIOGRAPHY

Akyürek, B., Bilginer, E., Akbaþ, B., Hepþen, N., Pehlivan , Þ., Sunu, O., Soysal, Y., Çatal, E., Daðer, Z., Sözeri, B., Yýldýrým, H. and Hakyemez, Y. 1982. Ankara - Elmadað - Kalecik dolayýnýn temel jeolojisi Mineral Research and Exploration General Directorate, Report no: 7298, Ankara (unpublished).

Aziz, A.1972. Ýskilip civarý ile güney ve güney batýsýnýn jeolojisi ve petrol olanaklarý: Mineral Research and Exploration General Directorate, Report no: 6132 (unpublished).

Birgili, S.,Yoldaþ, R. and Ünalan, G. 1975. Çankýrý-Çorum havzasýnýn jeolojisi ve petrol olanaklarý: Mineral Research and Exploration General Directorate, Report no. 5621. (unpublished).

Çelik, E., Kayakýran S. and Kartalkanat A., 1987 Çayýrhan doðal sodyum yataðý maden jeolojisi raporu ve dünyada sodyum sülfat, Mineral Research and Exploration General Directorate. Report, no: 8206 Ankara (unpublished).

Dromart, G. and Dumas, D., 1997. The Salt Basin of Valence (France): In: (Sedimentary deposition in Rift and Foreland Basins in France and Spain (Eds. G. Busson and B.Ch. Schreiber) pp. 195-239, Columbia University Press, New York.

Ergun, O.N., 1977. Sedimentology and Tertiary evaporites, Uðurludað Area Çankýrý - Çorum basin, Turkey. PhD Thesis, Imperial College, London, 260 p. (unpublished).

Görür, N., Oktay, F. Y., Seymen, Ý. and Þengör , A. M. C. 1984. Paleotectonic evolution of the Tuzgölü Basin complex, Central Turkey. Sedimentary record of a Neo-Tethyan closure, In: (Eds. Dixon, J. E. and Robertson, A. H. F.) The geological evolution of the eastern mediterranean: Geological Society of London Special Paper, 17, 467-482.

Gündoðan, Ý., 1994, Geology, mineralogy, geochemistry and economic potential of the Bolluk Lake and the adjacent area Cihanbeyli - Konya. Yüksek Lisans Tezi, Dokuz Eylül Üniversitesi, Ýzmir, 79s (unpublished).

_____, 2000. Geology, mineralogy - petrography and economic potential of the Upper Miocene evaporites in the Beypazarý and Çankýrý-Çorum Basins. PhD Thesis, Dokuz Eylül University, 254 p (unpublished).

_____ and Helvacý, C., 2001. Sedimentological and petrographical aspects of Upper Miocene evaporites in Beypazarý and Çankýrý - Çorum Basins, Turkey. International Geology Reviews. 43, 818-829.

Hakyemez, Y., Barkurt, M.Y., Bilginer, E., Pehlivan, Þ., Can, B.; Daðer, Z. and Sözeri, B., 1986. Yapraklý Ilgaz - Çankýrý - Çandýr dolayýnýn jeolojisi: Mineral Research and Exploration General Directorate Report no: 7966 (unpublished).

Helvacý, C., Ýnci, U., Yýlmaz, H. and Yaðmurlu, F., 1989. Geology and Neogene Trona Deposit of the Beypazarý region, Turkey, Doða Türk Mühendislik ve Çevre Dergisi, 13/2, 245-256.

Karadenizli, L. 1999. Çankýrý - Çorum Havzasý'ndaki Orta Eosen - Erken Miyosen Tortullarýnýn Sedimantolojisi, PhD Thesis Ankara University, 189 p (Unpublished).

_____ and Kazancý, N. 2000. Çankýrý-Çorum havzasýndaki paleo - yükselti ve alt havzalar. Cumhuriyetin 75. yýldönümü yerbilimleri ve madencilik kongresi, Mineral Research and Exploration General Directorate, Ankara, Bildiriler 209-227.

_____, Saraç, G., Þen, Þ., Seyitoðlu, G., Antoine, P.O., Kazancý, N., Varol, B., Alçiçek, M.C., Gül, A., Erten, H., Esat, K., Özcan, F., Savaþçý, D., Antoine, A., Filoreau, X., Hervet, S., Bouvrain, G., De Bonis, L. and Hakyemez, Y., 2004. Çankýrý-Çorum Havzasýnýn batý ve güney kesiminin memeli fosillere dayalý Oligo-Miyosen biyostratigrafisi ve dolgulama evrimi. Mineral Research and Exploration General Directorate, Report no: 10706 Ankara (unpublished).

Kaymakçý, N., 2000. Tectono-stratigraphical evolution of the Çankýrý basin (Central Anatolia Turkey). PhD Thesis, Univ. Utrecht, Geologia Ultraiectina. 190, 247 p.

Koçyiðit, A., 1991. Changing stress orientation in progressive intracontinental deformation is indicated by the Neotectonics of the Ankara Region (NW Central Anatolia). Bulletin of Turkish Petroleum Geologists, 3 (1), 43-55.

Ordonez, S. and Garcia del Cura, M.A., 1994. Deposition and diagenesis of sodium-calcium sulfate salts in the Tertiary saline lakes of the Madrid basin, Spain. In: (Eds. R.W. Renault and W.M. Last). Sedimentology and Geochemistry of modern and ancient saline lakes SEPM Spec. Publ., 50, 229-238.

Orti, F. and Rosell, L., 2000. Evaporative systems and diagenetic patterns in the Calatayud Basin (Miocene, central Spain). Sedimentology, 47, 665-685.

Salvany, J. M., 1997. Continental evaporitic sedimentation in Navarra during the Oligocene to Lower Miocene: Falces and Lerin Formations. In: Sedimentary deposition in rift and foreland basins Ýn France and Spain, Paleogene and Lower Neogene (Eds. G. Busson and B. Ch. Schreiber), 397-419, Columbia University Press, New York.

_____ and Orti,F., 1994. Miocene glauberite deposits of Alcanadre, Ebro Basin, Spain, sedimentery and diagenetic processes, Sedimentology and Geochemistry of modern and ancient saline lakes (Eds R. W. Renault and W. M. Last), SEPM Special Publucation, 50, p. 203-215.

_____, Veigas, J. G., and Orti F., 2007. Glauberite-halite association of the Zaragoza Gypsum Formation (Lower Miocene, Ebro Basin, NE Spain), Sedimentology 54, 443-467.

Seyitoðlu. G., Kazancý, N., Karakuþ, K., Fodor, L., Araz. H. and Karadenizli, L., 1997. Does continuous compressive tectonic regime exist during Late Palaeogene to Late Neogene in NW Central Anatolia, Turkey? Preliminary observations. Turkish Journal of Earth Sciences, 6, 77-83.

Seyitoðlu, G., Kazancý,N., Karadenizli, L., Þen, Þ., Varol, B. and Karabýyýkoðlu, T., 2001. Rockfall avalanche deposits associated with normal faulting in the NW of Çankýrý basin: Implication for the post-collisional tectonic evolution of the Neo-Tethyan suture zone. Terra Nova, 12/6, 245-251.

Þengör, A. M. C. and Yýlmaz, Y. 1981. Tethyan evolution of Turkey: A plate tectonic approach. Tectonophysics, 75, 181-241.

Türkel, K. and Ertok, H., 2001. 8. Beþ Yýllýk Kalkýnma Planý, Özel Ýhtisas Komisyonu Raporu, Endüstriyel Hammaddeler Alt Komisyonu, Cilt II, Sodyum Sülfat Çalýþma Raporu, s 113-150.

Tüysüz, O. and Dellaloðlu, A.A., 1992. Çankýrý havzasýnýn tektonik birlikleri ve havzanýn Jeolojik evrimi. Türkiye 9. Petrol Kongresi Bildirileri özeti, 180 .

Varol, B., Araz, H., Karadenizli, L., Kazancý, N., Seyitoðlu, G. and Þen, Þ., 2002. Sedimentology of the Miocene evaporitýc succession in the North of Çankýrý - Çorum Basin, central Anatolia, Turkey. Carbonates and Evaporites, 17/2, 197-209.

Yoldaþ, R., 1982 Tosya (Kastamonu) ile Bayat (Çorum) arasýndaki bölgenin jeolojisi. PhD Thesis, Ýstanbul Üniversity, 311s (unpublished).

bos sayfa

Mineral Res. Expl. Bull., 140, 55-71, 2010

INVESTIGATION OF CRUSTAL STRUCTURE OF TURKEY BY MEANS OF GRAVITY DATA

Selim ARSLAN*, Uður AKIN* and Atakan ALACA**

ABSTRACT.- During this work, the regional gravity data acquired earlier were used and in order to investigate the relations between geology - tectonics and elevation, isostatic map of Turkey, free air anomaly map and Bouguer anomaly maps were obtained, and comparisons with respect to elevations were carried out. For the thickness of the earth crust T = 0.32 - 0.08g relation was used. The best relation was obtained from Bouguer anomaly with +0.65 coefficient; the relation function was obtained as Y = - 72E + 7.77. Thickness of the crust of Turkey is estimated to be 31.4 km where it is the shallowest and 50 km where it is deepest.

Key Words: Turkey, Geophysics, Gravity, Free Air, Boguer, Crustal Thickness, Isostasy, Tectonics

INTRODUCTION

Regional gravity investigations were started in 1973 by General Directorate of Mineral Research and Exploration (MTA), during this work which lasted 15 years measurements were taken from 60648 stations and the work was finished in 1988. The measurements were taken from survey control points at intervals of 3 to 5 km and from points where coordinates could be provided on 1: 25000 scale topographical maps such as schools, mosques, road junctions, stream diversion points, etc. Limited gravity data obtained from Turkish Petroleum Company (TPAO) and General Command of Mapping (HGK) were included in our data.

During the field work Worden Master LaCoste Romberg 344 and 347 gravity meters were used. The international base value taken from Potsdam was transported to airports by HGK. HGK and MTA distrubuted these values throughout Turkey to establish the National Gravity Base Network.

Seismology which is a branch of geophysical disciplines provides very useful information on the structure of earth crust. Seismic refraction, seismic reflection and distibution of velocity of surface waves as well provide useful information to understand the crustal structure to some extent. Another auxiliary branch is gravity studies. Although it can not provide some adequate resolutions by itself, it provides useful information to support and to contravene the seismic investigations. For crustal structure, isostasy - topographical elevation and topographical elevation - geological factors can be related to propose geological models applicable. Besides, crustal structure and heat flow can be related (Woollard, 1959). The interrelations of Bouguer and elevation values play an important role in understanding the crustal structure (Qureshy, 1970).

In this study, free air, isostasy (Airy) and Bouguer maps were prepared to investigate their relations with elevations, tectonics and geology and then a crustal thickness map of Turkey prepared by use of Bouguer anomaly and elevation data was obtained. The relation T = 32 - 0.08g was used for the crustal thickness of the world during this work (Wollard, 1959).

The Eastern Mediterranean Region which is located on an earthquake belt between Gibraltar and Indonesia and forming an interesting belt

* MTA Genel Müdürlüðü, Jeofizik Etütleri Dairesi - Ankara
** MTA Genel Müdürlüðü, Orta Anadolu I. Bölge Müdürlüðü - Sivas

with its structures similar to island arcs has been investigated by many researchers for gravity anomalies since 1930s. Recent developments have attributed significance to these investigations. Gravity anomalies of the Eastern Mediterranean and Anatolian were combined and related in order to seek a lineer relation between the gravity values and topographical elevations along these profiles (Özelçi, 1973).

In seismology and seismic works, measurement of the crustal waves or interpretation of the data obtained by artifical blasts have been significant for understanding the crustal structure and composition. During these works realized in Marmara, central Anatolia, Eastern Anatolia and Southeastern Anatolia, dynamites blasted in quarries and wells were used. The average crustal thickness for Central Anatolia is calculated as 36 - 40 km, and it was observed that the crust displaying lateral changes is thinner in northwest Anatolia compared to eastern Anatolia. Crustal thickness was measured as 41 km in Aðrý. A 220 km long and NW-SE trending profile transected a tectonically complex structure such as the Arabian - Anatolian plate. Thickness of the crust was measured to be between 38 - 42 km by seismic refraction studies (Bekler et al., 2005).

The surficial waves of the 1999 Turkish earthquakes obtained from the seismic stations located in western Greece were studied mainly for diffractions of Love waves and the crustal thickness of the northwestern Anatolia was calculated as about 33 km (Novotny et al., 2001).

By application of experimental relations to gravity anomaly data, it was determined that the crustal thickness values for Anatolia varies between 26.4 km and 49.5 km (Maden et al., 2005). Later on, two dimensional radial mean power spectrum technique was applied to anomaly map to find the average regional depth as 47 km. At the second stage, the one dimensional sliding window power spectrum method was applied to the same map to investigate the change in structural depths. It was determined as a result of this application that the depths varied between 38 - 52 km and the average crustal thickness is determined as 45 km (Akçýð et al., 2005).

GENERAL GEOLOGICAL STRUCTURE OF TURKEY

Geological structure of Turkey which is located in Alpine - Himalayan Orogenic Belt is dominated by Pan - African basement cropping out locally in some zones and continental zones formed during the evolution process of Tethyan Ocean (Paleo - and Neo - Tethys) and the paleotectonic zones formed by the oceanic suture belts located between them (Figure 1). These tectonic units extending in E - W diection in general were investigated by some researchers (i.e. Ketin 1966; Özgül 1976, 1984; Þengör and Yýlmaz, 1981; Þengör et al., 1984; Þengör 1985; Görür 1987, 1988, 1991; Okay 1989; Koçyiðit et al., 1991; Tüysüz 1993; Görür et al., 1983; Yýlmaz et al., 1994, 1995; Okay et al., 1996; Okay and Tüysüz 1999) for their forms, positions, distributions, contact relations, regional correlations and tectonical evolutions.

When the continental zones and suture belts with tectonic contacts were investigated from north the south, the Istranca Zone is located in northwest Turkey. Gneiss and metamorphic rocks are observed at the basement of the Istranca Zone which is comprised of Istranca Massif and Thrace Basin. On these lithologies, Triassic - Early Jurassic clastic and carbonate rocks which have undergone metamorphism in Middle Jurassic period are observed. These metamorphic rocks were unconformably overlain by Thrace Basin sequence which is comprised of clastics and carbonate rocks deposited during Middle Eocene - Recent (Aydýn, 1974; Kasar and Okay, 1992; Okay et al., 2001). The Istranca Zone is separated by a tectonic contact of a strike slip fault from the Istanbul Zone (Okay and

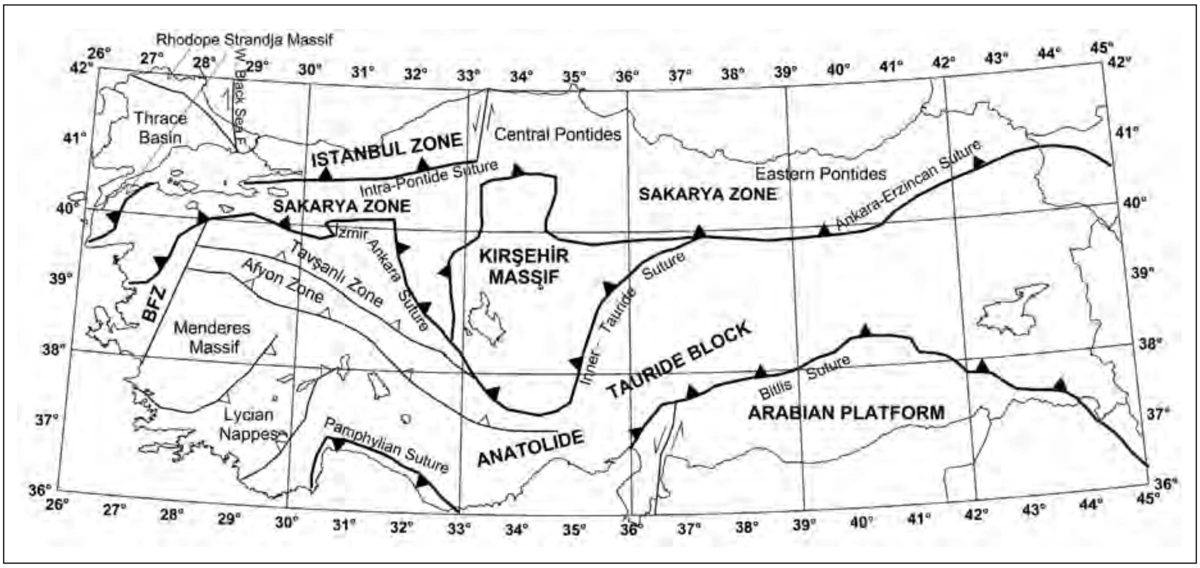

Figure 1- Map showing the structural units and suture zones of Turkey (changed from Okay and Tüysüz, 1999).

Tüysüz, 1999). At the basement of the Istanbul - Zonguldak Zone Pan - African basement rocks comprised of Precambrian gneiss, metagranite and amphibolite are located. This basement is overlain by an unmetamorphosed sedimentary sequence of Ordovician - Carboniferous age comprised of clastic and carbonate rocks (Kozur and Göncüoðlu, 1999; Ustaömer and Robertson, 2005). These Triassic clastics and carbonates unconformably overlie the lower sequences (Þengör and Yýlmaz 1981; Yýlmaz et al.,1995). Late Cretaceous - Eocene volcano - clastic rocks and carbonates are the cover rocks of the Ýstanbul - Zonguldak Zone (Okay et al., 1994; Görür and Okay 1996). Th eInner Pontide Suture separate the Ýstanbul - Zonguldak Zone from the Sakarya Zone (Þengör and Yýlmaz, 1981). Late Cretaceous - Paleocene ophiolitic melange and Late Cretaceous - Eocene blocky flysch are located in Inner Pontide Suture (Okay and Görür,1995; Görür and Okay, 1996). The continental rock assemblage extending between Biga Peninsula and Eastern Black Sea forms the Sakarya Zone. The metamorphic massifs, namely Kazdað, Uludað and Pulur which are comprised of gneiss, marble and metaperidotites located at the basement of the Sakarya Zone have been affected by Hercynian orogeny. These massifs were tectonically overlain by Late Paleozoic - Triassic volcano - sedimentary rock assemblages (Karakaya Complex) which were affected by low grade metamorphism and intensely deformed and include limestone blocks (Bingöl et al., 1973; Okay et al.,1996; Duru et al., 2004). These rocks were transgressively overlain by Early Jurassic - Eocene carbonates and flysch sequence. In this sequence, especially in Eastern Black Sea volcanic products are quite widespread since Late Cretaceous period. Besides, intensive granitic intrusions of Late Paleozoic - Miocene age in Sakarya Zone were observed. The Ýzmir - Ankara - Erzincan Suture located south of the Sakarya Zone represent the north dipping subduction zone (Þengör and Yýlmaz, 1981). This suture is accompanied by highly sheared ophiolitic rocks of Triassic - Cretaceous age and Late Cretaceous blocky flysch (Bornova Flysch Zone) and blueschists and ophiolitic rocks in Tavþanlý Zone (Okay, 1984, 1986; Erdoðan et al.,, 1990). To the south of the Ýzmir - Ankara - Erzncan Suture, the Central Anatolian Massif comprised of high grade metamorphic rocks is located. This crystalline massif which is intruded by Late Cretaceous granitic intrusions was unconformably overlain by clastic and carbonate rocks deposited between Late Maastrichtian - Recent (Erkan, 1975; Göncüoðlu, 1981; Seymen 1982; Gökten, 1986). The Central Anatolian massif is separated from the Tauride platform by the Inner Tauride Suture which is comprised of Late Cretaceous - Eocene ophiolitic rocks (Þengör and Yýlmaz, 1981). To the south of Ýzmir - Ankara - Erzincan Suture and Ýnner Tauride Suture, the Menderes Massif and Taurus Platform are located. The Menderes Massif includes a core and cover units enclosing it (Dürr et al., 1978; Þengör et al., 1984; Konak, 2003). The core is comprised of augen gneiss and migmatites which represent the Pan - African basement. On the other hand, the cover units are constituted by Late Paleozoic - Eocene carbonate and clastic rocks. These lithologies were affected by regional metamorphism. The Taurus Platform is comprised of different tectonostratigraphic units and nappes which include platform, continental margin and oceanic lithologies deposited between Early Paleozoic - Tertiary were thrusted onto each other by Late Cretaceous - Eocene movements and were affected by metamorphism locally (Özgül, 1976; 1984). The Bitlis Suture which the boundary between Taurus Platform and Arabian Platform represents the southern branch of the Neo-Tethys Ocean which existed between Late Triassic and Early Miocene. The widespread ophiolitic nappes in Eastern and Southeastern Anatolia are the remnants of this ocean (Þengör and Yýlmaz, 1981; Dewey et al., 1986). The Arabian Platform located to the south of Bitlis Suture is represented by a basement of oceanic and continental relicts which is intensively deformed and overlying clastic rocks deposited in pre-Late Permian times. The transgressively overlying Late Permian - Tertiary carbonate dominated sequence were deposited on and at the margins of the Arabian Platform (Perinçek, 1980; Perinçek et al., 1991; Þengör and Natal'in 1996).

BOUGUER, ISOSTASY AND CRUST MAPS OF TURKEY

Gravity method is used to analyse the structure of the crust and geological structures. In order to shape the basic scientific frame, and to include the early investigations carried out and the regional research, it is a primary tool to interprete the system. The regional gravity anomaly maps are useful for geographical distributions and the appearance of the basement rocks, for structural and lithological areas, crustal thinning regions, for areas in the lithosphere where masses are missing, for the geometry of the sedimentary basins, and for mapping the volcanic intrusive rocks and their distributions (Kwang et al., 1999).

In this study, density was taken as 2.67 gr/cm^3 for Bouguer anomaly map (Figure 2). During calculation of Bouguer value corrections for tides, latitude, topographical and elevations were made. Density was taken as 2.4 gr/cm^3 for topographical corrections. For latitude correction 1967 international gravitation Formula was used (Blakely, 1995). In latitude corrections the reduction surface is taken as sea level.

The total change of Bouguer anomaly map of Turkey is located between -205 to + 80 mgal. The mean Bouguer value is -66 mgal.

On the Bouguer anomaly map, a positive belt extending between Eastern Black Sea and Mediterranean Sea is observed. This belt probably represents the masses with high density. A negative belt emerging from the east of the Salt Lake and extending to Eastern Anatolia, dominant over the high topography is observed. This belt is observed to reach negative values down to -185 mgal. Here, the thickness of the crust is higher with respect to coastal areas. The Great

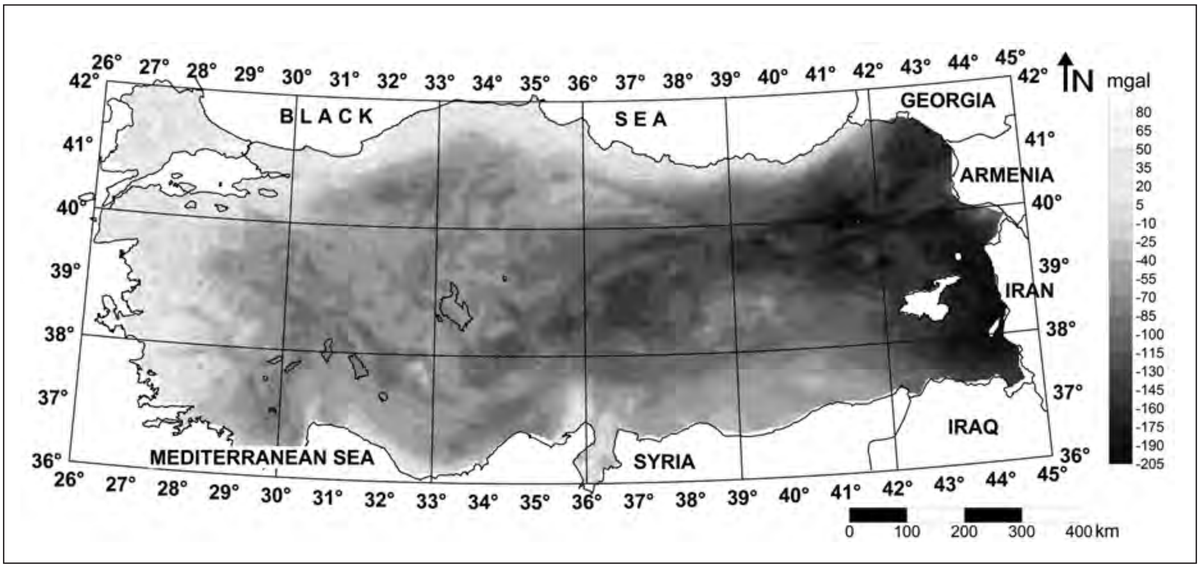

Figure 2- Bouguer gravity map of Turkey.

Menderes, Lesser Menderes and Gediz grabens can clearly be observed on the map.

Whee inconsistencies between the free air gravity and topographical maps are observed geological structures with different densities were indicated. When we look at the free air anomaly map, the positive anomalies extending between the Central Black Sea and Eastern Black Sea, the positive belt to the south of Lake Van, the positive belt to the east of Gulf of Antalya represent mountain ranges located here (Figure 3).

Airy and Pratt explained isostasy concept by two different hyphotheses in 1854 and 1855. Isostasy states the outer layer of the earth and dynamic equlibrium state of the surficial elevations based on the average densities of the underlain rocks. As a result of this theory, the surface of the earth, due to new loads and emoval of loads, move in up and down directions. For this reason, the isostasy concept is very important in describing the lithosphere. The isostatic correction is made to remove the gravity effect of the isostatic root. For isostatic correction and to acquire the maps Oasis Montaj 7.1 software and elevation and bathymetry data of NGDC (NOAA's National Geophysical Data Center) were used provided from the internet address http://www.ngdc.noaa.gov/mgg/topo/gltiles.html.

For regional isostasy calculation the Airy model was adopted (Simpson et al., 1983, 1986). First of all, the Moho depth was calculated from topographical data and then, three dimensional gravity effect extending down to 166.7 km depth of the root (Figure 4). The regional isostatic gravity data was extracted from the Bouguer gravity data to obtain the isostatic residual gravity map (Figure 5). It was observed that Kýrþehir Massif, Sakarya Zone in the north, Arabian Platform in southeast, Anatolide - Tauride Block, and the NW - SE trending Tavþanlý and Afyon Zones are in good harmony with regional isostasy map of Turkey (Figure 4).

On Bouguer Map of Turkey changes between -205 to +80 mgal, and on residual isostasy map changes between -60 to +110 mgal were

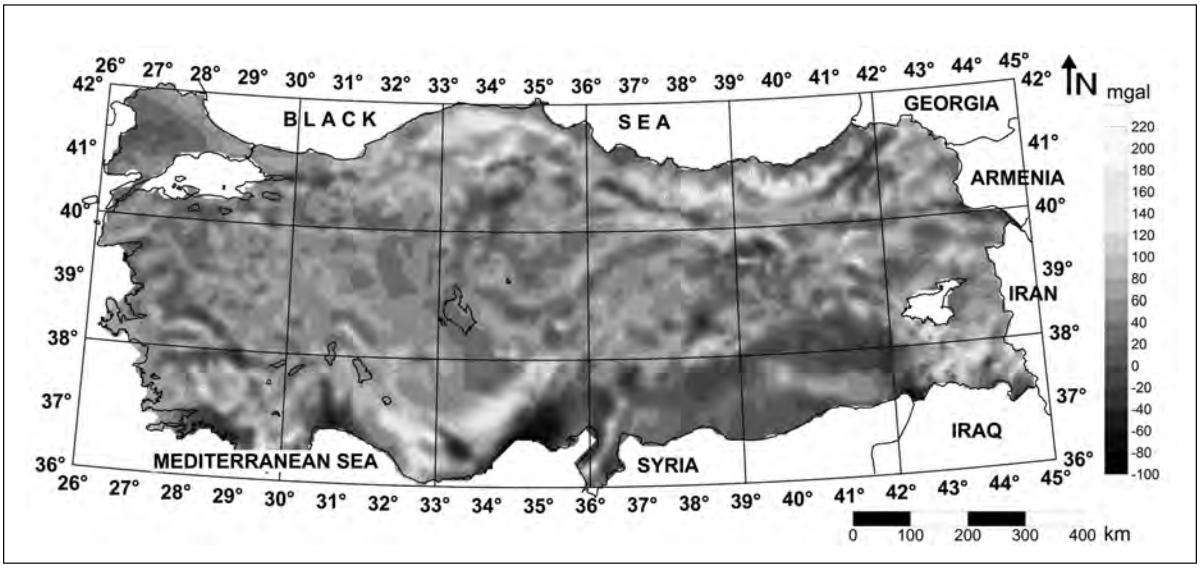

Figure 3- Free air gravity map of Turkey.

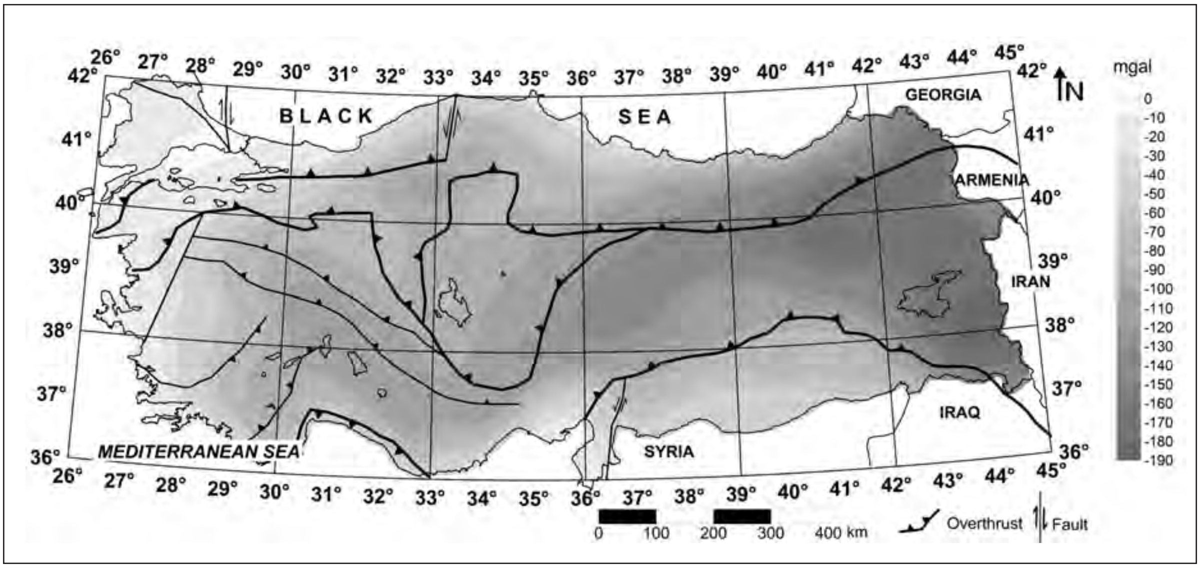

Figure 4- Regional isostasy map of Turkey.

observed. The root effect on Bouguer map was removed up to +110 mgal. The most prominent feature of the isostatic residual map is the removal of the large negative belt observed on the Bouguer map in Eastern Anatolia. This indicates that the effect of isostatic root is quite high.

The Bouguer, free air and isostasy maps were examined and the relations between gravity and elevation were studied. The lineer relation between the gravity data and elevation data were plotted on graphics (Figure 6) and the related information was transferred in Table 1. There are

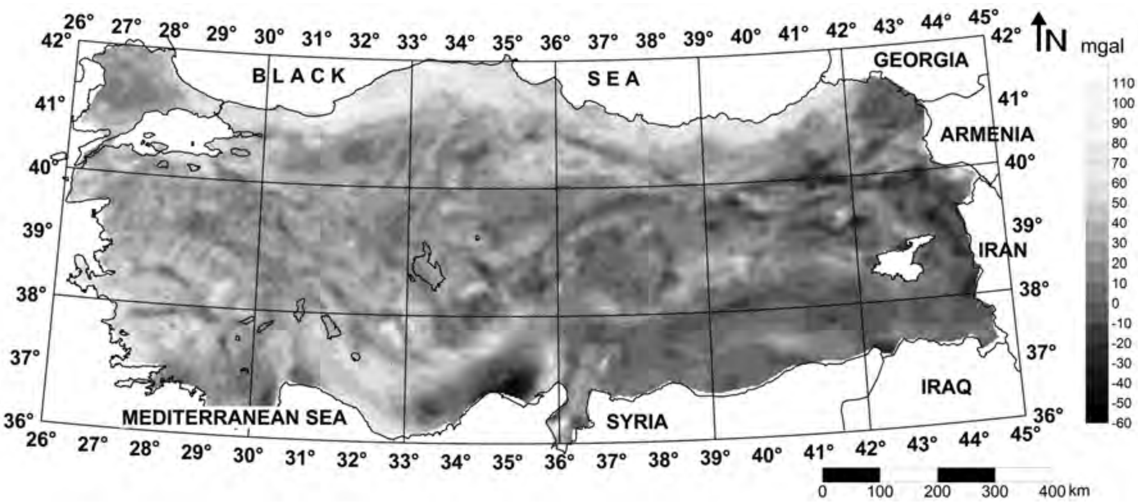

Figure 5- Residual isostasy map of Turkey.

60648 stations in dataset. Statistical relations of each anomaly type was revealed (regression) and their relation coefficients were calculated. The most appropriate relation coefficient (+0.65) was obtained from Bouguer anomaly values.

The regressional equivalence, Y=-72.2E+ 7.77, found for the Bouguer anomaly type as observed in Table 1 is used in Woollard (1959) equation and

$$T = 32-0.08(-72.2E+7.77) = 31.38+5.77E$$

was obtained and crustal thickness map of Turkey was prepared (Figure 7).

The change in crustal thickness was found as 18.6 km. Although the highest crustal thickness was observed in Eastern Anatolia, it was observed that the thickness of crust changed between 34 - 36 km along the Arabian Platform. The abrupt change in thickness between Ýstanbul and Sakarya Zones is remarkable.

Relation of Bouguer Anomaly with Geology and Tectonics

The Bouguer anomaly values observed in Figure 2 changes between -205 to +80 mgal, in total 285 mgal, throughout Turkey. The areas characterized by the lowest average Bouguer anomaly values on the map are: 1. Anatolide - Tauride Block, 2. Kýrþehir Massif, 3. Afyon Zone, 4. Arabian Platform, 5. Lycian Nappes, 6. Tavþanlý Zone, 7. Sakarya Zone, 8. Menderes Massif.

The areas with the highest average values are:

1. Bornova Flysch Zone, 2. Ýstanbul Zone, 3. Thrace Basin (Rhodope - Istranca Massifs).

The lineer relation information obtained from the dataset, intercept values of related geological / tectonic units, dip, relation coefficients, average elevation information, average Bouguer anomaly values and the number of stations were calculated (Table 2).

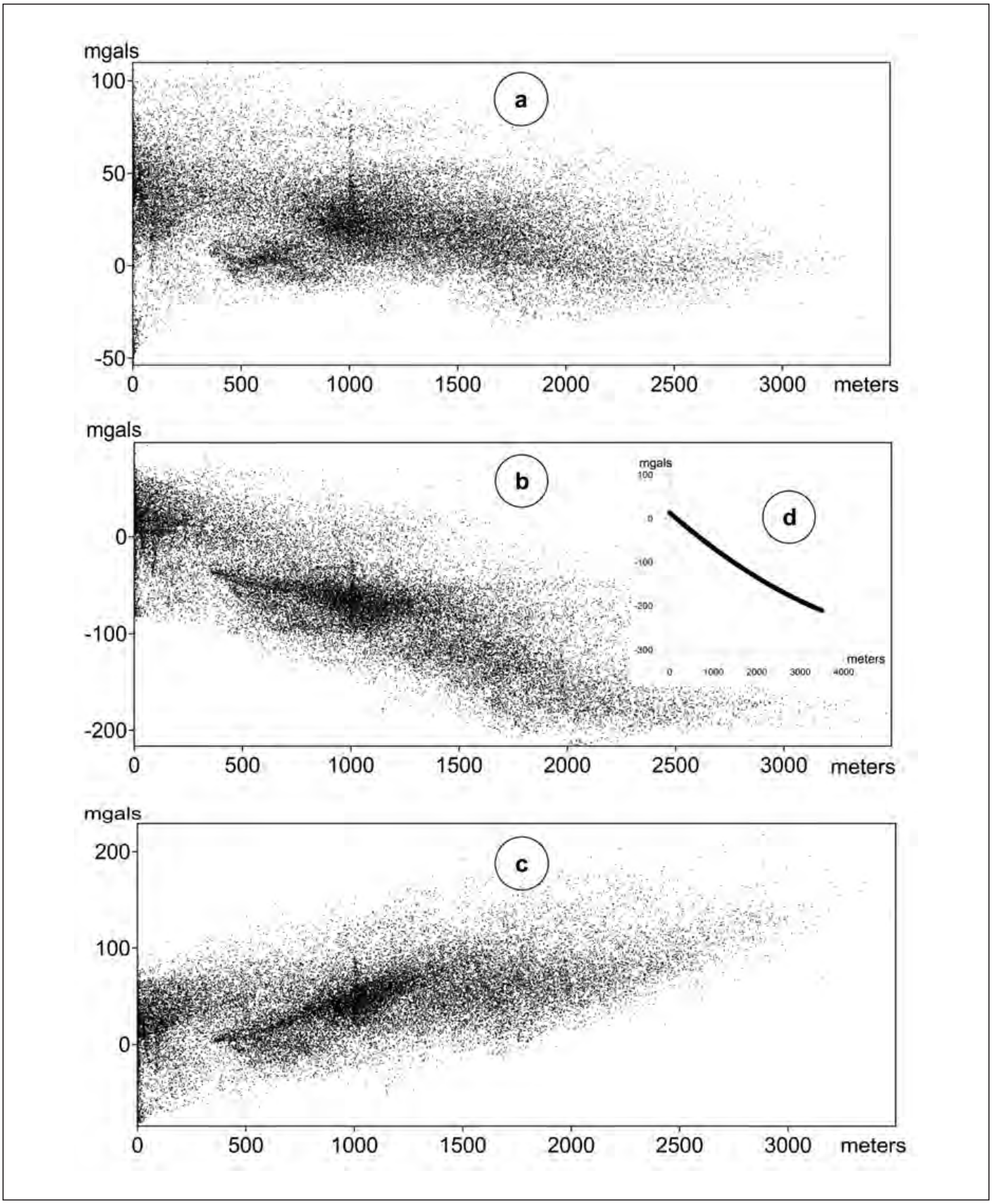

Figure 6- Behaviour of the isostasy (a), Bouguer (b) and free air anomalies (c) by altitude changes; The polynomial relation of second degree between Bouguer and altitude (d).

Table 1- Regressional equivalence for gravity data of Turkey.

Anomaly Type	Regressional equivalence Y mgal, E km	Coefficient of relation	Number of points
Bouguer	Y= -72.2 E +7.77	+0.65	60648
Free Air	Y= 32.7 E +11.9	+0.33	60648
Isostasy - Airy	Y= -11 E +34.75	+0.11	60648

Table 2- Relations between Bouguer anomaly and elevation for different geological and tectonic units.

Geological / Tectonic Unit	Intercept mgal	Dip mgal/km	Relation coefficient	Average elevation (m)	Average Bouguer anomaly (mgal)	Number of stations
Anatolide – Tauride Block	-6.08	-67	0.6	1269	-91.2	29866
Afyon Zone	-27.5	-35	0.3	1117	-66.7	3097
Bornova Flysch Zone	13.2	-5.5	0.006	283	11.7	1032
Lycian Nappes	-10	-45	0.4	1018	-56	2798
Menderes Massif	2.7	-23	0.1	515	-14.6	2809
Tavşanlı Zone	-17.1	-39.7	0.3	960	-55.3	2427
Arabian Platform	-33.9	-41	0.3	765	-65.4	7830
İstanbul Zone	40.6	-50.5	0.37	521	14.27	1603
Rhodope - Istranca Massif	33.9	-24	0.1	228	28	715
Kırşehir Massif	-51.8	-25.3	0.2	1097	-79.5	3577
Sakarya Zone	13.3	-61.7	0.6	1031	-50.3	11617
Thrace Basin	15.4	15.3	0.01	139	17.6	1645

Regression relations were calculated for free air anomaly, Bouguer anomaly and isostasy map. Graphics showing the relation between the elevation and isostasy, Bouguer and free air were plotted (Figure 6). The points of isostasy anomaly versus elevation were scattered between -50 mgal and +100 mgal, the dip was found as -11 and the intercept value as 34.75. The relation coefficient is +0.11 (Figure 6a).

The general scattering in Bouguer anomaly versus elevation behaviour was betwen +60 and -200 mgal; the dip was -72.2 and the intercept value was calculated as 7.77 mgal. The relation coefficient is +0.65 (Figure 6b).

The intercept value of the free air anomaly was calulated as 11.9 mgal and the dip is 32.7; the relation coefficient was calculated as +0.33. The general scattering of the points was between -80 and +200 mgal (Figure 6c).

The relation between the Bouguer and elevation obtained by a polynom of second degree is

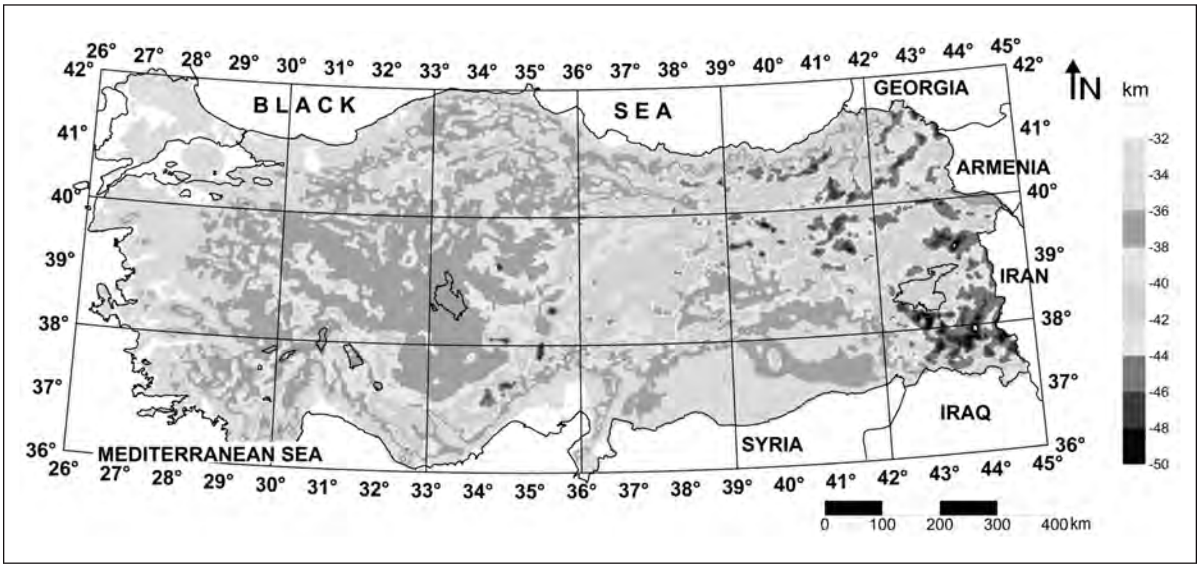

Figure 7- Crustal thickness map of Turkey.

shown in figure 6d. This graphic obtained is in good harmony with the Bouguer anomaly calculated for the world by Woollard (1959).

When we consider the relation coefficient, in relation of Bouguer, free air and isostasy anomalies with elevation, the best harmony was provided in Bouguer anomaly with the value of +0.65.

Five different profiles were shot considering the geology and the structural units in the region. The first four profiles were in roughly N - S direction and were 400 - 600 km long. The fifth profile was in E - W direction and was 1500 km long (Figure 8). In order to see the change in crustal thickness the fault systems and zones (Koçyiðit et al., 2005) cut by the five profiles were shown with abbreviated names such as KAFS: North Anatolian Fault System, IEFZ: Ýnönü - Eskiþehir Fault Zone, TGFZ: Salt Lake Fault Zone, KDAFZ: Northeast Anatolian Fault Zone, DAFS: East Anatolian Fault Zone, OAFZ Central Anatolian Fault Zone.

Along the profile 1 which emerges in Thrace Basin and extends to Anatolide - Tauride Block, the crustal thickening begins at 32 km and the same thickness continues along the Sakarya Zone and reaches to 36 km around the mid - Menderes Massif. In Lycian Nappes region in the southeast, the thickness vary between 37 - 39 km and at the southern end of the profile the crustal thickness drops drastically to 34 km (Figure 9).

The profile 2 which extends between the Ýstanbul Zone and Anatolide - Tauride Zone is 45 km long. The crustal thickness for the Ýstanbul Zone on profile 2 is 32 km and along the Sakarya Zone it reaches to 36 - 37 km. Towards the southern end of the profile, the thickness varies at levels of 1 - 2 km (Figure 10).

The profile 3 extends between the Sakarya Zone and Anatolide - Tauride Block. The crustal thickness is about 36 - 37 km at the beginning of the profile and where the Sakarya Zone is cut by the North Anatolian Fault, it reaches to 40 km. The crustal thickness at Kýrþehir Massif decrease

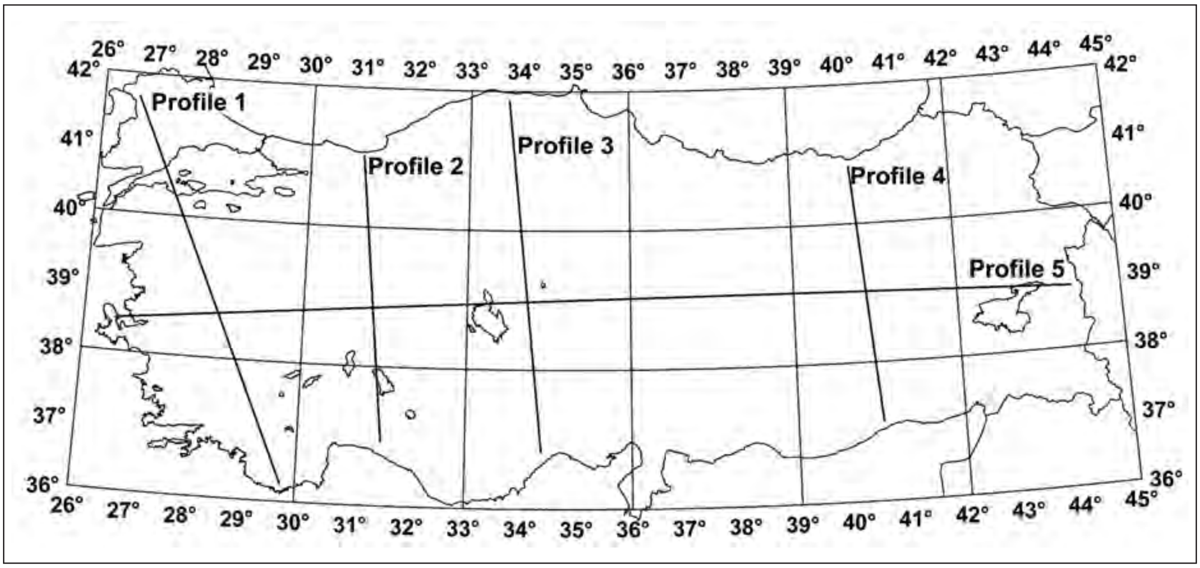

Figure 8- The location of the profiles for determining the crustal thickness.

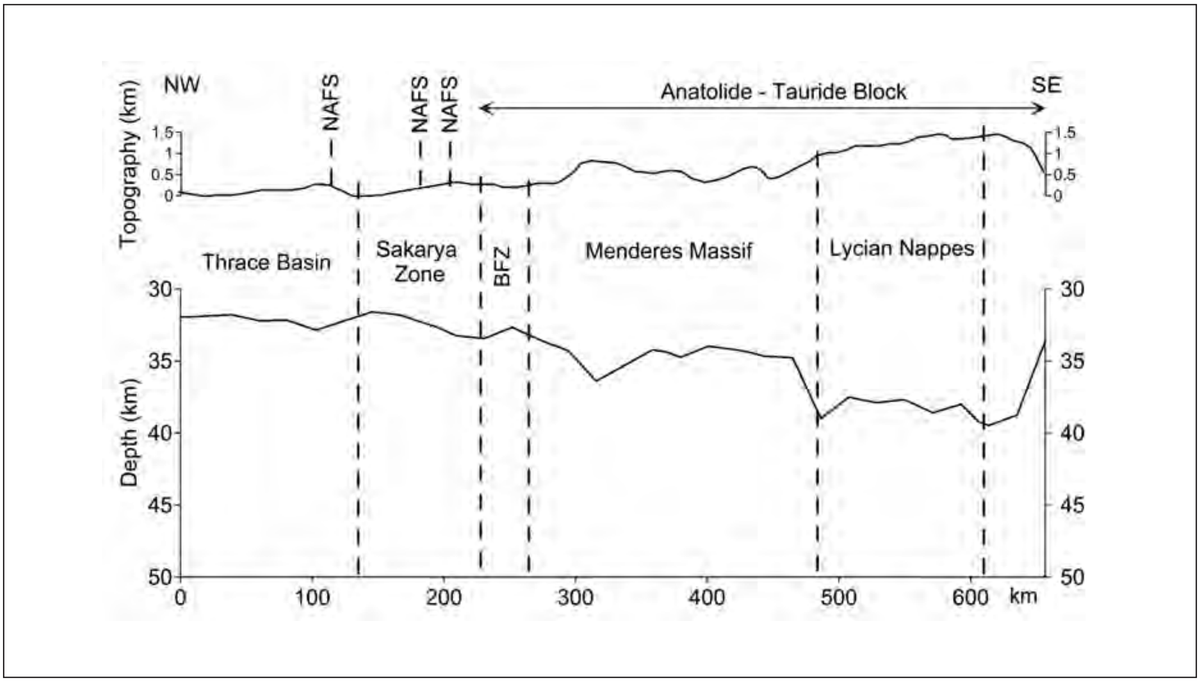

Figure 9- The vertical section of the profile 1 in NW-SE direction showing topography and crustal thickness.

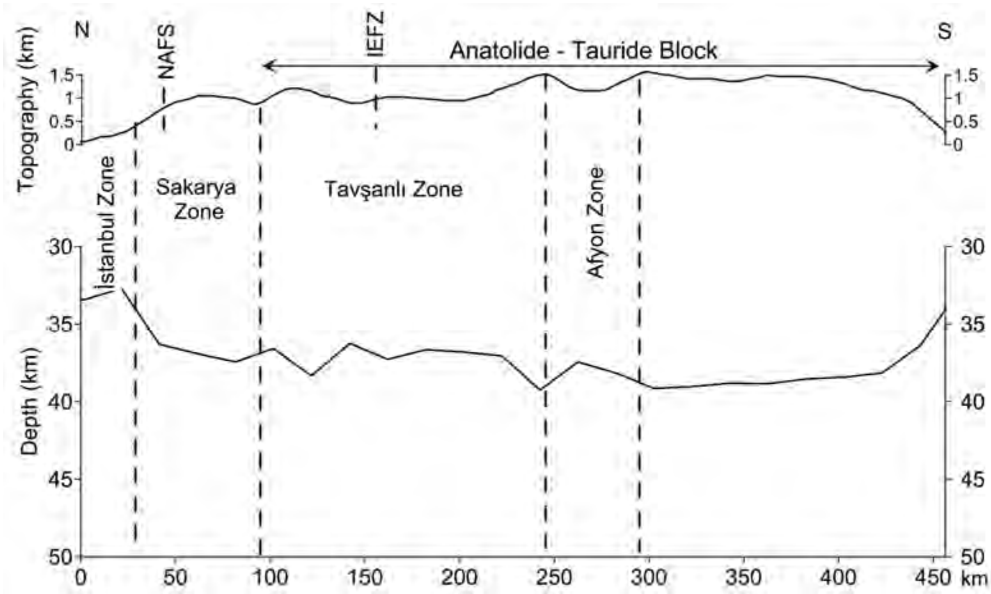

Figure 10- The vertical of the profile 2 in N-S direction slowing topography and crustal thickness.

down to 35 km gradually southward. Where the profile cuts the Afyon Zone the crustal thickness reaches its maximum, 44 km. At the end of this zone, with the emerge of the Anatolide - Tauride Block the thickness drops down to 35 km (Figure 11).

The 400 km long profile 4 which extends between the Sakarya Zone and Arabian Platform the crustal thickness begins with 36-37 km, however, depth reaches to 42-43 km. The crustal thickness of the Anatolide - Tauride Block traversed in this section gets thinner from north to south and drops down to 37 km. Here the crustal thickness of the Arabian Platform is observed as 35 - 36 km (Figure 12).

Along the profile 5 which extends in E - W direction, the amounts of crustal thickness along the traversed sections are as follows: 32 - 34 km at Bornova Flysch Zone, 33 - 37 km at tectonically active Menderes Massif, 37 km at Afyon Zone, 36 -39 km at Tavþanlý Zone, 37 km at Sakarya Zone, 36 - 39 km at Kýrþehir Massif, 37 - 44 km at Anatolide - Tauride Block. It is observed that along the profile 5 the crustal thickening is from west to east (Figure 13).

CONCLUSIONS

During this study using the gravity data Bouguer, free air and isostasy maps were produced. Data of the maps were related to elevation and the relation coefficients were calculated. With +0.65, Bouguer data has given the best results in relation coefficients compared to free air and isostatic data. Bouguer map was taken as basis to calculate the crustal thickness in Turkey.

As a result of calculating the crustal thickness of the whole Turkey regression equivalence was calculated as Y = -72.2 E + 7.77. Besides, different regression relations were found for each tectonic zone in Turkey.

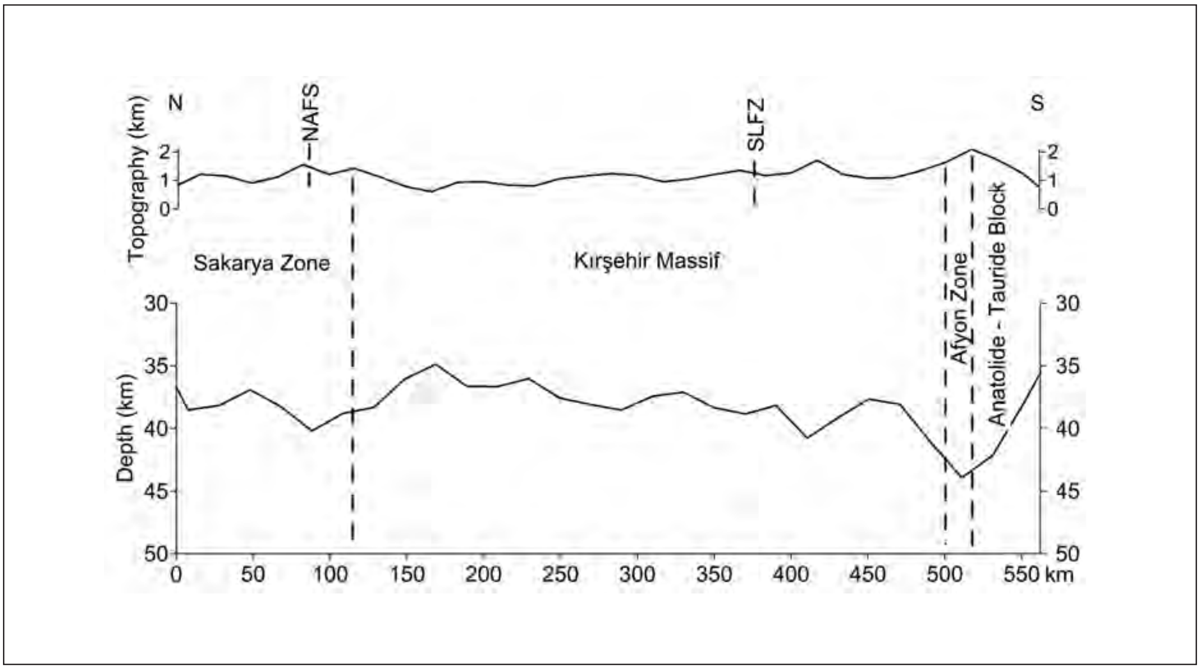

Figure 11- The vertical section of the profile 3 in N-S direction showing topography and crustal thickness.

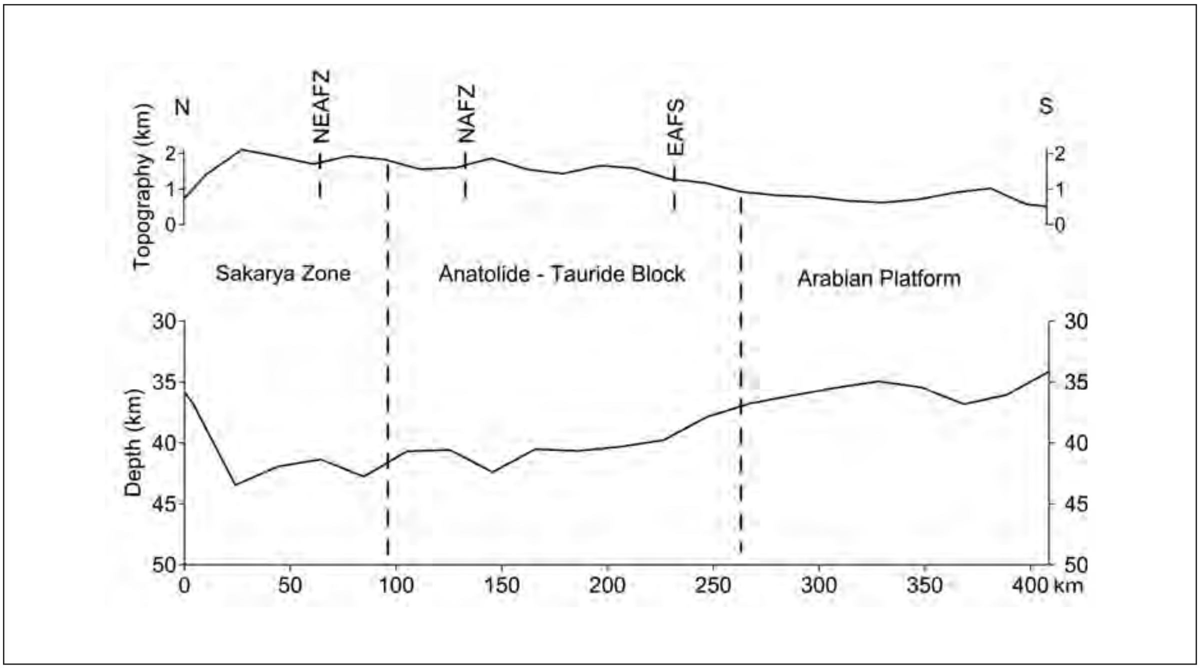

Figure 12- The vertical section of the profile 4 in N-S direction showing topography and crustal thickness.

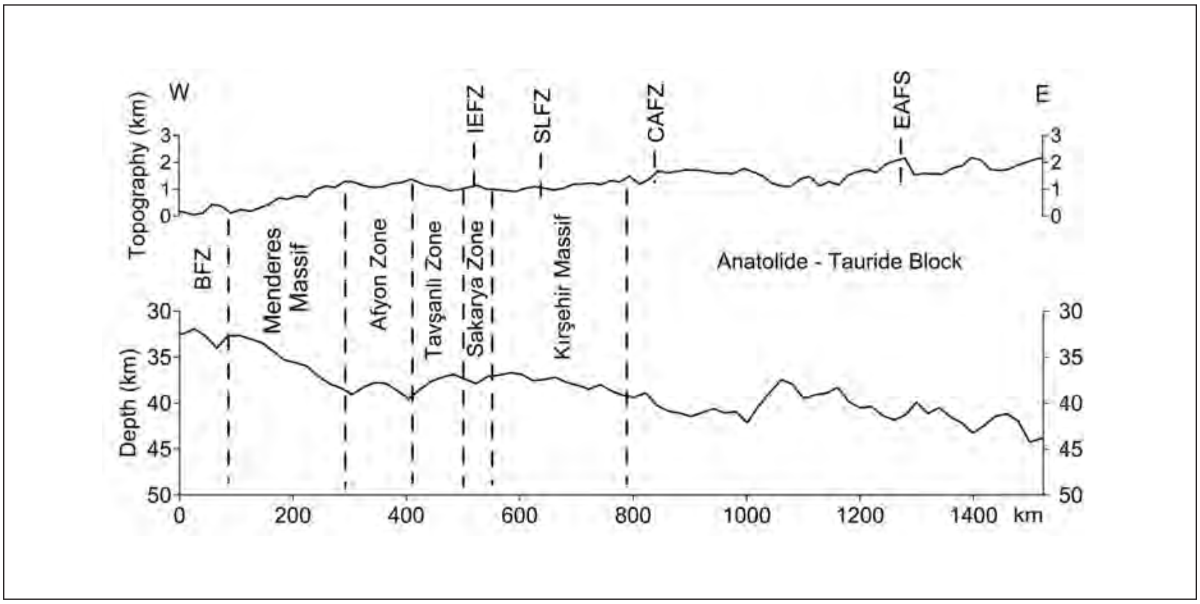

Figure 13- The vertical section of the profile 5 in N-S direction showing topography and crustal thickness.

In crustal thickness map of Turkey, complying with the tectonic activity, crustal thickness is observed in the east. Kýrþehir Massif and western Anatolia displays relative crustal thinning. It was observed that the isostatic regional gravity map and the map showing the tectonic zones and suture boundaries prepared by Okay and Tüysüz (1999) were found to be consistent with each other.

Where the tectonic zones are present, in order to investigate the regional crustal thickness, the crustal thickness data were detailed along 5 profiles. As it can be seen on the crustal thickness map of Turkey, the shallowest crust is measured as 31.4 km while the deepest crust is 50 km.

ACKNOWLEDGEMENTS

We would like thank Dr. Mehmet Duru for their kind help in geological interpretations.

Manuscript received April 21, 2009

REFERENCES

Akçýð, Z., Pýnar, R., Türkelli, N., Gürbüz C., Pamukçu, O. A., Özyalýn, Þ.,Demirbaþ, Þ., and Tosun S., 2005. Doðu Anadolu bölgesindeki yapýsal sorunlarýn gravite ve manyetik yöntemlerle araþtýrýlmasý Tübitak Raporu Proje No: 101Y124.

Aydýn, Y., 1974. Etude petrographique et géochimique de la partie centrale du Massif d'Istranca (Turquie). Thése de Docteur Ingénieur, Univ. Nancy, 1, 131pp.

Bekler, T., Gürbüz, Kalafat, D., and Toksöz N., 2005. Anadolu'da Kontrollü Sismik Kaynak Kullanarak Kabuk Yapýsý Araþtýrmalarý, Deprem Sempozyumu Kocaeli.

Blakely R.J., 1995. Potential Theory in Gravity & Magnetic Aplications. Cambridge University Press. 461 pp.

Bingöl, E., Akyürek, B. and Korkmazer, B., 1973. Biga Yarýmadasý'nýn jeolojisi ve Karakaya Formasyonu'nun bazý özellikleri. Cumhuriyetin 50. yýlý Yerbilimleri kongresi, 17-19 Aralýk 1973, Tebliðler, MTA, Ankara, 70-76.

Dewey, J.F., Hempton, M.R., Kidd, W.S.F., Þaroðlu, F. and Þengör, A.M.C., 1986. Shortening of continental lithosphere: the neotectonics of eastern Anatolia-a young collision zone. In: Covard, M.P. and Ries, A.C., (eds.), Collision Tectonics. Geol. Soc. London Spec. Publ., 19,3-36.

Duru, M., Pehlivan, Þ., Þentürk, Y., Yavaþ, F. and Kar, H., 2004. New results on the lithostratigraphy of the Kazdaðý Masif in NW Turkey, TUBÝTAK, Turkish Journal of Earth Sciences, 13/2, 177-186.

Dürr, S., Altherr, R., Keller, J., Okrusch, M. and Seidel, E., 1978. The Median Aegean crystalline belt: Stratigraphy, structure, metamorphism, magmatism. In: Cloos, H., Roeder, Schmidt, K., (eds), Alps, Apenines, Hellenides. Stuttgart: E. Schweizbart'sche Verlag, 455-477.

Erdoðan, B., Altýner, D., Güngör, T. and Özer, S., 1990. Karaburun Yarýmadasýnýn stratigrafisi. Maden Tetkik ve Arama Dergisi. 111, 1-21. (Foreign Edition: Stratigraphy of Karaburun peninsula. Bull. Min. Res. Exp., 111, 1-20).

Erkan, Y., 1975. Orta Anadolu Masifi'nin güneybatýsýnda (Kýrþehir bölgesinde) etkili rejyonal metamorfizmanýn petrolojik incelenmesi. Doçentlik tezi, H.Ü. Yerbilimleri Enst., Ankara, 147.

Gökten, Y.E., 1986. Paleocene carbonate turbidites of the Þarkýþla region, Turkey - Their significance in an orogenic basin. Sedimentary Geology, 49, 143-165.

Göncüoðlu, M.C., 1981. Niðde Masifi'nin jeolojisi. 35. Türkiye Jeoloji Bilimsel ve Teknik Kurultayý, Ankara, Ýç Anadolu'nun jeolojisi Simpozyumu, 16-19.

Görür, N., 1987. Earth Science Problems Along The First Turkish Geotraverse. Tübitak, Basic Sciences Research Group And Research Institute For Basic Sciences, Earth Sciences Department, Gebze, Kocaeli, Turkey, 5-33.

Görür, N., 1988. Timing Of Opening Of The Black Sea Basin. Tectonophysics, 14, 247-262.

______, 1991. Aptian-Albian Palaeogeography Of Neo-Tethyan Domain. Palaeogeology, Palaeoclimatology, Palaeoecology, 871, 267-288.

______, Þengör, A.M.C., Akkök, R. and Yýlmaz, Y., 1983. Pontidler'de Neo-Tetis'in Kuzey Kolunun Açýlmasýna Iliþkin Sedimentolojik Veriler. T.J.K. Bülteni, 26/1, 11-20

______ and Okay, A.Ý., 1996. A fore-arc origin for the Thrace Basin, NW Turkey. Geologische Rundschau, 85, 662-668.

Kasar, S. and Okay, A. Ý., 1992. Silivri-Kýyýköy-Ýstanbul Boðazý arasýndaki alanýn jeolojisi. T.P.A.O. Raporu, No: 3119, 79s.

Ketin, Ý., 1966. Anadolu'nun tektonik birlikleri. MTA Dergisi, 66, 20-34, Ankara.

Koçyiðit, A., Altýner, D., Farinacci, A., Nicosia, U. and Conti, M.A., 1991. Late Triassic-Aptian Evolution Of The Sakarya Divergent Margin: Implications For The Opening History Of The Northern Neo-Tethys, In North-Western Anatolia, Turkey. In: Farinacci, A., Et Al., (Eds.), Geology And Paleontology Of Western Pontides, Turkey; Jurassic - Early Cretaceous Stratigraphy, Tectonics And Paleogeographic Evolution. Cnr - Tubitak Project, 81-100.

______ and Özacar, A. A., 2003. Extensional neotectonic regime through the NE edge of the Outer Isparta Angle, SW Turkey: New field and seismic data, Turkish J. Earth Sci., 12,67-90.

Konak, N., 2003. Menderes Masifi'nin güneydoðusundaki naplý yapýlar. 56.Türkiye Jeoloji Kurultayý, Bildiri Özleri, 304-306.

Kozur, H.W., Göncüoðlu, M.C., 1999. Differences in the geological evolution of the Istanbul and

Zonguldak terranes, northern Turkey. In: Talent, J., Khan,F., Mawson, R. (Eds.), IGCP 421: Mid-Palaeozoic bioevent/biogeography patterns in relation to crustal dynamics. North Ryde (Macquarie University Printery), Peshawar, Pakistan, pp. 16-18.

Kwang, S. C., Kumar, G.V.R. and Kim K. Y., 1999. Qualitative interpretation of Bouguer anomaly in the southern part of the Korean peninsula. Geosciences Journal Vol. 3, No. 1, p. 49-54.

Maden, N., Geliþli, K., Bektaþ, O. and Eyüboðlu, Y., 2005. Anadolu'da Kabuk Yapýsý ve Tektonik Yapý ile Ýliþkisi II. Mühendislik Bilimleri Genç Araþtýrmacýlar Kongresi MBGAK 2005 Ýstanbul 17-19 Kasým 2005.

Novotn , O., Zahradník, J., and Tselentis, G-A., 2001. Northwestern Turkey Earthquakes and the Crustal Structure Inferred from Surface Waves Observed in Western Greece. Bulletin of the Seismological Society of America; August 2001; v. 91; no. 4; p. 875-879.

Okay, A.Ý., 1984. Distribution and characteristics of the north-west Turkish blueschists. In: Dixon, J.F. and Robertson, A.H.F. (eds.), The Geological Evolution of the Eastern Mediterranean. Geol. Soc. London, Spec. Publ., 17, 297-308.

_____, 1986, High pressure/low temperature metamorphic rocks of Turkey. Geol. Soc. Amer. Mem., 164, 333-348.

_____, 1989. Tectonic Units And Structures In The Pontides, Northern Turkey. In: Þengör, A.M.C. (Ed.), Tectonic Evolution Of The Tethyan Region. Nato Asi Series, Kluwer Academic Publishers, 109-116.

_____, Þengör, A.M.C. and Görür, N., 1994. Kinematic history of the opening of the Black Sea and its effect on the surrounding regions. Geology, 22, 267-270.

_____ and Görür, N., 1995. Batý Karadeniz ve Trakya havzalarýnýn kökenleri arasýnda zaman ve mekan iliþkisi. Trakya Havzasý Jeolojisi Simpozyumu, Bildiri Özleri, TPAO - Ozan Sungurlu Bilim, Eðitim ve Yardým Vakfý, 9-10.

Okay, A.Ý., Satýr, M.,Maluski, H., Siyako, M., Monie, P., Metzger, R. and Akyüz, S., 1996. Paleo-And Neo-Tethyan Events In Northwestern Turkey: Geological And Geochronological Constraints. In: Yin, A. And Harrison, T.M. (Eds), The Tectonic Evolution Of Asia. Cambridge Univ. Press., 420-441.

_____ and Tüysüz, O., 1999. Tethyan Sutures Of Northern Turkey. In: Durand, B., Jolivet, L., Horvath, F., Seranne, M. (Eds.), Mediterranean Basins: Tertiary Extension Within The Alpine Orogen. Geological Society Of London Special Publication, 156, 475-515.

_____ Satýr, M., Tüysüz, O., Akyüz, S. and Chen, F., 2001. The tectonics of the Strandja Massif; late Variscan and mid-Mesozoic deformation and metamorphism in the northern Aegean. International Journal of Earth Sciences 90 (2), 217-233.

Özelçi, F., 1973. Doðu Akdeniz Bölgesi Gravite Anomalileri MTA Dergisi, Sayý 80 Sayfa 54-89 MTA Genel Müdürlüðü Ankara-Türkiye

Özgül, N., 1976. Toroslarýn Bazý Temel Jeoloji Özellikleri. TJK Bülteni, 19/1, 65-78.

_____, 1984. Stratigraphy And Tectonic Evolution Of The Central Taurides. In: Tekeli, O. And Göncüoðlu, M.C. (Eds), Geology Of The Taurus Belt. Int. Symp. Proc., M.T.A., Ankara, 77-90.

Perinçek, D., 1980. Arabistan kýtasý kuzeyindeki tektonik evrimin kýta üzerinde çökelen istifteki etkileri. Türkiye 5. Pet. Kong., Jeoloji-Jeofizik Bildirileri, 77-94.

_____, Duran, O., Bozdoðan, N. and Çoruh, T., 1991. Stratigraphy and paleogeographical evolution of the autochthonous sedimentary rocks in the SE Turkey. Ozan Sungurlu Semp. Bildirileri, Kasým 1991, Ozan Sungurlu Bilim, Eðitim ve Yardým Vakfý, 274-305.

Qureshy, M. N., 1970. Relation of gravity to elevation, geology and tectonics in India. Proceedings of the second symposium on upper manle project 28-31 December 1970, Hyderabad.

Seymen, Ý., 1982. Kaman dolayýnda Kýrþehir Masifi'nin jeolojisi. Doçentlik Tezi, Ý.T.Ü. Maden Fak., 164s.

Simpson, Robert W., Jachens, Robert C. and Blakely, Richard J., 1983. Airyroot: A Fortran Program for Calculating the Gravitational Attraction of an Airy Isostatic Root Out to 166.7 KM: U.S.G.S. Open-File Report 83-883, 66 p.

_____, _____, _____ and Saltus, Richard W., 1986. A New Isostatic Residual Gravity Map of the Conterminous United States With a Discussion on the Significance of Isostatic Residual Anomalies: JGR, 91, 8348-8372.

Þengör, A. M. C. 1985. Türkiye'nin Tektonik Tarihinin Yapýsal Sýnýflamasý. Ketin Simpozyumu, T.J.K., Ankara, 37-61.

_____ and Yýlmaz, Y., 1981. Tethyan Evolution Of Turkey: A Plate Tectonic Approach. Tectonophysics, 75, 181-241.

_____, ______, and Sungurlu, O., 1984. Tectonics Of The Mediterranean Cimmerides: Nature And Evolution Of The Western Termination Of Paleo-Tethys. In: Dixon, J.F. And Robertson, A.H.F. (Eds.), The Geological Evolution Of The Eastern Mediterranean. Geol. Soc. London, Spec. Publ., 17, 117-152.

Þengör, A.M.C. and Natal'in, B., 1996. Palaeotectonics of Asia: Fragments of a synthesis. In: Yin, A. and Harrison, M. (eds), The tectonic evolution of Asia. Rubey Colloquium, Cambridge University Press, Cambridge, 486-640.

Tüysüz,. O.,1993. Karadeniz'den Orta Anadolu'ya bir jeotravers; Kuzey Neo-Tetisin Tektonik Evrimi, Türkiye Petrol Jeologlarý Derneði Bülteni, 5, 1-33.

Ustaömer, T. and Robertson, A.H.F., 2005. Tectonic evolution of the Intra-Pontides suture zone in the Armutlu Peninsula, NW Turkey; reply. Tectonophysics 405 (1-4), 223-231.

Yýlmaz Y., Genç, Þ.C., Yiðitbaþ, E., Bozcu, M. and Yýlmaz, K., 1994. Kuzeybatý Anadolu'da Geç Kretase Yaþlý Kýta Kenarýnýn Jeolojik Evrimi; Türkiye 10. Pet. Kong. ve Sergisi, Bildiriler, Jeoloji, 37-55.

_____, _____, _____, _____ and _____, 1995. Geological Evolution Of The Late Mesozoic Continental Margin Of Northwestern Anatolia. Tectonophyscics, 243, 155-171.

Woollard, G.P., 1959. Crustal Structure from Gravity and Seismic Measurements, J. Geophys. Res., 64 (10), 1524-1544.

Mineral Res. Expl. Bull., 140, 73-79, 2010

PRELIMINARY FINDINGS ON THE FOSSIL TRACES IN THE MASSIVE SULPHITE DEPOSITS OF EASTERN BLACK SEA REGION (LAHANOS, KILLIK AND ÇAYELI)

M. Kemal REVAN*, Taner ÜNLÜ** and Yurdal GENÇ***

ABSTRACT.- Tube worm fossils have been found in the Upper Cretaceous aged massive sulphite deposits of the Eastern Black Sea Region. Similar ones of these tube worm fossils have been found in the massive sulfide deposits of Umman, Cyprus, Ireland and Urals. This fossil community defined in very few massive sulfide deposits in the world is the important evidences of the sea floor hydrothermal vents in Pontids. These worm-like forms can be considered as the ancestral forms of the unusual vent communities defined in places where modern hydrothermal vents are observed such as East Pacific Rise, Galapagos and Juan de Fuca Ridge.

Key Words: Eastern Black Sea, massive sulphide, fossil, hydrothermal vent

INTRODUCTION

Discovery of the faunas living around the hydrothermal sulfur vents on the sea floor drew the interest of the researchers. Some of the most impressive of the unusual organisms are the tube-worms which live in a symbiotic relationship with bacteria. Modern deep-sea hydrothermal vent fields where the present-day deposit occurrences are observed and unusual organisms live extensively have been studied and defined in detail (Hannington et al. 2005; Little, 2002; Rona et al. 1983; Rona, 1984) in several places in the world (for example, East Pacific Rise, Juan de Fuca ridge, Galapagos Ridge). Various researchers stated that iron, zinc and copper sulfide mineral deposit to the sea floor and create massive sulphite deposits because of sudden cooling of the metal and sulfur rich hot fluids by mixing with the sea water while being discharged to the sea floor from the vents (Spooner and Fyfe, 1973; Hebert and Constantin, 1991; Haymon et al. 1984; Qudin and Constantinou, 1984). The reduced sulfur in the hydrothermal solutions constitute the base of a food chain for unusual organisms clustered around the vents. Most common communities observed in the modern hot spring fields include mussel, crab, vestimentiferan tube worm and several fish species. Living areas of the species mussels, anemones, barnacles, limpets and siphonophores are restricted to some hot spring fields (Haymon et al. 1984). It has been observed that some species of vent worms live in fields very close to hydrothermal solutions rising along with these hot spring vents with a temperature of up to 350 ºC (Haymon et al. 1984). Among the relicts of these tube worms, only those that are replaced by the sulphite and sulphate minerals can be preserved. Traces of ecological actualism of these unique organisms that found near present-day vents are rarely encountered in the massive sulfide paleohydrothermal fields (Kuznetzov et al. 1988; Little et al. 1997). Therefore the finding of these fossil traces in the Upper Cretaceous aged massive sulfide deposits in the Eastern Black Sea Region (Figure 1) is a significant data.

STUDY METHOD

Macro structure, texture and mineralogical definitions of the fossil ore samples collected in the Lahanos, Killik and Çayeli beds by cutting to obtain equatorial and axial cross sections and correcting their surfaces in the abrasive machine. In order to determine the opaque and gang mi-

* Maden Tetkik ve Arama Genel Müdürlüðü, Maden Etüt ve Arama Dairesi, 06800, Balgat-Ankara
** Ankara Üniversitesi, Mühendislik Fakültesi, Jeoloji Mühendisliði Bölümü, Tandoðan-Ankara
*** Hacettepe Üniversitesi, Mühendislik Fakültesi, Jeoloji Mühendisliði Bölümü, Beytepe-Ankara

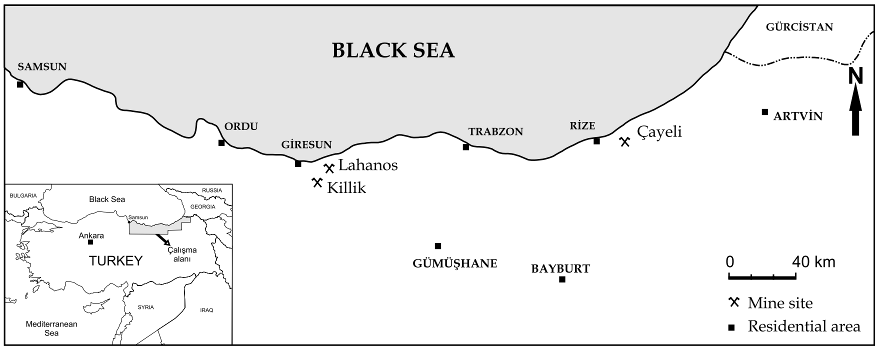

Figure 1 - The location map of mine sites where the fossil findings were detected.

neral content of the fossil traces and fillings, polished and thin sections have been prepared from the samples representing each deposit. Polishing and opaque mineral studies have been carried out in the Ore Microscopy Laboratory of the Geological Engineering Department of the Hacettepe University. Gang minerals that can not be defined with the ore microscope have been determined in the form of dot based mineralogical analyses by using high resolution, analytical Raman microscope Horiba Jobin Yvon Brand Labraun HR (633 laser power) Konfokal Raman Spectrometer in the laboratories of the Geological Engineering Department of Ankara University.

Mineralized fossil traces observed in the massive sulphite deposits of Lahanos, Killik and Çayeli

The dimensions of the of the tube worm fossil traces defined in the Lahanos, Killik and Çayeli deposits reach up to 25 mm diameter and 8 cm length. Worm fossil traces are preserved in the black ore usually consisting of the pyrite and sphalerite (Figure 2B, C, D).

In all three deposit, mineralized tube worm samples are preserved in a sulfide matrix. It has been observed that few fossil traces are replaced by opaque and gang mineral from the exterior to the interior while the inside of the tube fossil traces is filled with mineral fragments such as pyrite, sphalerite, chalcopyrite and galena. As much as it can be observed from the axial and equatorial sections, these replacement cover all of the fossil trace in some samples while it is only in the side sections and the internal part of the fossil trace is left in the shape of a cavity (Figure 3A). In some samples however, side sections of the fossil traces, are replaced by opaque minerals (pyrite and galena), while internal sides are filled by opaque mineral clasts like pyrite, sphalerite, chalcopyrite and galena.

In Lahanos samples, in the fossil traces replaced by opaque minerals from the sides, the sequence of mineral zoning, from the exterior to the interior, is sfalerit + pyrite >> chalcopyrite + pyrite.

The mineral zoning sequence observed in Çayeli samples, from the exterior to the interior is pyrite >> galena (Figure 2B).

In some samples of Killik mine, outer sections of the tube fossil traces are replaced by barite, while the internal sides are infilled by clasts consisting of sulphite minerals (Figure 3B). In a sample taken from Lahanos, whole of the tube worm fossil trace is infilled with barite. This sample contains only barite in the outer sections

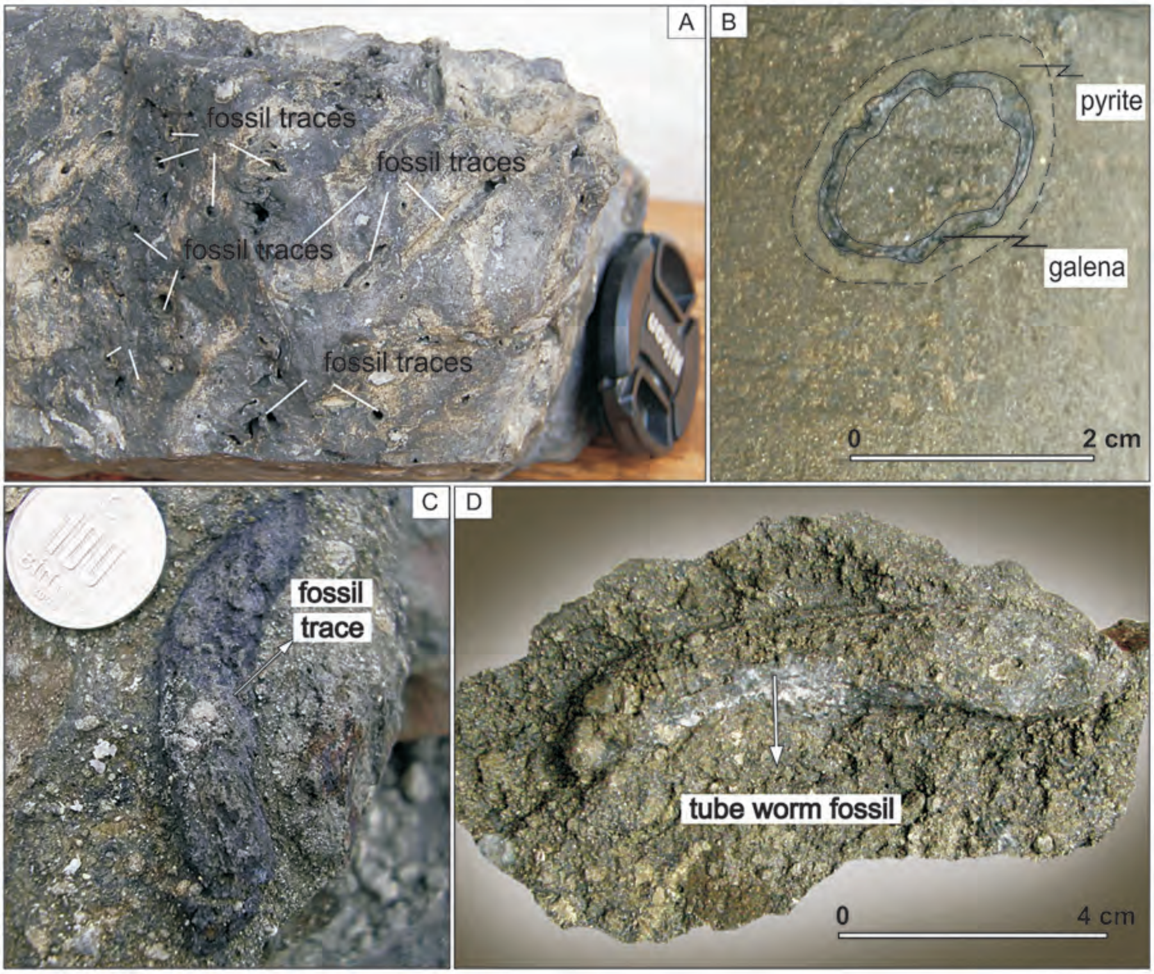

Figure 2 - A - Various forms of tube fossils found in the massive sulphide deposit in the Urals region. Different cross sections of the tube worm fossils in the brecciated sulphides found in massive sulfide deposits of B- Çayeli C- Lahanos and D- Killik.

while the inner sides contain sulphite minerals (pyrite, chalcopyrite, covellite, sphalerite) as well as barite. In the fossil trace fillings, apart from barite (Figure 4) the existence of secondary minerals such as goethite [FeO(OH)], serpierite [$Ca(Cu,Zn)_4(SO4)_2(OH)_6.3(H_2O)$], native sulfur [S] and jarosite [$KFe_3(SO4)_2(OH)_6$] and dolomite [$CaMg(CO_3)$] in amounts that cannot be differentiated by microscope, has detected by Raman Spectrometry (Figure 5).

DISCUSSION AND COMMENTS

Traces of these unique organisms that found near present-day vents are rarely encountered in the massive sulfide paleo-hydrothermal fields. The tubular worm fossil relics were found for the first time by Ivanov (1947) among pyrite minerals in Sybai deposit (Urals). Later, the similar fossil findings were defined in the massive sulfide deposits in Umman (Haymon et al. 1984), Cyprus

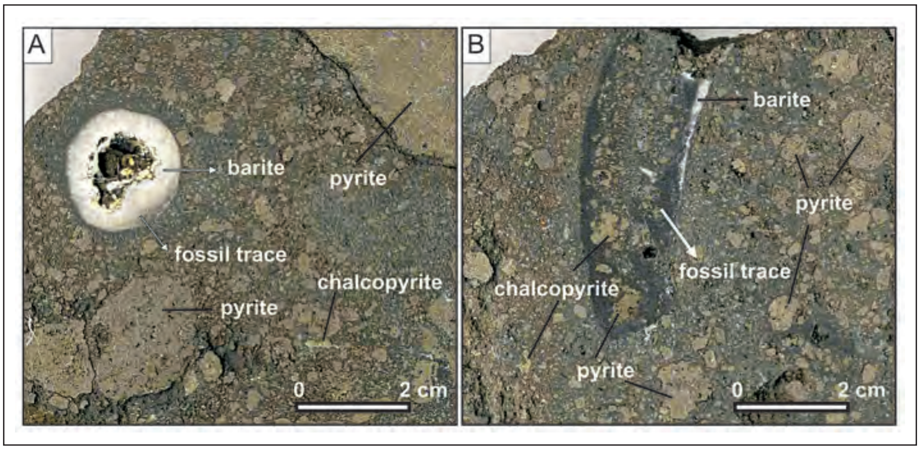

Figure 3 - A - In Killik mine, the worm fossil trace replaced by the sulphate mineral within the clastic ore, internal part is empty, doesn't contain filling; (B) The worm fossil trace filled with sulphide and sulphate mineral fragments.

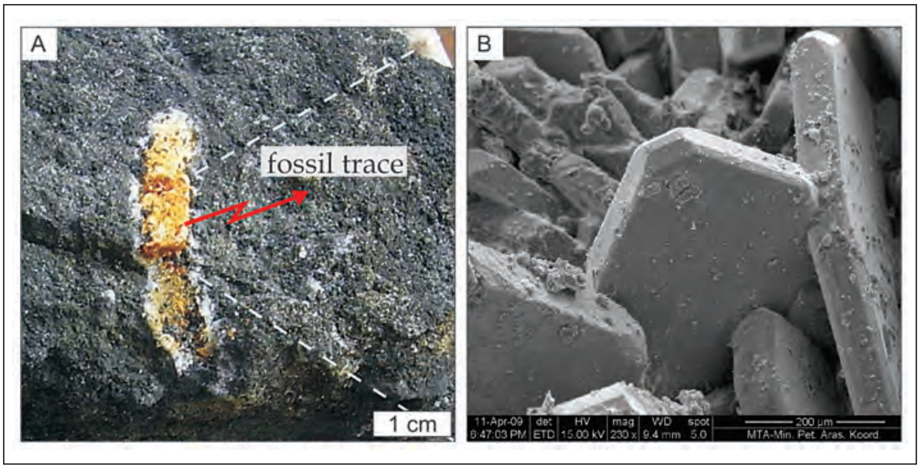

Figure 4- A- SEM image of barite minerals (B) from tube worm fossil replaced by sulphate and sulphide minerals. Sample is taken from black ore zone of Lahanos deposit.

(Qudin and Constantinou, 1984) and Ireland (Banks, 1986). Apart from these, findings and information (Kuznetzov et al. 1993; Zaykov et al. 1995) regarding the tubular worm fossil community (Figure 2A) have been obtained in the massive sulfide deposits in Urals (Yaman-Kasy, Buribaiskoye, Yubileinoye, Safyanovskoye, Komsomolskoye). However, the abundance and preservation of this mineralized fauna are dissimilar in different deposits (Prokin et al. 1985; Kuznetzov et al. 1993; Zaykov et al. 1995). The data obtained from the levels where the fauna fragments are located in massive sulfide deposits (Malahova, 1969; Bitter et al. 1992) indicate that the concerned faunas can survive in very special environmental conditions. In this environment, hydrosulfuric environment conditions which are inconvenient for the survival of

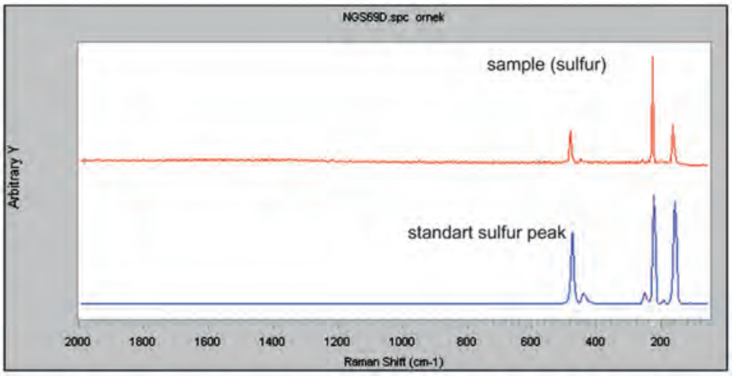

Figure 5- Raman spectrum of native sulphur from tube worm fossil replaced by sulphate and sulphide.

many other organisms except bacteria are dominant. These habitat conditions refer to sea environment deeper than 1300 meters (person. comm. Maslennikov, 2009). The organisms that survive in such a hydrothermal field have such special living conditions that it is almost impossible for them to maintain their lives in other environments (Lob'e, 1990). The existence of modern tube worms in the present-day oceans could presumably be evidence of evaluation of fossil tube worms detected in the paleo-massive sulfide deposits (such as Urals, Pontids and Samail Ophiolite) (Monroe and Wicander, 2005). However, it has not been proven yet that whether these fossil worms are ancestral forms that have evolved since the Cretaceous into the types of worms found at vents today (Haymon, et al. 1984).

The geologic setting where the Lahanos, Killik and Çayeli massive sulfide deposits formed and the mineralogical and textural features of the fossils they contain are the evidences of the existence of the hydrothermal vent on the bottom of paleo-ocean. Besides, the mineralogical findings obtained in this study demonstrate that, for the preservation of the tube worm fossils, the substitution of them by the sulfite and sulfate minerals starting from the sides is very important for the preservation of the forms. The replaced fossils became more resistant and could maintain their tube shapes. On the other hand, the existence of the microscopic and milimetric sized clastic opaque minerals filling the internal sides of the fossils indicates that the erosional effect under sea is significant and therefore they are mobile due to gravity, undersea currents or tectonic effects. The fact that the grain size of the clastic fossil fillings are in milimetric size refers to that the tube worms live relatively far away to the hot spring vent chimneys or that only fossils of the tube worms not living in a close environment to the hot spring vent chimneys can be preserved.

Within the scope of this study, Upper Cretaceous aged deposits in the Eastern Black Sea region are included in massive sulfide districts where findings of this unique fauna are found. The fossil fauna discovered in Pontid deposits are well- preserved when compared to the similar ones found in the other regions (person. comm. Valery Maslennikov, 2009).

ACKNOWLEDGEMENT

This study includes a special section of the findings related to the PhD thesis "Determining the Typical Features of the VMS Deposits of the

Eastern Black Sea Region" carried out by the first author under the supervision of the third author in the Geological Engineering Department of the Hacettepe University under the "Determining New Criteria in the Exploration of VMS Deposits" by the Department of the Mineral Research of the General Directorate of Mineral Research and Exploration (MTA)".

We would like to thank for their contribution and support to Halil Türkmen (MTA); to Þenol Karslý (MTA) and Prof. Dr. Valery Maslennikov (Russian Academy of Science) for their help in the field studies; to Okan Zimitoðlu (MTA), Dr. Okan Delibaþ (MTA) and Prof. Dr. Yusuf Kaan Kadýoðlu (Ankara University, Geological Engineering Department); to Mining Engineer Hasan Yaðcý working at the Lahanos Mine and to all mine employees.

Manuscript received January 18, 2010

REFERENCES

Banks, D.A. 1986. Hydrothermal chimneys and fossil worms from the Tynagh Pb-Zn deposits, Ireland, Geology and genesis of mineral deposits in Ireland, 441-447.

Bitter, P.H., Scott, S.D. and Schenk, P.E. 1992. Chemosynthesis; an alternate hypothesis for carboniferous biotas in bryozoan/microbial mounds Newfoundland, Canada, Palaios, 7, 466-484.

Hannington, M.D., de Ronde, C.E.J. and Petersen, S. 2005. Seafloor tectonics and submarine hydrothermal systems. Econ Geol 100th Ann vol: 111-141

Haymon, R.M., Koski, R.A. and Sinclair, C. 1984. Fossils of hydrothermal vent forms discovered in Cretaceous sulfide ores of The Semail ophiolite, Oman, Science, 223, 1407-1409.

Hebert, R. and Constantin, M. 1991. Petrology of hydrothermal metamorphism of oceanic Layer 3; implications for sulphide parageneses and redistribution, Economic Geology, 86, (3), 472-485.

Ivanov, S. N. 1947. Study experience of geology and mineralogy of the Sibay massive sulphide deposit, Akademii Nauk SSSR, Uralskiy Filial, 2, 1-109 (in Russian).

Kuznetzov, A.P., and Sobetskii, V.A. 1988. Fosil fauna in the sulphide hydrothermal hills from the middle Devonian paleo-ocean of the Ural area. Doklady Akademii Nauk SSSR, 303, 1481 (in Russian).

_____, Maslennikov, V. V. and Zaikov, V.V. 1993. The near hydrothermal fauna of the Silurian paleo-ocean in the South Ural. Izvestia Akademii Nauk SSSR. Seria Biologicheskaya, 4, 534-535 (in Russian).

Little, C.T.S. 2002. The fossil record of hydrothermal vent communities. Cahiers Biol Marine 43: 313-316.

Little, C. T. S., Maslennikov, V. V., Morris, N. J. and Zaykov, V.V. Silurian high temperature hydrothermal vent community from the Southern Urals, Russia, Nature, 1997. v. 385, no. 9, 3-6.

Lob'e, L. 1990. Oasises on the ocean floor. Moscow. Hydrometeoizdat (in Russian).

Malahova, N. P. 1969. Fauna and host sequence of massive sulphide deposits of the South Urals, Akademii Nauk SSSR, Uralskiy Filial, 81, 3-84 (in Russian).

Maslennikov, V. V. 2009. Oral communication; Institute of Mineralogy, Russia Academy of Science, Ural Division of RAS.

Monroe, J.S. and Wicander, R. 2005. Fiziksel jeoloji, yeryuvarý'nýn araþtýrýlmasý (türkçe baskýya hazýrlayanlar: Dirik, K. ve Þener, M.), TMMOB Jeoloji Mühendisleri Odasý Çeviri Serisi No 1, 642s., 2007, Ankara.

Prokin, V.A., Bogoyavlenskaya, O.V. and Maslennikov, V.V. 1985. Conditions of locations of fosil at massive copper sulphide deposits in the Urals. Geology of Ore Deposits, 1, 114-117 (in Russian).

Rona, P.A. 1984. Hydrothermal mineralization at seafloor spreading centers. Earth Sci Rev 20: 1-104.

_____, Bostrom, K., Laubier, L., and Smith, K.L. (edt). 1983. Hydrothermal processes at seafloor spreading centers. Plenum, Newyork, 796 pp.

Qudin, E. and Constantinou, G. 1984. Black smoker chimney fragments in Cyprus sulphide deposits, Nature, 308, 349-353.

Spooner, E.T.C. and Fyfe, W.S. 1973. Sub-seafloor metamorphism, heat and mass transfer. Contribution Mineralogy and Petrology. 42, 287-304.

Zaykov, V.V., Shadlun, T.N., Maslennikov, V.V. and Bortnikov, N.S. 1995. Yaman-Kasy sulphide deposits - ancient "black smoker" of Urals paleoocean. Geology of ore deposits, 37, 511-529.